

UNIVERSIDAD DE CANTABRIA
E.T.S. de Ingenieros Industriales y de Telecomunicación
Departamento de Ingenierías Química y Biomolecular

Memoria de tesis doctoral presentada para optar al título de Doctor
por la Universidad de Cantabria

**PROGRESS AND
CHALLENGES IN THE
PHOTOCATALYTIC
REMOVAL OF EMERGING
CONTAMINANTS**

**Avances y retos en la
eliminación fotocatalítica
de contaminantes
emergentes**

Sara Domínguez Suárez

Directores de tesis:
Prof. Dra. Inmaculada Ortiz Uribe
Dra. María José Rivero Martínez

Santander, 2017



Universidad de Cantabria

Escuela Técnica Superior de Ingenieros Industriales y de Telecomunicación

Departamento de Ingenierías Química y Biomolecular

**PROGRESS AND CHALLENGES IN THE
PHOTOCATALYTIC REMOVAL OF EMERGING
CONTAMINANTS**

**“Avances y retos en la eliminación fotocatalítica de
contaminantes emergentes”**

Memoria de tesis doctoral presentada para optar al título de
Doctor por la Universidad de Cantabria. Programa de Doctorado en Ingeniería
Química, de la Energía y de Procesos

Sara Domínguez Suárez

Directores de tesis:

Prof. Dra. Inmaculada Ortiz Uribe

Dra. María José Rivero Martínez

Santander, 2017

*Programa de Doctorado en Ingeniería Química, de la Energía y de
Procesos (BOE núm. 16, de 19 de enero de 2015. RUCT: 5601000)*

The research described in this thesis was conducted at the Advanced Separation Processes Group in the Department of Chemical and Biomolecular Engineering at the University of Cantabria.

This research was financially supported by the Spanish Ministry of Economy and Competitiveness and the European Regional Development Fund through the projects: CTM2012-33917 (MINECO/FEDER, UE), “Advanced oxidation technologies for the improvement of landfill leachate treatment”; CTQ2012-31639 (MINECO/FEDER, UE), “New separation processes with kinetic control based on the use of functionalized materials”; CTM2015-69845-R (MINECO/FEDER, UE), “New developments in photocatalysis for environmental applications”; CTQ2015-66078-R (MINECO/FEDER, UE), “Advanced separation applications. Modeling and experimental validation”.

Sara Domínguez also would like to express her gratitude to the Spanish Ministry of Economy and Competitiveness for the FPI postgraduate research grant (BES-2013-064055) and the two predoctoral mobility grants for conducting short stays in R&D Centers (EEBB-I-15-09465; EEBB-I-17-12013). The first research stay, which lasted four months, was in the Department of Biomedical, Chemical and Environmental Engineering at the University of Cincinnati (United States of America) under the supervision of the professor Dr. Dionysios D. Dionysiou. The second one lasted two months and a half and was conducted under the supervision of the professor Dr. Gianluca Li Puma in the Department of Chemical Engineering at the Loughborough University (United Kingdom).

During the elaboration of this thesis six papers have been published in international scientific indexed journals:

1. **Dominguez, S.**, Laso, J., Margallo, M., Aldaco, R., Rivero, M.J., Irabien, Á., Ortiz, I., 2017. Comparative LCA of greywater management within a water circular economy restorative thinking framework. *Sci. Total Environ.*, article in press.
2. Gómez-Pastora, J., **Dominguez, S.**, Bringas, E., Rivero, M.J., Ortiz, I., Dionysiou, D.D., 2017. Review and perspectives on the use of magnetic nanophotocatalysts (MNPCs) in water treatment. *Chem. Eng. J.* 310, 407–427.
3. **Dominguez, S.**, Huebra, M., Han, C., Campo, P., Nadagouda, M.N., Rivero, M.J., Ortiz, I., Dionysiou, D.D., 2017. Magnetically recoverable TiO₂-WO₃ photocatalyst to oxidize bisphenol A from model wastewater under simulated solar light. *Environ. Sci. Pollut. R.* 24, 12589–12598.
4. Escudero, C.J., Iglesias, O., **Dominguez, S.**, Rivero, M.J., Ortiz, I., 2017. Performance of electrochemical oxidation and photocatalysis in terms of kinetics and energy consumption. New insights into the p-cresol degradation. *J. Environ. Manage.* 195, 117–124.
5. **Dominguez, S.**, Rivero, M.J., Gomez, P., Ibañez, R., Ortiz, I., 2016. Kinetic modeling and energy evaluation of sodium dodecylbenzenesulfonate photocatalytic degradation in a new LED reactor. *J. Ind. Eng. Chem.* 37, 237–242.
6. **Dominguez, S.**, Ribao, P., Rivero, M.J., Ortiz, I., 2015. Influence of radiation and TiO₂ concentration on the hydroxyl radicals generation in a photocatalytic LED reactor. Application to dodecylbenzenesulfonate degradation. *Appl. Catal. B - Environ.*, 178, 165–169.

Acknowledgements

Deseo expresar mi más sincero agradecimiento a mis directoras de tesis, la Prof. Dra. Inmaculada Ortiz Uribe y la Dra. María José Rivero Martínez, por la gran confianza que han depositado en mí. Sin su ayuda, comprensión y paciencia la realización de esta tesis no hubiera sido posible.

I would like to acknowledge Prof. Dr. Dionysios D. Dionysiou for giving me the chance to work in the Department of Biomedical, Chemical and Environmental Engineering of the University of Cincinnati. I would also like to thank to the Dr. Changseok Han for helping me with the photocatalysts development and for his patient and to Vasileia Vogiazzi for her advice and support. Finally, I would like to show my gratitude to the Dr. Pablo Campo-Moreno, thank you for helping me with all the intermediate compounds analysis and for showing me Cincy. It was a positive experience from a professional and personal point of view.

I am very grateful to Prof. Dr. Gianluca Li Puma for allowing me to work in the Department of Chemical Engineering of the Loughborough University and to the Dr. Miguel Ángel Mueses for helping me with the modeling. I sincerely thank my co-workers Andrea, Gurinder, Francesco I., Francesco M., Isabel, Marianna and Salvo for integrating me like one of them since the first day. It was a great professional and personal experience.

Me gustaría mostrar mi gratitud de igual manera por la asistencia recibida por parte del personal administrativo, personal técnico y profesorado del Departamento de Ingenierías Química y Biomolecular de la Universidad de Cantabria. Particularmente, no puedo dejar pasar la oportunidad de agradecer a Gema su inestimable ayuda, ya que siempre que lo he necesitado me ha ayudado tanto profesionalmente como personalmente, mil gracias por todo.

Ampliar mi agradecimiento a todos los antiguos y actuales compañeros del departamento, especialmente a los más cercanos, Antía, Ana F., Ana H., Andrés, Azucena, Elia, Carolina, Esther, Gabi, Germán, Isa, Lucía, Mariana, Pablo y Sandra, creo que he sido una afortunada contando con vosotros como compañeros. Mención especial merecen mis super investigadores, Carlos, Olaia y Paula, sin vosotros haciendo mejor mi día a día no hubiera sido lo mismo, no sólo sois buenos compañeros, sino que me llevo unos grandes amigos, gracias por estos años.

No puedo dejar de dar las gracias a mis amigos por apoyarme siempre, aunque muchas veces no sepan ni de lo que les hablo.

Finalmente me gustaría agradecer que mi familia siempre haya confiado en mí y me haya apoyado tanto en las pequeñas decisiones como en las no tan pequeñas, os quiero. Especialmente me gustaría dar las gracias a Víctor, no hay palabras suficientes para agradecerte todo lo que has hecho por mí durante estos años ni por lo que sigues haciendo por mí día a día, no podía haber elegido mejor compañero para este gran viaje que es la vida.

¡MUCHÍSIMAS GRACIAS! / THANK YOU VERY MUCH!

Table of contents

Summary / Resumen	xv
<hr/>	
Chapter 1. Introduction	1
<hr/>	
1.1. Water as resource and its pollution	5
1.2. Advanced oxidation processes applied to the removal of emerging contaminants	9
1.3. Photocatalysis	11
1.3.1. Fundamentals and state of the art	11
1.3.2. Main challenges	14
1.4. Background and scope	20
1.5. References	21
Chapter 2. Materials and methods	33
<hr/>	
2.1. Chemical reagents	37
2.2. Photocatalytic oxidation experiments	38
2.2.1. Methodology	38
2.2.2. Experimental set-ups specifications	39
2.2.3. Radiation measurement	42
2.3. Synthesis of magnetic photocatalysts	43
2.4. Analytical measurements	46
2.4.1. Analysis of the target pollutants and their intermediate compounds	46
2.4.2. Quantification of the degree of mineralization	48
2.4.3. Analysis of the hydroxyl radicals concentration	49
2.4.4. Solids characterization	51
2.5. References	52

Chapter 3. Development of magnetic photocatalysts	53
<hr/>	
3.1. Photocatalyst characterization	57
3.2. Photocatalytic activity	63
3.3. Final remarks	70
3.4. References	72
Chapter 4. Progress on reaction mechanisms	75
<hr/>	
4.1. Hg lamp photoreactor	79
4.1.1. Influence of the photocatalyst dosage	79
4.1.2. Kinetic modeling	81
4.2. 1 st generation light emitting diodes photoreactor	83
4.2.1. Influence of the photocatalyst dosage	83
4.2.2. Influence of the radiation intensity	86
4.2.3. Kinetic modeling	89
4.3. Upgraded light emitting diodes photoreactor	91
4.3.1. Influence of the radiation intensity	91
4.3.2. Kinetic modeling	94
4.4. Assessment of the energy efficiency	97
4.5. Final remarks	103
4.6. References	104
Chapter 5. Environmental assessment	107
<hr/>	
5.1. Life cycle assessment of two photocatalytic alternatives for the treatment of greywater	115
5.1.1. Estimation of the natural resources consumption	122
5.1.2. Determination of the environmental burdens	124

5.2. Comparison to the alternative treatment of greywater with a membrane biological reactor	127
5.2.1. Estimation of the natural resources consumption	132
5.2.2. Determination of the environmental burdens	134
5.2.3. MBR variation assessment	135
5.3. Final remarks	140
5.4. References	141
Chapter 6. Conclusions	147
<hr/>	
6.1. Conclusions	151
6.2. Challenges for future research	153
6.3. Conclusiones	154
6.4. Retos futuros	157
Annexes	159
<hr/>	
Annex I. Nomenclature	161
Annex II. Scientific contributions	164

Summary

Nowadays one of the most important challenges that the scientific community has to face is the sustainable management of the available water resources. One attractive solution is the treatment and reuse of wastewater. Thus, the development of environmentally friendly technologies that allow to treat wastewater with low-cost and high efficiency is crucial.

Emerging contaminants have gained attention over the last few years due to their presence in aquatic environments and their adverse ecological and human health effects. However, a large number of these contaminants are not totally removed by the conventional wastewater treatment processes.

Advanced oxidation processes, which are based on the in situ generation of reactive oxidizing species, are technologies for wastewater treatment with high effectiveness in the degradation of many emerging contaminants. Among them, heterogeneous photocatalysis, potentially driven by renewable energy, is a feasible alternative that operates at ambient temperature and pressure and minimizes the generation of secondary pollution. Although the technical viability of photocatalysis has been assessed, some challenges still need to be overcome to achieve an efficient and sustainable deployment of the technology.

Two of the main challenges are the recovery of the photocatalyst after the degradation treatment and the development of photocatalysts with high activity under sunlight. Moreover, the use of artificial light sources, makes photocatalysis an energy intensive process, thus, energy optimization

becomes a key issue. An additional critical question that deserves further research is the difficulty of comparing the results obtained in the numerous existent photoreactor configurations. Most of the kinetic expressions contained in literature are merely valid for the specific photoreactor where the treatment is performed, hence, the extrapolation for design and scale up purposes is inaccurate.

In light of these facts, this thesis aims at acquiring new knowledge on the current challenges presented by photocatalysis.

First, in Chapter 1, an overview of the background of the water scarcity scenario, the fundamentals of advanced oxidation processes and the main principles and challenges of photocatalysis are presented.

The chemical reagents, experimental set-ups, and experimental procedures, together with the analytical methods and techniques used, are detailed in Chapter 2.

Chapter 3 approaches the development of novel magnetic photocatalysts recoverable after the photocatalytic process and active under solar simulated light.

With the aim of obtaining a suitable index that allows the comparison of photocatalytic results obtained in different experimental configurations, Chapter 4 studies the mechanisms in photocatalysis when using different light sources and configurations and develops the energy assessment of the technology.

Finally, in order to study in depth the environmental impacts generated by photocatalysis, a complete environmental assessment through life cycle assessment is performed in Chapter 5.

To sum up, this thesis reports novel results in the fundamentals of photocatalysis and its applications to degrade emerging pollutants; thus, substantiate answer to the scientific challenges needed for full deployment of the technology is offered.

Resumen

Hoy en día uno de los desafíos más importantes que la comunidad científica tiene que afrontar es la gestión sostenible de los recursos hídricos disponibles. Una solución atractiva es el tratamiento y la reutilización de las aguas residuales. Por lo tanto, el desarrollo de tecnologías amigables con el medio ambiente, que permitan tratar las aguas residuales con bajo costo y alta eficiencia, resulta crucial.

Los contaminantes emergentes han ganado atención en los últimos años debido a su presencia en ambientes acuáticos y sus efectos adversos ecológicos y para la salud humana. Sin embargo, un gran número de estos contaminantes no son totalmente eliminados por los procesos convencionales de tratamiento de aguas residuales.

Los procesos avanzados de oxidación, que se basan en la producción in situ de especies oxidantes reactivas, son tecnologías para el tratamiento de aguas residuales con alta efectividad en la degradación de varios contaminantes emergentes. Entre ellos, la fotocatalisis heterogénea, potencialmente impulsada por energía renovable, es una alternativa factible que opera a temperatura y presión ambientales y minimiza la generación de contaminación secundaria. No obstante, a pesar de que su viabilidad técnica ha sido demostrada, todavía hay que superar algunos desafíos para lograr el desarrollo eficiente y sostenible de la tecnología.

Dos de los principales desafíos son la recuperación del fotocatalizador tras el tratamiento y el desarrollo de fotocatalizadores altamente activos bajo la luz solar. Además, cuando se utilizan fuentes de luz artificiales, la fotocatalisis puede resultar un proceso energético intensivo, por lo que la

optimización energética se convierte un problema clave. Otra cuestión crítica que todavía necesita investigación es la dificultad de comparar los resultados obtenidos en las innumerables configuraciones de fotorreactores existentes. Asimismo, la mayoría de las expresiones cinéticas obtenidas en la literatura son meramente válidas para el fotoreactor específico en el que se realiza el tratamiento, por lo que la extrapolación para fines de diseño y escalado es inadecuada.

A la luz de estos hechos, esta tesis pretende avanzar en el conocimiento sobre los retos actuales que plantea la fotocatalisis y sobre el progreso de los enfoques existentes para abordarlos.

Primero, en el Capítulo 1, se presenta una visión general de los antecedentes del escenario de escasez de agua, los fundamentos de los procesos de oxidación avanzada y los principales principios y retos de la fotocatalisis.

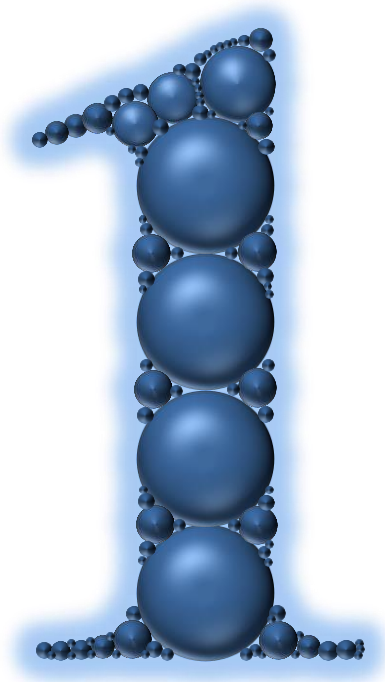
Los reactivos químicos, las configuraciones experimentales y los procedimientos experimentales, junto con los métodos analíticos y las técnicas utilizadas, se detallan en el Capítulo 2.

El Capítulo 3 aborda el desarrollo de nuevos fotocatalizadores magnéticos recuperables después del proceso fotocatalítico y activos bajo luz solar simulada.

Con el objetivo de obtener un índice adecuado que permita comparar los resultados fotocatalíticos obtenidos en diferentes configuraciones experimentales, el Capítulo 4 estudia el progreso de los mecanismos en la fotocatalisis cuando se utilizan diferentes fuentes de luz y configuraciones y desarrolla la evaluación energética de la tecnología.

Por último, para estudiar detalladamente los impactos ambientales generados por la fotocatalisis, se realiza una evaluación ambiental completa mediante análisis de ciclo de vida en el Capítulo 5.

En resumen, esta tesis presenta nuevos resultados sobre los fundamentos de la fotocatalisis y sus aplicaciones para la degradación de contaminantes emergentes; por lo tanto, se ofrece una respuesta sustancial a los desafíos científicos necesarios para el desarrollo completo de la tecnología.



INTRODUCTION

Chapter 1

Introduction

Abstract

Water scarcity and shortage of available water are two main environmental and societal worldwide concerns. Thus, an efficient and sustainable management of the water resources to guarantee freshwater accessible to everyone is required. Several methods have been employed for wastewater treatment, however, some of them are inefficient in degrading emerging contaminants. Hence, advanced oxidation processes have been presented as suitable technologies for wastewater treatment. Among them, photocatalysis represents a promising option, nevertheless, despite its technical viability has been proved, a few challenges need to be overcome to develop an efficient and sustainable photocatalytic process.

Therefore, in this chapter an overview of the importance of wastewater as resource is presented. Furthermore, the reader can find a summary of the applications of advanced oxidation processes to wastewater treatment, particularly focused on photocatalysis, its fundamentals, its main challenges and possible solutions. Finally, the background and scope of this thesis are briefly summarized.

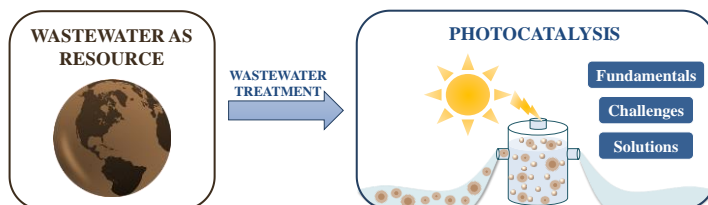


Fig. 1.1. Graphical abstract.

1.1. Water as resource and its pollution

The quantity of freshwater, which represents just the 2.50% of Earth's water, has decreased dramatically over the last decades due to the growth of human population and, thus, of the human activity (agriculture, industry, etc.), and to the trends of the climate change (longer dry spells, temperature rise, etc.) (Distefano and Kelly, 2017; Garrote, 2017; Quinteiro *et al.*, 2017). This situation has led to the deterioration of the wildlife and some aspects of the quality of human life.

It is estimated that near 4.30 billion people live under conditions of moderate to severe water scarcity and that this situation will get worse in the next years (Distefano and Kelly, 2017; Mekonnen and Hoekstra, 2016). Thus, water scarcity and shortage of available water have become two main environmental and societal worldwide concerns (Quinteiro *et al.*, 2017).

The efficient and sustainable management of water resources to provide freshwater with adequate quality for several designated uses is one of the main challenges that our society has to face nowadays (Ortiz *et al.*, 2015). With this purpose, the application of the circular economy thinking results a promising approach. This concept, which has been already taken into account in some environmental policy initiatives of the European Commission (European Commission, 2017), considers wastewater as a valuable non-conventional supply that should be used to sustain scarce life-essential resources (Abu-Ghunmi *et al.*, 2016). Hence, one attractive solution for water scarcity is the treatment and on-site reuse of wastewater or the treatment of wastewater in wastewater treatment plants (WWTPs), being crucial the development of low-cost and high efficiency technologies.

The recycling of treated wastewater is allowed by the Spanish Regulation under numerous circumstances (Real Decreto 1620/2007, 2007). Therefore, after its treatment, reclaimed water can be reused for car and window washing, fire extinguishing, groundwater discharge, irrigation, laundry or toilet flushing (Ghunmi *et al.*, 2011; Liberman *et al.*, 2016; Santasmasas *et al.*, 2013).

One of the most interesting alternatives in reuse of on-site wastewater is the recycling of greywater generated in hotel facilities, households, and sport centers (Fountoulakis *et al.*, 2016; Gabarró *et al.*, 2013; March *et al.*, 2004; Merz *et al.*, 2007; Sanchez *et al.*, 2010). Greywater is a domestic wastewater originated in hand basins, kitchen sinks, showers, and washing machines. In the developed countries the average volume of this kind of water varies from 90.0 to 120 L person⁻¹ day⁻¹, depending on numerous aspects such as the degree of water abundance, population characteristics (age, gender, etc.) or water installations (Li *et al.*, 2009).

Emerging contaminants, including additives, disinfectants, endocrine-disrupting compounds (EDCs), fragrances, micropollutants, personal care products, pesticides, pharmaceuticals, preservatives, and surfactants, have attracted increasing attention over the last few years owing to their presence in aquatic environments and their adverse ecological and human health effects (Barbosa *et al.*, 2016; Fagan *et al.*, 2016; Rodriguez-Narvaez *et al.*, 2017). However, frequently a large number of these contaminants is not totally removed by conventional wastewater treatment processes applied in the WWTPs (González *et al.*, 2016; Salimi *et al.*, 2017).

Among these contaminants, particular interest has been paid to EDCs, which are suspected of interfere and alter the endocrine system of living organisms (Salami *et al.*, 2017). One of the most representative EDCs is bisphenol A (BPA), $C_{15}H_{16}O_2$, which might cause damages to the reproductive system and provoke metabolic diseases and other health-related effects (Salimi *et al.*, 2017). Its chemical structure is shown in Fig. 1.2. Over 8.00 billion pounds of this synthetic monomer are annually produced worldwide (Resnik and Kevin, 2015), being widely employed in the plastic industry for the manufacturing of adhesives, beverage and food containers, dental sealants, and sheathing of electrical parts (Chiang *et al.*, 2004; Daskalaki *et al.*, 2011). According to estimates of the United States Environmental Protection Agency, more than 1.00 million pounds of BPA leach annually into the environment (Melcer and Klečka, 2011; Rodríguez *et al.*, 2010; Seachrist *et al.*, 2016). Since BPA has low biodegradability, its removal via the conventional treatments present in the WWTPs is difficult, thus, an effective treatment is required to protect the health of humans and the ecosystem from the adverse effects of this pollutant.

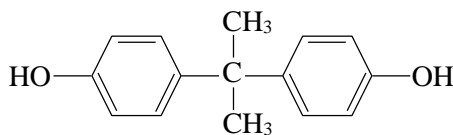


Fig. 1.2. Chemical structure of BPA.

Surfactants belong to a group of contaminants that has attracted attention; this is a group of chemical compounds with tensioactive properties that make them ideal for being the key ingredient in detergents and personal care products. Most surfactants can be found in the effluents of WWTPs and they represent an environmental hazard due to their low

biodegradability and their ability to form foams (Suárez-Ojeda *et al.*, 2007). Among them, sodium dodecylbenzenesulfonate (SDBS), $C_{18}H_{29}NaO_3S$, is an important anionic surfactant habitually employed in shampoo formulations and in detergents for washing machines (Bautista-Toledo *et al.*, 2014; Rivera-Utrilla *et al.*, 2012). Its structure is shown in Fig. 1.3.

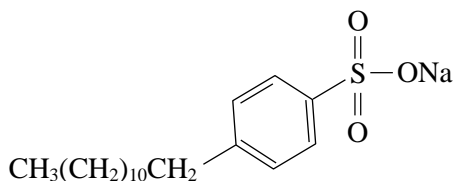


Fig. 1.3. Chemical structure of SDBS.

Several methods have been employed for the treatment of polluted waters, including biological, chemical, and physico-chemical processes (Ghunmi *et al.*, 2011; Jadhav *et al.*, 2015). Nevertheless, most of these treatments involve phase transfer of the pollutants, generate waste, require additional chemicals or use high amounts of energy (Wankhade *et al.*, 2013). Moreover, some of these conventional technologies such as activated carbon adsorption, biological treatment, and chemical oxidation seem to be too slow or inefficient in degrading some persistent emerging contaminants (Dimitroula *et al.*, 2012; Prieto-Rodriguez *et al.*, 2012; Wankhade *et al.*, 2013).

The use of membrane biological reactors (MBR) has been reported and awakened interest as promising technical alternative to treat wastewater containing emerging contaminants. An MBR combines traditional activated sludge biological treatment with membrane filtration (Chai *et al.*,

2013; Fountoulakis *et al.*, 2016; Gander *et al.*, 2000). It provides high removal degree of emerging contaminants, small space requirements, and reduced sludge production (De Gisi *et al.*, 2016; Dhouib *et al.*, 2005; Gander *et al.*, 2000; Merz *et al.*, 2007). Unfortunately, this technology still faces numerous problems for the removal of emerging contaminants, including long reaction times.

Over the last few decades advanced oxidation processes (AOPs) have been reported as environmentally friendly technologies for wastewater treatment. Their application showed high effectiveness in the degradation of several organic compounds, including different emerging contaminants (Boczka and Fernandes, 2017; Mejjide *et al.*, 2017; Vilhunen and Sillanpää, 2010; Wankhade *et al.*, 2013).

1.2. Advanced oxidation processes applied to the removal of emerging contaminants

AOPs are processes based on the in situ production of reactive oxidizing species, mainly hydroxyl radicals ($\cdot\text{OH}$). As it is detailed in Table 1.1, the $\cdot\text{OH}$ have the second highest oxidation potential known, 2.80 eV ($\cdot\text{OH}$, $\text{H}^+/\text{H}_2\text{O}$), and reaction rate constants for the degradation of several contaminants between $1.00 \cdot 10^6$ and $1.00 \cdot 10^{10} \text{ M}^{-1} \text{ s}^{-1}$ (Fernández-Castro *et al.*, 2014; Lee and Park, 2013; Moreira *et al.*, 2017). Hence, according to Eq. 1.1, they react non-selectively with most organic pollutants and decompose them into less harmful compounds such as carbon dioxide (CO_2) and water (H_2O) (Comninellis *et al.*, 2008; Moreira *et al.*, 2017).

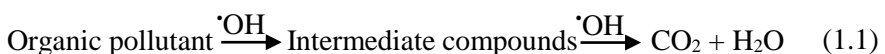


Table 1.1. Oxidation potential of some species used in wastewater treatment
(Domènech *et al.*, 2004; Lee and Park, 2013).

Reactive specie	Potential (eV)
Fluorine (F ₂)	3.03
Hydroxyl radical ([•] OH)	2.80
Ozone (O ₃)	2.07
Hydrogen peroxide (H ₂ O ₂)	1.78
Potassium permanganate (KMnO ₄)	1.68
Chlorine dioxide (ClO ₂)	1.57
Hypochlorous acid (HClO)	1.49
Chlorine (Cl ₂)	1.36
Oxygen (O ₂)	1.20
Bromine (Br ₂)	1.09
Iodine (I ₂)	5.40·10 ⁻¹

AOPs can be divided in non-photochemical processes and photochemical processes (Table 1.2) according to the origin of the [•]OH produced.

Table 1.2. Classification of the main AOPs (Domènech *et al.*, 2004).

Non-photochemical processes	Photochemical processes
Ozonization in alkaline medium (O ₃ / OH ⁻)	Water photolysis in vacuum ultraviolet
Ozonization with hydrogen peroxide (O ₃ / H ₂ O ₂)	UV / H ₂ O ₂
Fenton process (Fe ²⁺ / H ₂ O ₂)	UV / O ₃
Electrochemical oxidation	Photo-Fenton process
Radiolysis γ and treatment with bundles of electrons	Heterogeneous photocatalysis

One of the main advantages shown by the AOPs is that they provide non-selective oxidation, which make them useful to treat wastewater with several pollutants avoiding their displacement to a different phase (Vilhunen and Sillanpää, 2010). Therefore, the effectiveness of the AOPs has been already proved with the treatment of several kinds of effluents, including chemical, distillery, dyes, metal-plating, paper, pharmaceutical, and textile wastewaters (Boczkaj and Fernandes, 2017; Comninellis *et al.*, 2008).

Among this group of technologies, heterogeneous photocatalysis is an attractive instrument for the removal of emerging contaminants, operating at ambient temperature and pressure and avoiding the generation of secondary pollution (Lee and Park, 2013; Wankhade *et al.*, 2013). Additionally, contrary to other AOPs such as Fenton processes or ozonation, photocatalysis does not require the addition of expensive chemicals and it only needs a source of light and a semiconductor photocatalyst to work. Finally, since it can be solar-driven and the photocatalyst might be recovered, regenerated, and reused, it is extensively considered a sustainable technology (Malato *et al.*, 2009).

1.3. Photocatalysis

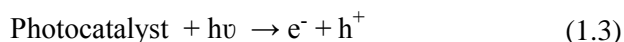
1.3.1. Fundamentals and state of the art

Heterogeneous photocatalysis is an advanced oxidation process in which a solid semiconductor material that acts as photocatalyst and a source of appropriate light promote the chemical reactions responsible for the generation of $\cdot\text{OH}$ (Kumar and Bansal, 2013; Wankhade *et al.*, 2013).

Fig. 1.4 depicts the schematic mechanism of photocatalysis where the excitation of a photocatalyst takes place when it is irradiated with an adequate source of light. When a photon with an energy ($h\nu$) equal or greater than the one of the band gap (E_g) is absorbed (Eq. 1.2) an electron (e^-) from the valence band (VB) is promoted into the conduction band (CB), leaving at the same time a photogenerated hole (h^+) in the VB and generating an electron-hole pair (e^-/h^+), as can be seen in Eq. 1.3. Then, the e^-/h^+ pairs created can further migrate to the surface of the photocatalyst, where they might react with water or oxygen molecules forming mainly $\cdot\text{OH}$ or superoxide anion radicals ($\text{O}_2^{\cdot-}$), Eq. 1.4 and Eq. 1.5, respectively; or they can recombine between themselves, liberating the previously absorbed energy as heat or light and avoiding the existence of redox reactions (Ab Aziz *et al.*, 2016; Byrne *et al.*, 2015).

$$E_g = h \cdot \nu = h \cdot c \cdot \lambda^{-1} \quad (1.2)$$

where E_g is the band gap energy, ν represents the frequency of light, h symbolizes the Planck's constant, c denotes the speed of light, and λ is the wavelength.



Taking into account that the E_g of the photocatalyst is a key parameter, the band gap of the material has to be considered for the selection of an adequate photocatalyst.

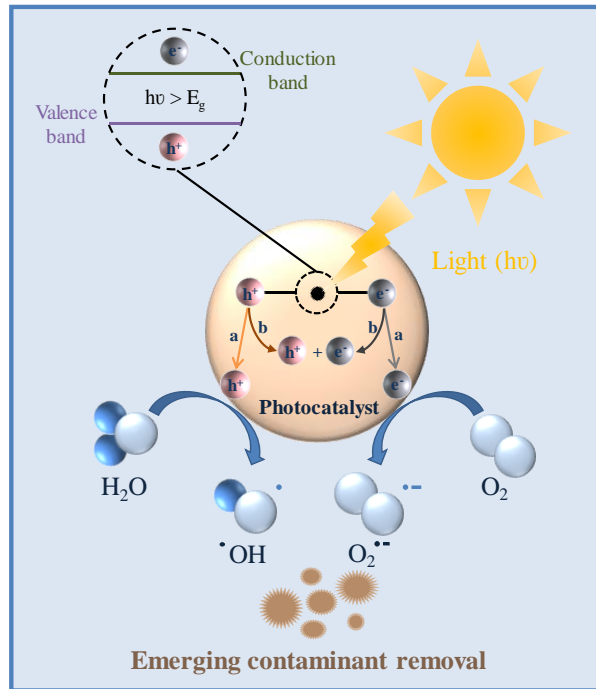


Fig. 1.4. Photocatalytic mechanism including the (a) migration of the e^-h^+ pairs to the surface and (b) recombination of the e^-h^+ pairs.

Several materials have been used as photocatalyst, including bismuth (III) sulfide (Bi_2S_3), niobium pentoxide (Nb_2O_5), russellite (Bi_2WO_6), silver carbonate (Ag_2CO_3), titanium dioxide (TiO_2), tungsten (VI) oxide (WO_3), zinc oxide (ZnO), and zinc sulfide (ZnS), among others (Boczkaj and Fernandes, 2017; Lee and Park, 2013). However, up to now, TiO_2 is the most widely employed material. This is due to its relatively high photocatalytic activity, chemical stability with respect to corrosion, nontoxicity, availability (0.44% of Earth's crust), safety, low cost, and reuse capacity (Friedmann, *et al.*, 2010; Gehrke *et al.*, 2015). There are three common crystalline forms of TiO_2 , which in order of abundance are rutile, anatase, and brookite. Anatase has the highest photocatalytic

activity, with a band gap of 3.20 eV, while brookite, which is unusual and unstable, has a band gap of 3.00 eV (Ibhadon and Fitzpatrick, 2013; Kumar and Bansal, 2013). The most commercial TiO₂ is the Aeroxide® P25 (Evonik Industries), which is formed by 70.0% of anatase and 30.0% of rutile and absorbs light with wavelengths below 387 nm (Ibhadon and Fitzpatrick, 2013; Kumar and Bansal, 2013).

1.3.2. Main challenges

With the aim of developing environmentally friendly photocatalytic treatments, the use solar light driven processes is highly desirable. Some works using solar-driven photocatalysis for the removal of emerging contaminants have reported positive results (Malato *et al.*, 2016), however, several issues still remain challenging for process scale-up and industrial implementation worldwide (Spasiano *et al.*, 2015).

The light emitted by the sun that reaches the Earth's surface has a heterogeneous distribution, depending of diverse aspects such as angle of incident light, changing atmospheric conditions, geographical area, height above sea level, ozone layer thickness and season of the year (Folli *et al.*, 2014). Another disadvantages for solar photocatalytic treatments are that large areas might be required, involving high environmental impact (Muñoz *et al.*, 2006), and that it is a discontinuous technology because the sun does not shine uninterruptedly.

Furthermore, commercial TiO₂ can be only excited at radiations below 387 nm, being this wavelength range mainly in the ultraviolet (UV) region of the solar spectrum. As less than 5.00% of the solar irradiation that reaches the Earth's surface is located within the UV region (Spasiano *et*

al., 2015), the use of artificial sources of illumination is required to obtain robust wastewater treatments. Two of the principal disadvantages of these sources of light, which usually contain mercury (Hg) or xenon (Xe) (Domènech *et al.*, 2004; Santiago-Morales *et al.*, 2013), are the low efficiency converting energy into light and their short useful life, being less than 10,000 h (Song *et al.*, 2016). Hence, the photocatalytic treatment results an energy intensive process, being the optimization of the energy consumption a key issue (Santiago-Morales *et al.*, 2013).

The employment of emerging semiconductor compact devices known as light emitting diodes (LEDs) results a suitable alternative to these traditional sources of light (Fig. 1.5). LEDs provide less toxic nature, high efficiency transforming electricity into light with a small amount of energy burned off into heat, stability, useful life longer than 100,000 h and compact size (Song *et al.*, 2016). Additionally, these devices are considerably cheaper than traditional lamps and can emit in a specific wavelength, making them appropriate for TiO₂ photocatalysis while they reduce the energy consumption (Jo and Tayade, 2014; Mioduska *et al.*, 2017). Aluminium gallium nitride, aluminum nitride, and gallium nitride are included among the most common materials use in the LEDs manufacture (Song *et al.*, 2016). Some works in literature have already shown the suitability of using LEDs in the photocatalytic removal of environmental pollutants such as acetaminophen, cyclohexane, diclofenac, dyes, formic acid, ibuprofen, phenol, and sulfamethoxazole (Eskandarian *et al.*, 2016; Jo and Tayade, 2014; Levchuk *et al.*, 2015; Mioduska *et al.*, 2017).

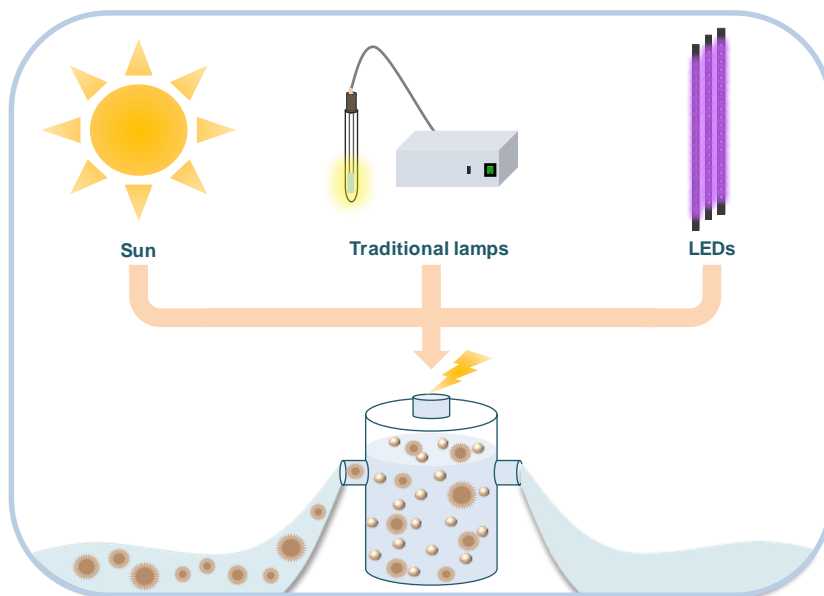


Fig. 1.5. Light source alternatives used in the photocatalytic treatment of wastewater.

Regarding the photocatalyst development two main problems need to be addressed, the development of efficient photocatalysts active under sunlight and the photocatalyst recovery after the photocatalytic process.

As it has been previously mentioned, TiO_2 , which is by far the most used photocatalyst, shows low activity under sunlight (Bai *et al.*, 2015). Thus, several approaches have been studied to enhance its activity under solar-driven photocatalysis. For instance, some works have combined the use of TiO_2 with additional components such as carbon nanotubes, dye sensitizers (azure, methylene blue, etc.), metals or metallic elements (cobalt, gold, etc.), non-metals (nitrogen, sulfur, etc.) or other semiconductors with narrow band gaps (Bi_2S_3 , WO_3 , etc.) (Barndök *et al.*, 2013; Daghrir *et al.*, 2013; Pelaez *et al.*, 2012).

One of the most promising options is the synthesis of $\text{TiO}_2\text{-WO}_3$ composites. WO_3 possesses a suitable narrow band gap, 2.80 eV, which can enhance the absorption of visible light, and it is more acidic than TiO_2 , allowing the adsorption of emerging contaminants and $\cdot\text{OH}$ on the surface of the photocatalyst (Daghrir *et al.*, 2013).

On the other hand, the recovery of the photocatalyst from the reaction medium after the treatment still remains difficult when it is used in powder form, which implies an additional separation step. A possible solution to this problem is the fixation of the photocatalyst into an inert support, avoiding the recovery stage after treatment (Byrne *et al.*, 2015). Nevertheless, this configuration diminishes the number of available active sites in the surface of the photocatalyst, implying the reduction of the photocatalytic activity of the fixed photocatalyst compared to suspended configuration.

A promising alternative is the development of powder photocatalysts with magnetic properties that allow their easy recovery by application of external magnetic fields, as shown in Fig. 1.6, which boosts the design of intensified recovery systems (Linley *et al.*, 2013). Therefore, several magnetic photocatalysts have been tested for the photocatalytic treatment of wastewater.

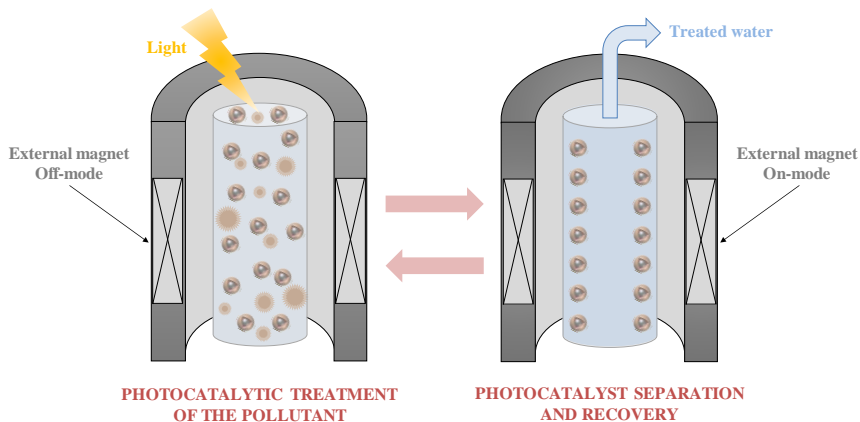


Fig. 1.6. Recovery of magnetic photocatalysts using an external magnetic field.

Most of these materials are composed of an inner core that provides the magnetic behavior, an intermediate protective shell to avoid the oxidation of the inner core, and an external photocatalytic active layer (Fig. 1.7). The core is normally formed by magnetic materials, like iron, nickel, maghemite ($\gamma\text{-Fe}_2\text{O}_3$) or magnetite (Fe_3O_4), the shell is habitually silica and the external layer is made of photocatalytic materials, such as TiO_2 or ZnO (Mamba and Mishra, 2016).



Fig. 1.7. General structure of magnetic photocatalysts.

However, since the development of these novel materials at large scale still needs to face several challenges, further work for the adequate evaluation of the structural and photocatalytic properties of the photocatalysts is required.

Another critical issue associated to the photocatalytic treatment that needs additional research is the existence of innumerable photoreactor designs with diverse dimensions, geometries, hydrodynamics, irradiances, and light sources, which highly contributes to the difficulty in the implementation of the technology (Grčić and Li Puma, 2013). Furthermore, the kinetic expressions obtained are merely valid for the specific photoreactor characteristics, thus, the extrapolation for design and scale-up resolutions is useless (Marugán *et al.*, 2013). A possible approach to address this issue is the development of simple kinetic models including key parameters for the photocatalytic reaction, such as the radiation intensity that allow comparative analysis of the performance of different photoreactors designs.

Finally, for the adequate progress of photocatalysis in wastewater treatment, its application should consider not only the degradation and mineralization achieved during the treatment but also the environmental impacts generated (Chatzisymeon *et al.*, 2013; Giménez *et al.*, 2015; Rodríguez *et al.*, 2016). Hence, it is necessary to develop a complete environmental assessment. One of the most robust tools for process and products environmental assessment is the life cycle assessment (LCA), which evaluates, defines, and quantifies the potential impacts of the lifecycle stages from “cradle” to “grave” (Corominas *et al.*, 2013; Garcia-Herrero *et al.*, 2017; Margallo *et al.*, 2014). The LCA categorizes and quantifies the inputs (energy, materials, and reagents), and outputs (emissions, waste, and environmental impacts) of the process (Chong *et al.*, 2010; Serra *et al.*, 2011). It is remarkable that scarce works can be found in literature that apply LCA to photocatalysis and most of them were performed in lab scale, limiting the utility of the results for real large-scale application (Giménez *et al.*, 2015; Muñoz *et al.*, 2005).

1.4. Background and scope

This thesis has been performed in the Advanced Separation Processes research group of the University of Cantabria. In previous works of this group, Sanchez *et al.* (2010) studied the photocatalysis of greywater from hotels with commercial TiO₂ as photocatalyst. The TiO₂ concentration was varied and positive results regarding the removal and mineralization of anionic surfactants were obtained. Afterwards, Sanchez *et al.* (2011) evaluated the kinetics of the photocatalytic treatment of SDBS using TiO₂. Several operation parameters, such as pH and TiO₂ dosage, were optimized for different SDBS concentrations. The experimental results showed that the natural pH of the solution (5.80–6.50) and an increase of the TiO₂ concentration from $5.00 \cdot 10^{-1}$ to 5.00 g L^{-1} were favorable for SDBS degradation, assessing the technical viability of the photocatalytic removal of this surfactant. Moreover, the adsorption of SDBS onto TiO₂ was evaluated in terms of the Langmuir-Hinshelwood isotherm.

Based on the aforementioned results, the main objective of this thesis is to contribute and make progress to the fundamental knowledge of the phenomena involved in photocatalysis aimed to facilitate its implementation as an environmentally friendly and sustainable wastewater treatment technology. Therefore, Chapter 1, contains an overview of the water scarcity situation, the fundamentals of AOPs, and the main challenges of photocatalysis. Chapter 2 includes the experimental set-ups, methodology and analytical methods used. Chapter 3 studies novel magnetic recoverable photocatalysts active under visible light. Chapter 4 approaches the progress on reaction mechanisms in photocatalysis when using different light sources and photoreactor configurations. Chapter 5 comprises a complete environmental assessment of photocatalysis.

1.5. References

- [1] Ab Aziz, N.A., Palaniandy, P., Abdul Aziz, H., Dahlan, I., 2016. Review of the mechanism and operational factors influencing the degradation process of contaminants in heterogenous photocatalysis. *J. Chem. Res.* 40, 704–712.
- [2] Abu-Ghunmi, D., Abu-Ghunmi, L., Kayal, B., Bino, A., 2016. Circular economy and the opportunity cost of not ‘closing the loop’ of water industry: the case of Jordan. *J. Clean. Prod.* 131, 228–236.
- [3] Bai, S., Liu, H., Sun, J., Tian, Y., Chen, S., Song, J., Luo, R., Li, D., Chen, A., Liu, C.C., 2015. Improvement of TiO₂ photocatalytic properties under visible light by WO₃/TiO₂ and MoO₃/TiO₂ composites. *Appl. Surf. Sci.* 338, 61–68.
- [4] Barbosa, M.O., Moreira, N.F.F., Ribeiro, A.R., Pereira, M.F.R., Silva, A.M.T., 2016. Occurrence and removal of organic micropollutants: an overview of the watch list of EU Decision 2015/495. *Water Res.* 94, 257–279.
- [5] Barndök, H., Peláez, M., Han, C., Platten III, W.E., Campo, P., Hermosilla, D., Blanco, A., Dionysiou, D.D., 2013. Photocatalytic degradation of contaminants of concern with composite NF-TiO₂ films under visible and solar light. *Environ. Sci. Pollut. Res.* 20, 3582–3591.
- [6] Bautista-Toledo, M.I., Rivera-Utrilla, J., Méndez-Díaz, J.D., Sánchez-Polo, M., Carrasco-Marín, F., 2014. Removal of the surfactant sodium dodecylbenzenesulfonate from water by processes based on adsorption/bioadsorption and biodegradation. *J. Colloid Interf. Sci.* 418, 113–119.

- [7] Boczkaj, G., Fernandes, A., 2017. Wastewater treatment by means of advanced oxidation processes at basic pH conditions: a review. *Chem. Eng. J.* 320, 608–633.
- [8] Byrne, J.A., Dunlop, P.S.M., Hamilton, J.W.J., Fernández-Ibáñez, P., Polo-López, I., Sharma, P.K., Vennard, A.S.M., 2015. A review of heterogeneous photocatalysis for water and surface disinfection. *Molecules* 20, 5574–5615.
- [9] Chai, H., Bao, Y., Lin, H., 2013. Engineering applications on reclaimed water treatment and reuse of hotel's high grade gray water. *Adv. Mat. Res.* 610–613, 2391–2396.
- [10] Chatzisymeon, E., Foteinis, S., Mantzavinos, D., Tsoutsos, T., 2013. Life cycle assessment of advanced oxidation processes for olive mill wastewater treatment. *J. Clean. Prod.* 54, 229–234.
- [11] Chiang, K., Lim, T.M., Tsen, L., Lee, C.C., 2004. Photocatalytic degradation and mineralization of bisphenol A by TiO₂ and platinized TiO₂. *Appl. Catal. A - Gen.* 261, 225–237.
- [12] Chong, M.N., Jin, B., Chow, C.W.K., Saint, C., 2010. Recent developments in photocatalytic water treatment technology: a review. *Water Res.* 44, 2997–3027.
- [13] Comninellis, C., Kapalka, A., Malato, S., Parsons, S.A., Poullos, I., Mantzavinos, D., 2008. Perspective advanced oxidation processes for water treatment: advances and trends for R&D. *J. Chem. Technol. Biotechnol.* 83, 769–776.
- [14] Corominas, Ll., Foley, J., Guest, J.S., Hospido, A., Larsen, H.F., Morera, S., Shaw, A., 2013. Life cycle assessment applied to wastewater treatment: state of the art. *Water Res.* 47, 5480–5492.

- [15] Dagherir, R., Drogui, P., Robert, D., 2013. Modified TiO₂ for environmental photocatalytic applications: a review. *Ind. Eng. Chem. Res.* 52, 3581–3599.
- [16] Daskalaki, V.M., Frontistis, Z., Mantzavinos, D., Katsaounis, A., 2011. Solar light-induced degradation of bisphenol-A with TiO₂ immobilized on Ti. *Catal. Today* 161, 110–114.
- [17] De Gisi, S., Casella, P., Notarnicola, M., Farina, R., 2016. Grey water in buildings: a mini-review of guidelines, technologies and case studies. *Civ. Eng. Environ. Syst.* 33, 35–54.
- [18] Dhouib, A., Hdiji, N., Hassaïri, I., Sayadi, S., 2005. Large scale application of membrane bioreactor technology for the treatment and reuse of an anionic surfactant wastewater. *Process Biochem.* 40, 2715–2720.
- [19] Dimitroula, H., Daskalaki, V.M., Frontistis, Z., Kondarides, D.I., Panagiotopoulou, P., Xekoukoulotakis, N.P., Mantzavinos, D., 2012. Solar photocatalysis for the abatement of emerging micro-contaminants in wastewater: synthesis, characterization and testing of various TiO₂ samples. *Appl. Catal. B-Environ.* 117–118, 283–291.
- [20] Distefano, T., Kelly, S., 2017. Are we in deep water? Water scarcity and its limits to economic growth. *Ecol. Econ.* 142, 130–147.
- [21] Domènech, X., Jardim, W.F., Litter, M.I., 2004. Procesos avanzados de oxidación para la eliminación de contaminantes. Eliminación de contaminantes por fotocátalisis heterogénea, 3–26. Blesa, M. A., Sánchez, B., CIEMAT, Madrid, Spain.
- [22] Eskandarian, M.R., Choi, H., Fazli, M., Rasoulifard, M.H., 2016. Effect of UV-LED wavelengths on direct photolytic and TiO₂ photocatalytic degradation of emerging contaminants in water. *Chem. Eng. J.* 300, 414–422.

- [23] European Commission 2017. <https://ec.europa.eu/commission/> (accessed 10.02.2017).
- [24] Fagan, R., McCormack, D.E., Dionysiou, D.D., Pillai, S.C., 2016. A review of solar and visible light active TiO₂ photocatalysis for treating bacteria, cyanotoxins and contaminants of emerging concern. *Mat. Sci. Semicon. Proc.* 42, 2–14.
- [25] Fernández-Castro, P., Vallejo, M., San Román, M.F., Ortiz, I., 2015. Insight on the fundamentals of advanced oxidation processes. Role and review of the determination methods of reactive oxygen species. *J. Chem. Technol. Biot.* 90, 796–820.
- [26] Folli, A., Bloh, J.Z., Strøm, M., Madsen, T.P., Henriksen, T., Macphée, D.E., 2014. Efficiency of solar-light-driven TiO₂ photocatalysis at different latitudes and seasons. Where and when does TiO₂ really work? *J. Phys. Chem. Lett.* 5(5), 830–832.
- [27] Fountoulakis, M.S., Markakis, N., Petousi, I., Manios, T., 2016. Single house on-site grey water treatment using a submerged membrane bioreactor for toilet flushing. *Sci. Total Environ.* 551–552, 706–711.
- [28] Friedmann, D., Mendive, C., Bahnemann, D., 2010. TiO₂ for water treatment: parameters affecting the kinetics and mechanisms of photocatalysis. *Appl. Catal. B-Environ.* 99, 398–406.
- [29] Gabarró, J., Batchellí, L., Balaguer, M.D., Puig, S., Colprim, J., 2013. Grey water treatment at a sports centre for reuse in irrigation: a case study. *Environ. Technol.* 34, 1385–1392.
- [30] Gander, M., Jefferson, B., Judd, S., 2000. Aerobic MBRs for domestic wastewater treatment: a review with cost considerations. *Sep. Purif. Technol.* 18, 119–130.

- [31] Garcia-Herrero, I., Laso, J., Margallo, M., Bala, A., Gazulla, C., Fullana-i-Palmer, P., Vázquez-Rowe, I., Irabien, A., Aldaco, R., 2017. Incorporating linear programming and life cycle thinking into environmental sustainability decision-making: a case study on anchovy canning industry. *Clean Techn. Environ. Policy*. 19(7), 1897–1912.
- [32] Garrote, L., 2017. Managing water resources to adapt to climate change: facing uncertainty and scarcity in a changing context. *Water Resour. Manage.* 31, 2951–2963.
- [33] Gehrke, I., Geiser, A., Somborn-Schulz, A., 2015. Innovations in nanotechnology for water treatment. *Nanotechnol. Sci. Appl.* 8, 1–17.
- [34] Ghunmi, L.A., Zeeman, G., Fayyad, M., Van Lier, J.B., 2011. Grey water treatment systems: a review. *Crit. Rev. Env. Sci. Tec.* 41, 657–698.
- [35] Giménez, J., Bayarri, B., González, Ó., Malato, S., Peral, J., Esplugas, S., 2015. Advanced oxidation processes at laboratory scale: environmental and economic impacts. *ACS Sustainable Chem. Eng.* 3, 3188–3196.
- [36] González, O., Bayarri, B., Aceña, J., Pérez, S., Barceló, D., 2016. Treatment technologies for wastewater reuse: fate of contaminants of emerging concern. *Handbook of Environmental Chemistry*, 45, 5–37. Barceló, D., Kostianoy, A.G., Springer, Berlin, Germany.
- [37] Grčić, I., Li Puma, G., 2013. Photocatalytic degradation of water contaminants in multiple photoreactors and evaluation of reaction kinetic constants independent of photon absorption, irradiance, reactor geometry, and hydrodynamics. *Environ. Sci. Technol.* 47, 13702–13711.

- [38] Ibhaddon, A.O., Fitzpatrick, P., 2013. Heterogeneous photocatalysis: recent advances and applications. *Catalysts* 3, 189–218.
- [39] Jadhav, S.V., Bringas, E., Yadav, G.D., Rathod, V.K., Ortiz, I., Marathe, K.V., 2015. Arsenic and fluoride contaminated groundwaters: a review of current technologies for contaminants removal. *J. Environ. Manage.* 162, 306–325.
- [40] Jo, W.K., Tayade, R.J., 2014. New generation energy-efficient light source for photocatalysis: LEDs for environmental applications. *Ind. Eng. Chem. Res.* 53, 2073–2084.
- [41] Kumar, J., Bansal, A., 2013. Photocatalysis by nanoparticles of titanium dioxide for drinking water purification: a conceptual and state-of-art review. *Mater. Sci. Forum* 764, 130–150.
- [42] Lee, S.-Y., Park, S.-J., 2013. TiO₂ photocatalyst for water treatment applications. *J. Ind. Eng. Chem.* 19, 1761–1769.
- [43] Levchuk, I., Rueda-Márquez, J.J., Suihkonen, S., Manzano, M.A., Sillanpää, M., 2015. Application of UVA-LED based photocatalysis for plywood mill wastewater treatment. *Sep. Purif. Technol.* 143, 1–5.
- [44] Li, F., Wichmann, K., Otterpohl, R., 2009. Review of the technological approaches for grey water treatment and reuses. *Sci. Total Environ.* 407, 3439–3449.
- [45] Liberman, N., Shandalov, S., Forgacs, C., Oron, G., Brenner, A., 2016. Use of MBR to sustain active biomass for treatment of low organic load grey water. *Clean Techn. Environ. Policy* 18, 1219–1224.
- [46] Linley, S., Leshuk, T., Gu, F.X., 2013. Magnetically separable water treatment technologies and their role in future advanced water treatment: a patent review. *Clean-Soil Air Water* 41, 1152–1156.

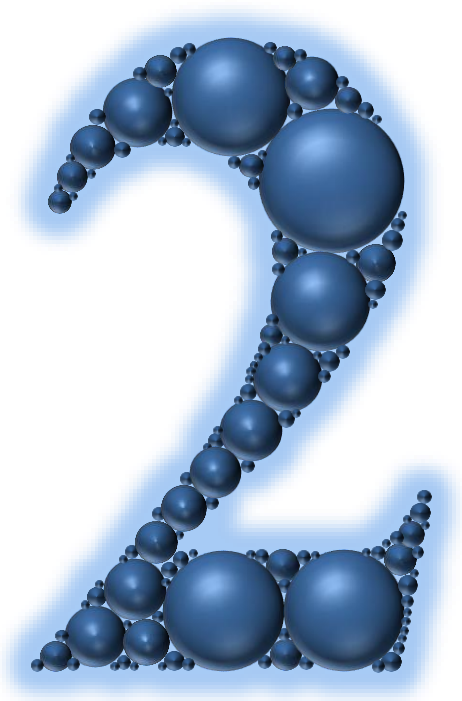
- [47] Malato, S., Fernández-Ibáñez, P., Maldonado, M.I., Blanco, J., Gernjak, W., 2009. Decontamination and disinfection of water by solar photocatalysis: recent overview and trends. *Catalysis Today* 147, 1–59.
- [48] Malato, S., Maldonado, M.I., Fernández-Ibáñez, P., Oller, I., Polo, I., Sánchez-Moreno, R., 2016. Decontamination and disinfection of water by solar photocatalysis: the pilot plants of the Plataforma Solar de Almeria. *Mat. Sci. Semicon. Proc.* 42, 15–23.
- [49] Mamba, G., Mishra, A., 2016. Advances in magnetically separable photocatalysts: smart, recyclable materials for water pollution mitigation. *Catalysts* 6(6), 79.
- [50] March, J.G., Gual, M., Orozco, F., 2004. Experiences on greywater re-use for toilet flushing in a hotel (Mallorca Island, Spain). *Desalination* 215, 37–43.
- [51] Margallo, M., Dominguez-Ramos, A., Aldaco, R., Bala, A., Fullana, P., Irabien, A., 2014. Environmental sustainability assessment in the process industry: a case study of waste-to-energy plants in Spain. *Resour. Conserv. Recy.* 93, 144–155.
- [52] Marugán, J., Van Grieken, R., Pablos, C., Satuf, M.L., Cassano, A.E., Alfano, O.M., 2013. Modeling of a bench-scale photocatalytic reactor for water disinfection from laboratory-scale kinetic data. *Chem. Eng. J.* 224, 39–45.
- [53] Meijide, J., Rosales, E., Pazos, M., Sanroman, M.A., 2017. p-nitrophenol degradation by electro-Fenton process: pathway, kinetic model and optimization using central composite design. *Chemosphere* 185, 726–736.
- [54] Mekonnen, M.M., Hoekstra, A.Y., 2016. Four billion people facing severe water scarcity. *Science Advances* 2(2), pp. e1500323.

- [55] Melcer, H., Klečka, G., 2011. Treatment of wastewaters containing bisphenol A: state of the science review. *Water Environ. Res.* 83(7), 650–666.
- [56] Merz, C., Scheumann, R., El Hamouri, B., Kraume, M., 2007. Membrane bioreactor technology for the treatment of greywater from a sports and leisure club. *Desalination* 215, 37–43.
- [57] Mioduska, J., Zielińska-Jurek, A., Hupka, J., 2017. Photocatalytical degradation of toluene and cyclohexane using LED illumination. *Pol. J. Environ. Stud.* 26(3), 1159–1164.
- [58] Moreira, F.C., Boaventura, R.A.R., Brillas, E., Vilar, V.J.P., 2017. Electrochemical advanced oxidation processes: a review on their application to synthetic and real wastewaters. *Appl. Catal. B-Environ.* 202, 217–261.
- [59] Muñoz, I., Peral, J., Ayllón, J.A., Malato, S., Passarinho, P., Domènech, X., 2006. Life cycle assessment of a coupled solar photocatalytic–biological process for wastewater treatment. *Water Res.* 40, 3533–3540.
- [60] Muñoz, I., Rieradevall, J., Torrades, F., Peral, J., Domènech, X., 2005. Environmental assessment of different solar driven advanced oxidation processes. *Sol. Energy* 79, 369–375.
- [61] Ortiz, I., Mosquera-Corral, A., Lema, J.M., Esplugas, S., 2015. Advanced technologies for water treatment and reuse. *AIChE J.* 61, 3146–3158.
- [62] Pelaez, M., Nolan, N.T., Pillai, S.C., Seery, M.K., Falaras, P., Kontos, A.G., Dunlop, P.S.M., Hamilton, J.W.J., Byrne, J.A., O’Shea, K., Entezari, M.H., Dionysiou, D.D., 2012. A review on the visible light active titanium dioxide photocatalysts for environmental applications. *Appl. Catal. B-Environ.* 125,331–349.

- [63] Prieto-Rodriguez, L., Miralles-Cuevas, S., Oller, I., Agüera, A., Li Puma, G., Malato, S., 2012. Treatment of emerging contaminants in wastewater treatment plants (WWTP) effluents by solar photocatalysis using low TiO₂ concentrations. *J. Hazard. Mater.* 211-212, 131–137.
- [64] Quinteiro, P., Ridoutt, B.G., Arroja, L., Dias, A.C., 2017. Identification of methodological challenges remaining in the assessment of a water scarcity footprint: a review. *Int. J. Life Cycle Ass.*, article in press.
- [65] Real Decreto 1620/2007, de 7 de diciembre, por el que se establece el régimen jurídico de la reutilización de las aguas depuradas, BOE no. 294, 2007.
- [66] Resnik, D.B., Elliott, K.C., 2015. Bisphenol A and risk management ethics. *Bioethics* 29(3), 182–189.
- [67] Rivera-Utrilla, J., Sánchez-Polo, M., Bautista-Toledo, M.I., Méndez-Díaz, J.D., 2012. Enhanced oxidation of sodium dodecylbenzenesulfonate aqueous solution using ozonation catalyzed by base treated zeolite. *Chem. Eng. J.* 180, 204–209.
- [68] Rodríguez, E.M., Fernández, G., Klammerth, N., Maldonado, M.I., Álvarez, P.M., Malato, S., 2010. Efficiency of different solar advanced oxidation processes on the oxidation of bisphenol A in water. *Appl. Catal. B-Environ.* 95, 228–237.
- [69] Rodríguez, R., Espada, J.J., Pariente, M.I., Melero, J.A., Martínez, F., Molina, R., 2016. Comparative life cycle assessment (LCA) study of heterogeneous and homogeneous Fenton processes for the treatment of pharmaceutical wastewater. *J. Clean. Prod.* 124, 21–29.

- [70] Rodriguez-Narvaez, O.M., Peralta-Hernandez, J.M., Goonetilleke, A., Bandala, E.R., 2017. Treatment technologies for emerging contaminants in water: a review. *Chem. Eng. J.* 323, 361–380.
- [71] Salimi M., Esrafil, A., Gholami, M., Jafari, A.J., Kalantary, R.R., Farzadkia, M., Kermani, M., Sobhi, H.R., 2017. Contaminants of emerging concern: a review of new approach in AOP technologies. *Environ. Monit. Assess.* 189(8), 414.
- [72] Sanchez, M., Rivero, M.J., Ortiz, I., 2010. Photocatalytic oxidation of grey water over titanium dioxide suspensions. *Desalination* 262, 141–146.
- [73] Sanchez, M., Rivero, M.J., Ortiz, I., 2011. Kinetics of dodecylbenzenesulphonate mineralisation by TiO₂ photocatalysis. *Appl. Catal. B-Environ.* 101, 515–521.
- [74] Santasmasas, C., Rovira, M., Clarens, F., Valderrama, C., 2013. Grey water reclamation by decentralized MBR prototype. *Resour. Conserv. Recy.* 72, 102–107.
- [75] Santiago-Morales, J., Gómez, M.J., Herrera-López, S., Fernández-Alba, A.R., García-Calvo, E., Rosal, R., 2013. Energy efficiency for the removal of non-polar pollutants during ultraviolet irradiation, visible light photocatalysis and ozonation of a wastewater effluent. *Water Res.* 47, 5546–5556.
- [76] Seachrist, D.D., Bonk, K.W., Ho, S.M., Prins, G., Sotod, A.M., Keria, R.A., 2016. A review of the carcinogenic potential of bisphenol A. *Reprod. Toxicol.* 59, 167–182.
- [77] Serra, A., Brillas, E., Domènech, X., Peral, J., 2011. Treatment of biorecalcitrant α -methylphenylglycine aqueous solutions with a solar photo-Fenton-aerobic biological coupling: biodegradability and environmental impact assessment. *Chem. Eng. J.* 172, 654–664.

- [78] Song, K., Mohseni, M., Taghipour, F., 2016. Application of ultraviolet light-emitting diodes (UV-LEDs) for water disinfection: a review. *Water Res.* 94, 341–349.
- [79] Spasiano, D., Marotta, R., Malato, S., Fernandez-Ibañez, P., Di Somma, I., 2015. Solar photocatalysis: materials, reactors, some commercial, and pre-industrialized applications. A comprehensive approach. *Appl. Catal. B-Environ.* 170–171, 90–123.
- [80] Suárez-Ojeda, M.E., Kim, J., Carrera, J., Metcalfe, I.S., Font, J., 2007. Catalytic and non-catalytic wet air oxidation of sodium dodecylbenzene sulfonate: kinetics and biodegradability enhancement. *J. Hazard. Mater.* 144, 655–662.
- [81] Vilhunen, S., Sillanpää, M., 2010. Recent developments in photochemical and chemical AOPs in water treatment: a mini-review. *Rev. Environ. Sci. Biotechnol.* 9, 323–330.
- [82] Wankhade A.V., Gaikwad, G.S., Dhonde, M.G., Khat, N.T., Thakare, S.R., 2013. Removal of organic pollutant from water by heterogenous photocatalysis: a review. *Res. J. Chem. Environ.* 17, 84–94.



MATERIALS AND METHODS

Chapter 2

Materials and methods

Abstract

This chapter includes the characteristics of the chemicals used in the experimental part of present thesis, explains the methodology followed during the photocatalytic experiments, specifies the procedure used to synthesize the photocatalysts, and describes the analytical methods.

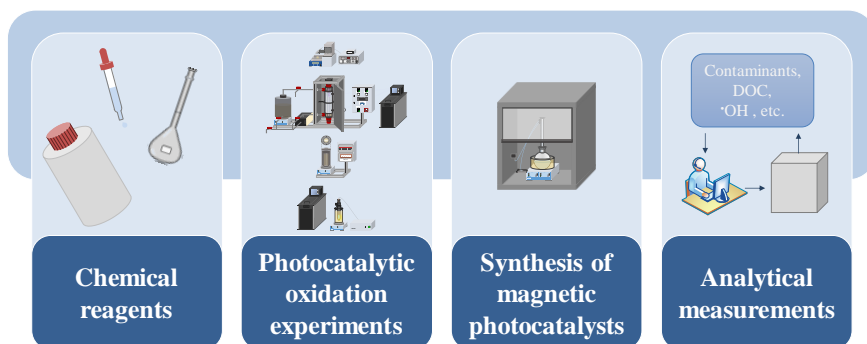


Fig. 2.1. Graphical abstract.

2.1. Chemical reagents

All the reagents and standards used in this thesis are detailed in Table 2.1 and Table 2.2.

Table 2.1. List of the chemicals used for the experimental work.

Reagent	Formula	Supplier	Use
2,4-dinitrophenylhydrazine (DNPH)	$C_6H_6N_4O_4$	Sigma-Aldrich	Hydroxyl radicals ($\cdot OH$) measurement
Acetonitrile	C_2H_3N	Fisher Scientific	BPA measurement
Ammonium hydroxide	NH_4OH	Fisher Scientific	Photocatalysts synthesis
Ammonium tungstate	$(NH_4)_{10}H_2(W_2O_7)_6$	Sigma-Aldrich	Photocatalysts synthesis
Bisphenol A (BPA)	$C_{15}H_{16}O_2$	Sigma-Aldrich	Target pollutant
Buffer solution pH 4	$H_3PO_4-NaH_2PO_4$	Panreac	$\cdot OH$ measurement
Cetyl trimethyl ammonium bromide (CTAB)	$C_{19}H_{42}BrN$	Sigma-Aldrich	Photocatalysts synthesis
Dimethyl sulfoxide (DMSO)	C_2H_6SO	Scharlau	$\cdot OH$ measurement
Ethanol	C_2H_6O	Fisher Scientific	Photocatalysts synthesis
Ferric sulfate pentahydrate	$Fe_2(SO_4)_3 \cdot 5H_2O$	ACROS Organics	Photocatalysts synthesis
Ferrous sulfate heptahydrate	$FeSO_4 \cdot 7H_2O$	ACROS Organics	Photocatalysts synthesis
Formaldehyde	CH_2O	Panreac	$\cdot OH$ measurement

Table 2.2. List of the chemicals used for the experimental work (continuation).

Reagent	Formula	Supplier	Use
Inorganic carbon (IC) standard	Na ₂ CO ₃ + NaHCO ₃	Panreac	Dissolved organic carbon (DOC) measurement
Isopropanol	C ₃ H ₈ O	GFS Chemicals	Photocatalysts synthesis
Methanol	CH ₃ OH	Sigma-Aldrich	[•] OH measurement
Natural surfactant Muscle 6013		VeruTEK	Photocatalysts synthesis
Sodium dodecylbenzenesulfonate (SDBS)	C ₁₈ H ₂₉ SO ₃ Na	Sigma-Aldrich	Target pollutant
Tetraethyl orthosilicate (TEOS)	SiC ₈ H ₂₀ O ₄	Sigma-Aldrich	Photocatalysts synthesis
Titanium (IV) isopropoxide (TTIP)	C ₁₂ H ₂₈ O ₄ Ti	ACROS Organics	Photocatalysts synthesis
Titanium dioxide (TiO ₂) Aeroxide [®] P25	TiO ₂	Evonik Industries	Photocatalyst
TOC Standard	C ₈ H ₅ O ₄ K	Panreac	DOC measurement

2.2. Photocatalytic oxidation experiments

2.2.1. Methodology

A fixed volume of solution with the target compound was mixed with a given amount of photocatalyst and kept for 24.0 h for BPA and 30.0 min for SDBS premixing in the dark to reach adsorption equilibrium. Meanwhile the source of light was switched on and stabilized. Then, the

suspension was added to the reactor and the photocatalytic experiment was started. The reaction medium was sampled at defined time intervals and filtered through a 0.45 μm syringe filter (Teknokroma) prior to analysis. The photocatalyst used was the commercial titanium dioxide (TiO_2) Aeroxide[®] P25 (Evonik Industries), except for the photocatalytic experiments for the evaluation of recoverable photocatalysts. Table 2.3 details the working photocatalyst dosage range, which was selected after the results obtained in previous works (Sanchez *et al.*, 2011). All the experiments were performed in duplicate at room temperature (25.0 $^\circ\text{C}$).

Table 2.3. Experimental conditions in the photocatalytic experiments.

Emerging contaminant	[Emerging contaminant] (mg L^{-1})	[Photocatalyst] (mg L^{-1})
BPA	10.0	$5.00 \cdot 10^{-1}$
		$1.00 \cdot 10^{-2}$
		$1.00 \cdot 10^{-1}$
		$5.00 \cdot 10^{-1}$
SDBS	50.0	1.00
		2.00
		3.00
		5.00

2.2.2. Experimental set-ups specifications

Four photocatalytic systems were used in this thesis.

Photoreactor 1 (Fig.2.2(a)) consisted in a 150 mL beaker irradiated with a 500 W solar simulator with a Xenon (Xe) lamp 67005 (Newport Corporation). The working volume was 100 mL. The power was supplied by an OPS-A500 69911 device (Newport Corporation).

Fig. 2.2(b) depicts photoreactor 2. It was integrated by a 1.00 L Pyrex reaction vessel (Heraeus Laboratory UV Reactor, Heraeus Noblelight GmbH, $d = 8.50$ cm, $h = 25.0$ cm) and a medium pressure mercury (Hg) lamp (TQ 150 z1, Heraeus Noblelight GmbH) immersed in a quartz sleeve in the center of the photoreactor. The working volume was 800 mL. The lamp emitted between 200 and 600 nm, it had maximum emission at 370 nm and it required 150 W. The radiation emitted in the UVC, UVB, UVA, and visible spectra was 21.0, 36.0, 30.0, and 194 mW cm^{-2} , respectively.

Photoreactor 3 (APRIA Systems S.L. laboratory UV LED reactor) is depicted in Fig. 2.2(c). It included a 1.00 L Pyrex glass cylindrical vessel ($d = 7.00$ cm, $h = 24.5$ cm), being the working volume 800 mL, and 180 1st generation LEDs (OCU-400 UA375, OSA Opto Light) assembled into 10 strips mounted around a dark PVC case arranged uniformly in the angular direction. LEDs had an emission wavelength between 375 and 380 nm. Total radiation ranged between $4.00 \cdot 10^{-3}$ and $2.40 \cdot 10^{-2}$ mW cm^{-2} , with an electrical power between 2.38 and 11.9 W.

Fig. 2.2(d) shows photoreactor 4 (APRIA Systems S.L. Photolab LED/160). It consisted of a 1.00 L jacketed annular Pyrex reaction vessel ($d = 6.00$ cm, $h = 50.0$ cm), a 5.00 L mixing tank, 40 upgraded LEDs (LZ1-00U600, LED Engin) assembled into 2 strips and a centrifugal pump (Grundfos CM1-2G). The working volume was 4.00 L. LEDs were located inside the inner tube of the photoreactor. Their emission was between 365 and 370 nm, the total radiation ranged from $3.30 \cdot 10^{-1}$ to 27.50 mW cm^{-2} and the electrical power varied from 1.00 to 100 W. The inner tube containing the LED strips was cooled using a fan to keep LEDs temperature below a suitable range (30.0 – 40.0 °C) that allowed to keep the radiation constant over time and increase the lamp lifetime.

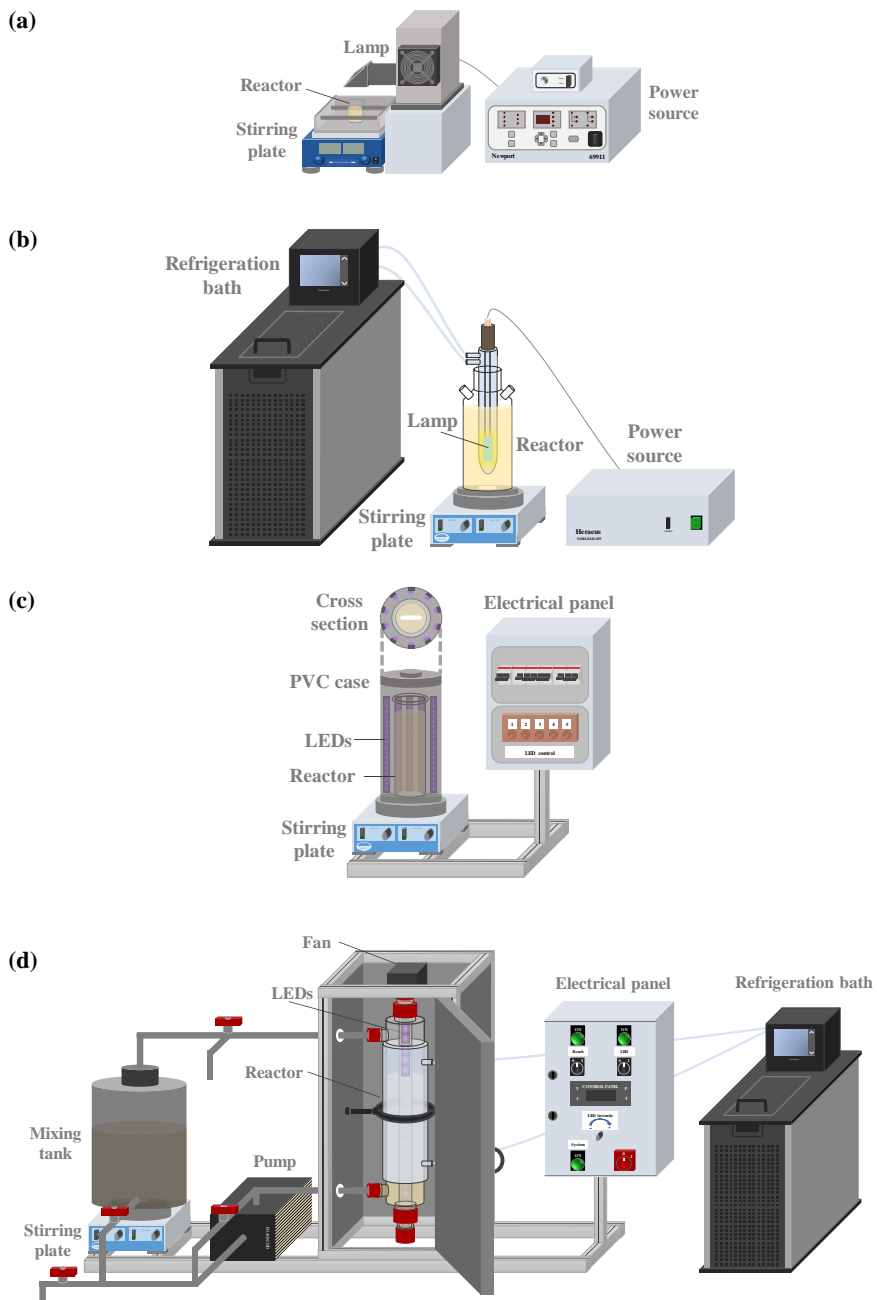


Fig. 2.2. (a) Photoreactor 1 (Xe lamp), (b) photoreactor 2 (Hg lamp), (c) photoreactor 3 (1st generation LEDs) and (d) photoreactor 4 (upgraded LEDs).

In the case of photoreactor 2 (Hg lamp) and photoreactor 4 (upgraded LEDs) a refrigeration bath (PolyScience Digital Temperature Controller) was required to keep the temperature constant at 25.0 °C. Stirring was used to provide proper mixing in the four systems, employing a mechanical KS 130 stirrer (IKA) in the case of photoreactor 1 (Xe lamp) and a magnetic Agimatic-E plate stirrer (J.P. Selecta S.A.) for the other systems. Dissolved oxygen, pH, and temperature were on-line measured with a Multimeter 44 (Crison) in photoreactor 3 (1st generation LEDs) and photoreactor 4 (upgraded LEDs).

2.2.3. Radiation measurement

A HD 2102.1 radiation meter (Delta OHM) was employed to quantify the mean radiation intensity. The radiation emitted for the different ranges of the spectrum was measured with the probes reported in Table 2.4. For the photoreactor 3 (1st generation LEDs), the measurements were carried out in the center of the empty reactor, while in the case of photoreactor 4 (upgraded LEDs) the radiation was quantified at different distances from the LED strips.

Table 2.4. Probes used for the radiation quantification. Rad range = $1.00 \cdot 10^{-5}$ – 200 mW cm^{-2} and resolution range = $1.00 \cdot 10^{-5}$ – $1.00 \cdot 10^{-2} \text{ mW cm}^{-2}$.

Spectrum range	λ (nm)	Probe
UVC	220 - 280	LP 471 UVC
UVB	280 - 315	LP 471 UVB
UVA	315 - 400	LP 471 UVA
Visible	400 - 1050	LP 471 RAD

2.3. Synthesis of magnetic photocatalysts

The synthesis of the magnetic iron-based nanoparticles with photocatalytic layer of tungsten (VI) oxide (WO_3) and TiO_2 , $\text{Fe}_3\text{O}_4@\text{SiO}_2@\text{TiO}_2\text{-WO}_3$, was performed in the 1.00 L round bottom flask reactor shown in Fig. 2.3.

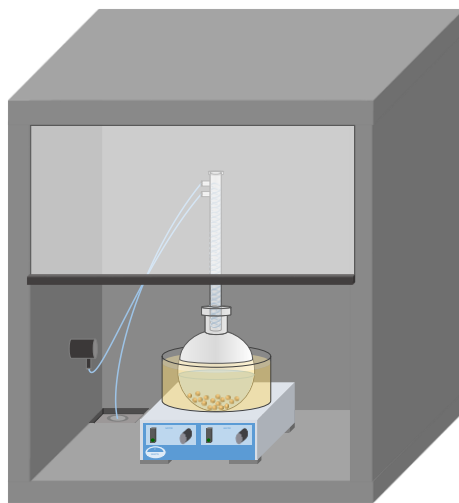


Fig. 2.3. Experimental set-up used in the synthesis of the magnetic photocatalysts.

For the preparation of the cores (Fig. 2.4), 16.7 g of ferrous sulfate heptahydrate (100 mM $\text{FeSO}_4 \cdot 7\text{H}_2\text{O}$, ACROS Organics) and 29.4 g of ferric sulfate pentahydrate (200 mM $\text{Fe}_2(\text{SO}_4)_3 \cdot 5\text{H}_2\text{O}$, ACROS Organics) were placed in the reactor. Then, 600 mL of a solution of ethanol (Fisher Scientific), ultrapure (UP) water and the natural surfactant Muscle 6013 (Verutek) (45.0:50.0:5.00 v/v) were added. 75.0 mL of ammonium hydroxide 20.0 – 22.0% (NH_4OH , Fisher Scientific) were added dropwise until a pH of 10.0 was reached. The reaction was stirred at 60.0 °C for 1.00 h and the ferrofluid obtained was sonicated 15.0 min at 20.0 kHz with a Sonics VCX 750 sonicator using a CV33 Probe (Vibra-Cell).

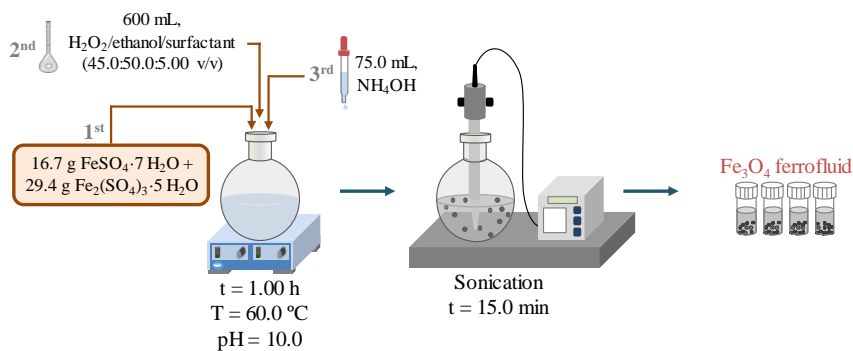


Fig. 2.4. Methodology scheme for the synthesis of the Fe_3O_4 cores.

To prevent the oxidation of the solid cores, a silica (SiO_2) layer was synthesized (Fig. 2.5) following a modified Stöber method by hydrolysis and condensation of tetraethyl orthosilicate (TEOS, Sigma-Aldrich) (Saiz *et al.*, 2013). 1.00 g of cetyl trimethyl ammonium bromide (CTAB, Sigma-Aldrich), 15.0 mL of UP water and 250 mL of ethanol were mixed at 60.0 °C. Then, 30.0 mL of the ferrofluid with the magnetic cores were introduced. Finally, 5.00 mL of TEOS were added dropwise and the suspension was stirred for 2.00 h. The precipitate obtained was washed with ethanol several times, dried at 90.0 °C for 12.0 h, calcined at 450 °C for 18.0 h, and ground.

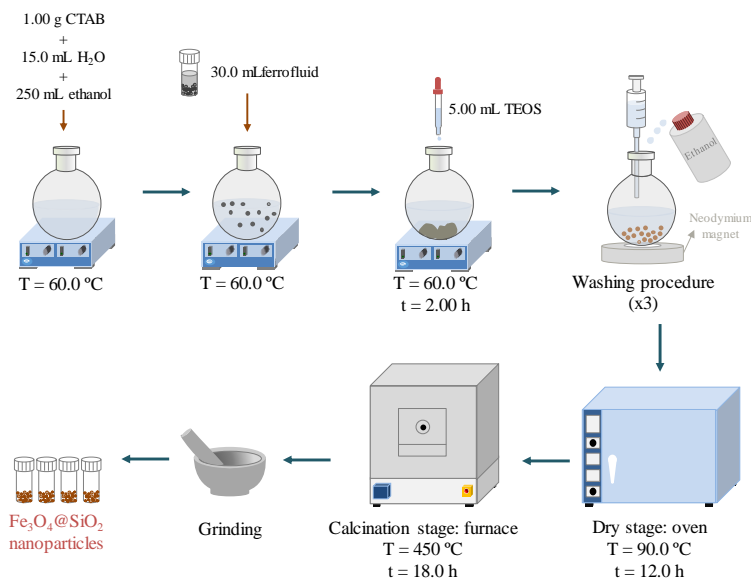


Fig. 2.5. Scheme for the synthesis of the Fe₃O₄@SiO₂ nanoparticles.

The external photocatalytic layer was synthesized via the sol-gel method showed in Fig. 2.6. $5.00 \cdot 10^{-1}$ g of the prepared Fe₃O₄@SiO₂ nanoparticles were dispersed in 100 mL of isopropanol (GFS Chemicals) at 80.0 °C. Titanium isopropoxide (TTIP, ACROS Organics) was employed as titanium precursor and an aqueous solution of ammonium tungstate ((NH₄)₁₀H₂(W₂O₇)₆, Sigma-Aldrich) was used as tungsten precursor. To get a 15.0% WO₃/TiO₂ molar ratio, the amount of TTIP added was 1.00 mL and the ammonium tungstate solution was obtained adding $12.9 \cdot 10^{-2}$ g of (NH₄)₁₀H₂(W₂O₇)₆ to 4.00 mL of UP water. They were added dropwise simultaneously, thus, their reactions started at the same time. Then, the reaction was kept for 24.0 h at 80.0 °C. The product obtained was washed three times with isopropanol, dried at 90.0 °C for 12.0 h, calcined at 450 °C for 8.00 h, and ground.

The photocatalysts without WO_3 , TiO_2 and $\text{Fe}_3\text{O}_4@\text{SiO}_2@\text{TiO}_2$, were also synthesized and, in this case, UP water was added dropwise at the same than the TTIP, instead of the ammonium tungstate solution, to facilitate TTIP hydrolysis.

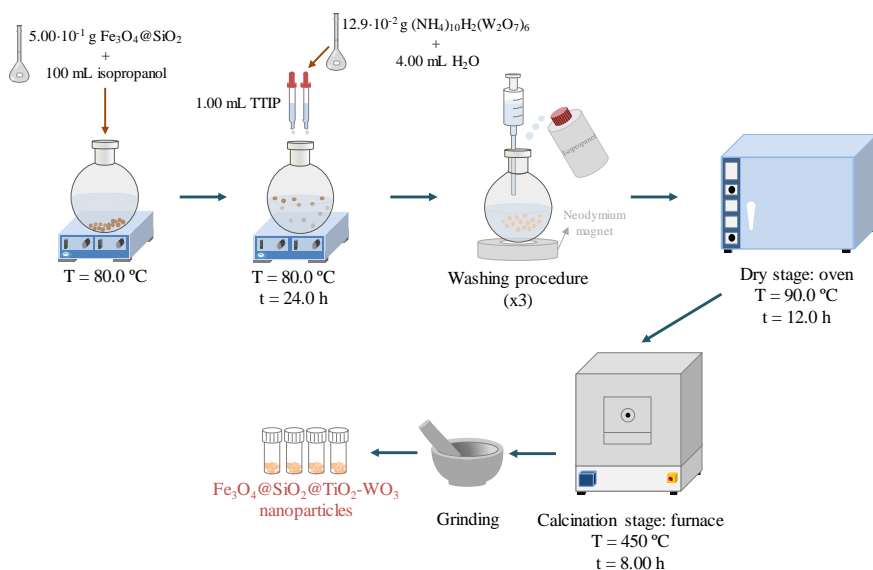


Fig. 2.6. Scheme for the synthesis of the $\text{Fe}_3\text{O}_4@\text{SiO}_2@\text{TiO}_2\text{-WO}_3$ nanoparticles.

2.4. Analytical measurements

2.4.1. Analysis of the target pollutants and their intermediate compounds

The BPA concentration was quantified via high performance liquid chromatography (HPLC) using the Agilent Series 1100 chromatograph (Agilent Technologies) depicted in Fig. 2.7 with a X Terra MS C18 $5 \mu\text{m}$ (4.60×250 mm) analytical column (Waters). The mobile phase used had a flow rate of 1.00 mL min^{-1} and was formed by a mixture of acetonitrile

(Fisher Scientific) and UP water (50.0/50.0, v/v). The operation wavelength was 214 nm and the temperature of the column was set at 30.0 °C. The signal generated was transformed to concentration using calibration curves ($[BPA] = 2.50 \cdot 10^{-1} - 15.0 \text{ mg L}^{-1}$).



Fig. 2.7. Agilent Series 1100 chromatograph.

The SDBS concentration was analyzed at 223 nm employing the UV-1800 spectrophotometer (Shimadzu) shown in Fig. 2.8. The measurements were performed using two quartz cuvettes with layer thickness of 10.0 mm Model 100-QS (Hellma Analytics), one for the sample and another one for the blank. The absorbance detected by the spectrophotometer was transform to concentration using a calibration curve ranging from 1.00 to 50.0 mg L⁻¹ of SDBS.



Fig. 2.8. UV-1800 spectrophotometer.

Identification of reaction intermediates by accurate mass measurements was carried out with an Agilent 1900 liquid chromatograph with an Agilent 6540 quadrupole time of flight/mass spectrometer (LC-Q-TOF/MS, Agilent Technologies). Nitrogen was used as drying gas at a flow rate of 7.00 L min⁻¹ at 300 °C and as sheath gas with a flow rate of 8.00 L min⁻¹ at 250 °C.

2.4.2. Quantification of the degree of mineralization

The measurement of the mineralization of the organic solutions was followed by means of the dissolved organic carbon (DOC) removal. First, samples were filtered and then they were analyzed in the TOC-VCPH analyzer with auto-sampler ASI-V (Shimadzu) shown in Fig. 2.9. The DOC was calculated from the subtraction of the inorganic carbon (IC) to the total carbon (TC) according to the Standard Methods 5310B (American Public Health Association, 1998). For the analysis of the TC 50.0 µL of the sample were introduced into the TC combustion tube, burned at 680 °C in a furnace and transformed to carbon dioxide (CO₂). Then the sample was transported by means of a carrier gas with a flow rate of 150 mL min⁻¹ to an electronic dehumidifier where it was dried and, finally, it was transported to the cell of a non-dispersive infrared (NDIR) gas analyzer, where the CO₂ formed was determined. The NDIR generated a signal and the software of the equipment registered a peak with a given area that was proportional to the amount of carbon present in the sample analyzed. In the case of the TIC analysis the sample was cooled down and acidified with phosphoric acid (25.0%), then the decomposition of the carbonates and bicarbonates of the sample generates CO₂ which was detected in the NDIR. Then, the procedure followed was the same that the one for TC.

It has to be remarked that the analyzer performed three measurements and an average DOC concentration was calculated. However, if the standard deviation was higher than $2.00 \cdot 10^{-1}$ (a.u.), it carried out two additional measurements and then chose the three values with the lowest deviation. The calibration curves were made with a 500 mg L^{-1} total organic carbon (TOC) solution (Panreac) and a 50.0 mg L^{-1} IC standard solution (Panreac).



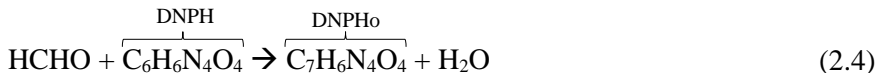
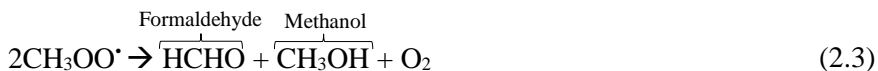
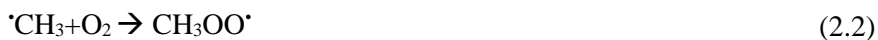
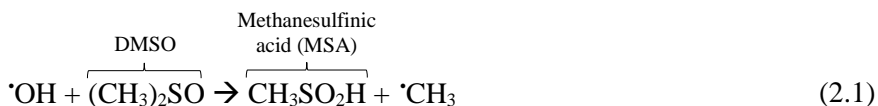
Fig. 2.9. TOC-VCPH analyzer with auto-sampler ASI-V.

2.4.3. Analysis of the hydroxyl radicals concentration

The method used in this thesis for the quantification of the $\cdot\text{OH}$ generated was initially proposed by Tai *et al.* (2004), and is based on the reaction between $\cdot\text{OH}$ and the compound dimethylsulfoxide (DMSO) to produce formaldehyde that reacts with 2,4-dinitrophenylhydrazine (DNPH) and forms the corresponding hydrazone (DNPHo), as can be seen from Eq. 2.1 to Eq. 2.4. Then, the quantification of the $\cdot\text{OH}$ generated was performed through the determination of the formaldehyde concentration when the DNPHo was analyzed by HPLC, assuming that all the $\cdot\text{OH}$ were consumed by the DMSO. Therefore, this indirect method provides the rate

of $\cdot\text{OH}$ generation, as it is the same as the rate of DMSO transformation into formaldehyde.

For the experiments, 250 mM of DMSO (Scharlau) were employed. The analysis was performed at 355 nm in an Agilent Series 1100 chromatograph (Agilent Technologies) with a XBridge C18 (5.00 μm , 4.60 x 250 mm) analytical column employing a methanol (Sigma-Aldrich)/water mixture (60.0:40.0 v/v) as mobile phase with a flow rate of $6.00 \cdot 10^{-1}$ mL min^{-1} . Then, the signal detected was converted to concentration using a calibration curve previously obtained with formaldehyde standards ($[\text{Formaldehyde}] = 1.00 \cdot 10^{-1} - 15.0$ mg L^{-1} , Panreac). The preparation of both the standards and samples for analysis was carried out through the derivatization of formaldehyde solutions with known concentration. With this aim, 2.00 mL of the formaldehyde solution or of the reaction sample were mixed with 2.50 mL of pH 4.0 H_3PO_4 - NaH_2PO_4 buffer solution (Panreac), $2.00 \cdot 10^{-1}$ mL of a 6.00 mM DNPH solution (Sigma-Aldrich) and diluted to 5.00 mL with UP water and kept at room temperature for 30.0 min before the analysis.



2.4.4. Solids characterization

The crystalline size and phases of the prepared photocatalysts were determined by X-ray diffraction (XRD) with a X'Pert PRO (Philips, Netherlands) with CuK α radiation source ($\lambda = 1.54 \text{ \AA}$) operating at 45.0 kV and 40.0 mA.

The synthesized photocatalysts morphology was characterized with scanning electron microscopy (SEM) using a JSM-6490LV microscope (JEOL) and with high-resolution transmission electron microscopy (HR-TEM) employing a JEM-2010F microscope (JEOL) with a field emission gun at 200 kV. Electron dispersion spectroscopy (EDS) installed in SEM was employed to observe the chemical composition of the samples.

The specific surface area of the nanoparticles was calculated by the Brunauer-Emmett-Teller (BET) method from the nitrogen adsorption-desorption isotherm data employing the ASAP 2000 surface area analyzer (Micromeritics) shown in Fig. 2.10.

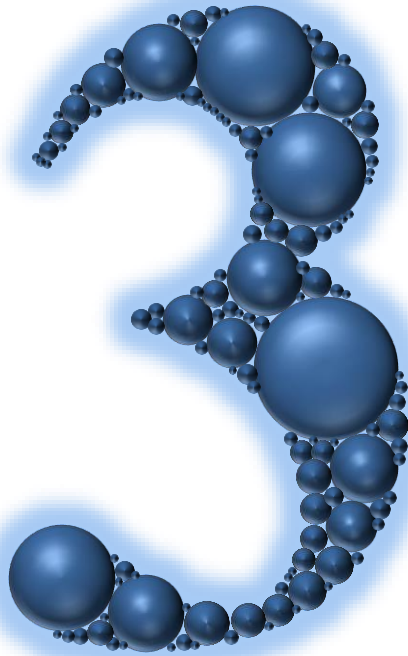


Fig. 2.10. ASAP 200 surface analyzer.

Magnetization measurements were performed on a Quantum Design MPMS magnetometer (SQUID) at 300 K in the magnetic field range from -50.0 to 50.0 kOe.

2.5. References

- [1] American Public Health Association (APHA), 1998. Standard methods for examination of water and wastewater, 20th ed. American Public Health Association, Washington DC, USA.
- [2] Saiz, J., Bringas, E., Ortiz, I., 2013. Functionalized magnetic nanoparticles as new adsorption materials for arsenic removal from polluted waters. *J. Chem. Technol. Biotechnol.* 89, 909–918.
- [3] Sanchez, M., Rivero, M.J., Ortiz, I., 2011. Kinetics of dodecylbenzenesulphonate mineralisation by TiO₂ photocatalysis. *Appl. Catal. B-Environ.* 101, 515–521.
- [4] Tai, C., Peng, J., Liu, J., Jiang, G., Zou, H., 2004. Determination of hydroxyl radicals in advanced oxidation processes with dimethyl sulfoxide trapping and liquid chromatography. *Anal. Chim. Acta* 527, 73–80.



**DEVELOPMENT OF MAGNETIC
PHOTOCATALYSTS**

Chapter 3

Development of magnetic photocatalysts

Abstract

Two of the main problems for the industrial implementation of the photocatalysis are the low activity of the commercial photocatalysts under sunlight and their recovery after the photocatalytic treatment. A novel magnetically recoverable $\text{TiO}_2\text{-WO}_3$ composite ($\text{Fe}_3\text{O}_4\text{@SiO}_2\text{@TiO}_2\text{-WO}_3$), which is also active under simulated solar light, was synthesized following the methodology indicated in Chapter 2. Its photocatalytic performance was evaluated for the treatment of bisphenol A. Moreover, with the aim to compare the results obtained, the photocatalytic activity of other materials such as non-magnetic $\text{TiO}_2\text{-WO}_3$, $\text{Fe}_3\text{O}_4\text{@SiO}_2\text{@TiO}_2$, TiO_2 and the commercial TiO_2 P25 was also studied under the same experimental conditions.

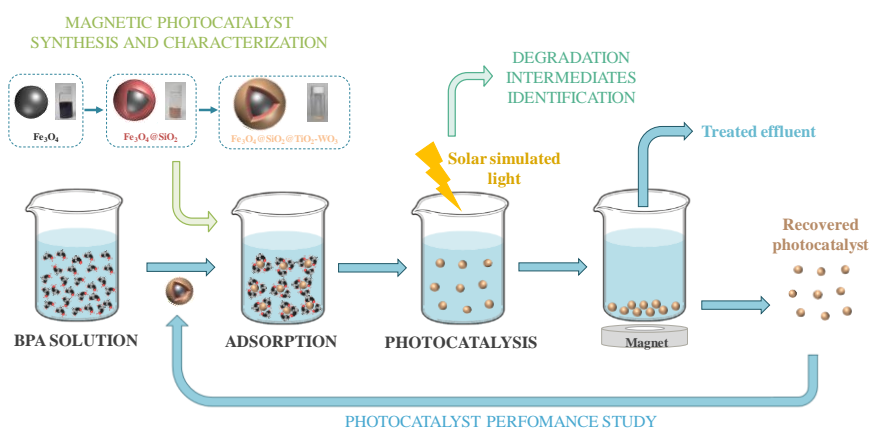


Fig. 3.1. Graphical abstract.

As it was previously stated in Chapter 1, for the development of suitable photocatalysts two main problems need to be solved, the low activity under sunlight and the recovery after the photocatalytic process. Since the most used photocatalyst, commercial titanium dioxide (TiO_2), shows low activity for solar-driven photocatalysis, increasing attention has been paid to the doping of TiO_2 with other semiconductors. Among them, tungsten (VI) oxide (WO_3), which has a suitable narrow band gap for sunlight, 2.80 eV, appears as an attractive alternative (Bai *et al.*, 2005; Daghrir *et al.*, 2013; Ramos-Delgado *et al.*, 2013). Therefore, a promising solution for addressing simultaneously both issues is the development of magnetic TiO_2 - WO_3 composites, $\text{Fe}_3\text{O}_4@ \text{SiO}_2@ \text{TiO}_2$ - WO_3 .

3.1. Photocatalyst characterization

The structure and morphology of the photocatalysts were studied by electron dispersion spectroscopy (EDS), high-resolution transmission electron microscopy (HR-TEM), scanning electron microscopy (SEM) and X-ray diffraction (XRD). Moreover, the Brunauer–Emmett–Teller (BET) surface area and the magnetic properties were also evaluated.

First, to verify the presence of W and Ti elements in the $\text{Fe}_3\text{O}_4@ \text{SiO}_2@ \text{TiO}_2$ - WO_3 photocatalyst and to check that the average molar ratio of WO_3 to TiO_2 reached the desired value, EDS was used to analyze the elemental composition (Fig. 3.2). Ti and W signals were observed, which confirmed the synthesis of the external layer of the photocatalyst. However, Fe and Si elements were detected, showing that the internal layers were not totally covered by the external one.

Additionally, using the weight content of WO_3 , the molar content was calculated, resulting 16.0%, which was close to the target value, 15.0%.

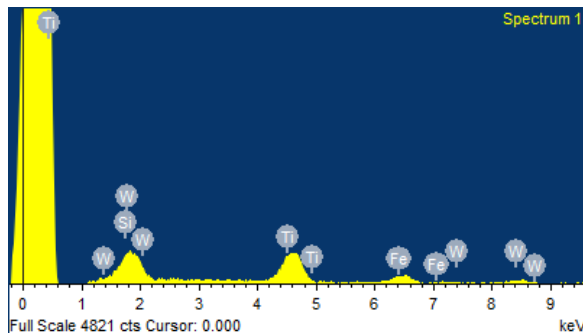


Fig. 3.2. EDS spectrum of the $\text{Fe}_3\text{O}_4@SiO_2@TiO_2-WO_3$ photocatalyst.

The structure of the photocatalysts was analyzed through the images obtained from the HR-TEM and SEM (Fig. 3.3). As it is observed in Fig. 3.3(a1), prepared primary Fe_3O_4 nanoparticles as cores of magnetic photocatalysts were spherical and their average diameter was 23.0 nm. Cores with similar size were obtained in literature; for instance, Jing *et al.* (2013) synthesized Fe_3O_4 nanoparticles of 17.0 nm. Nonetheless, Fig. 3.3(b1) demonstrates that the magnetic Fe_3O_4 cores were aggregated and formed large clusters. When the next layer was added, amorphous SiO_2 was covering completely the magnetic Fe_3O_4 cores (Fig. 3.3(a2) and Fig. 3.3(b2)). After addition of TiO_2 , crystallized nanoparticles on the surface of $\text{Fe}_3\text{O}_4@SiO_2$ samples were formed, as shown in Fig. 3.3(a3). The TiO_2 nanoparticles covered the whole area of $\text{Fe}_3\text{O}_4@SiO_2$ (Fig. 3.3(b3)), confirming that TiO_2 nanoparticles were effectively deposited on the surface of $\text{Fe}_3\text{O}_4@SiO_2$. In the case of the bare TiO_2 photocatalyst, Fig. 3.3(a5) shows that similar nanoparticles were formed. However, when WO_3 was added to the $\text{Fe}_3\text{O}_4@SiO_2@TiO_2$ interesting ring-like structures (Fig. 3.3(a4)) and micro-rods (Fig. 3.3(b4)) were also observed.

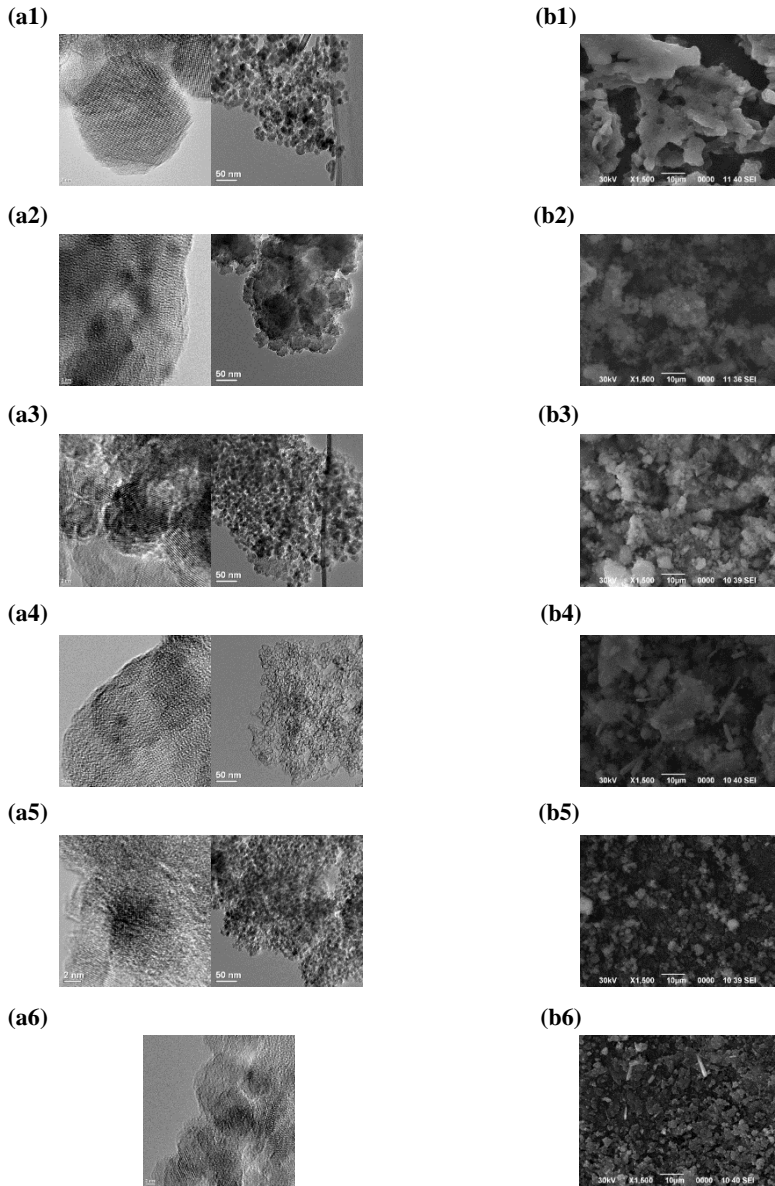


Fig. 3.3. Electronic microscopy characterization. HR-TEM images of (a1) Fe_3O_4 , (a2) $\text{Fe}_3\text{O}_4@\text{SiO}_2$, (a3) $\text{Fe}_3\text{O}_4@\text{SiO}_2@\text{TiO}_2$, (a4) $\text{Fe}_3\text{O}_4@\text{SiO}_2@\text{TiO}_2\text{-WO}_3$, (a5) TiO_2 and (a6) $\text{TiO}_2\text{-WO}_3$ nanoparticles. SEM images of (b1) Fe_3O_4 , (b2) $\text{Fe}_3\text{O}_4@\text{SiO}_2$, (b3) $\text{Fe}_3\text{O}_4@\text{SiO}_2@\text{TiO}_2$, (b4) $\text{Fe}_3\text{O}_4@\text{SiO}_2@\text{TiO}_2\text{-WO}_3$ (b5) TiO_2 and (b6) $\text{TiO}_2\text{-WO}_3$ nanoparticles.

Fig. 3.4. contains the XRD spectra of the synthesized photocatalysts. The strongest reflection for anatase was detected at 25.3° (101 plane). Furthermore, anatase generated other primary diffraction signals with lower intensities at 27.0 , 38.0 , 48.0 , 54.2 , 55.2 , 62.7 , 70.0 , 75.0 , and 82.8° , corresponding to the (110), (004), (200), (105), (211), (204), (220), (215), and (224) planes, respectively (JCPDS No. 21-1272). At 23.1 , 23.7 , 24.2 , and 33.9° , peaks corresponding to the primary reflections of monoclinic WO_3 were detected, which can be indexed as (002), (020), (200), and (202), respectively (JCPDS No. 43-1035). In the case of the magnetite, the strongest peak was observed at 35.6° , corresponding to the (311) plane. Moreover, the planes (220), (400), (422), (511), and (440) also corresponding to other magnetite phases were detected at 30.1 , 43.1 , 53.4 , 56.9 , and 62.5° , respectively (JCPDS No. 19-0629).

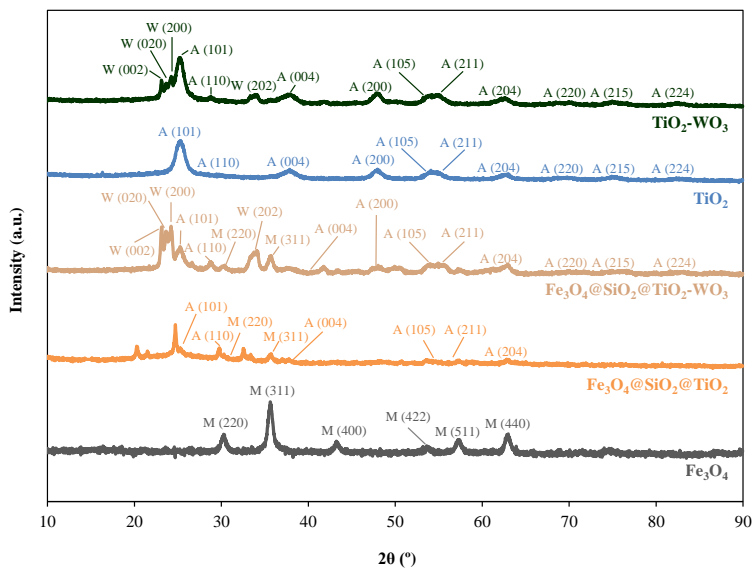


Fig. 3.4. XRD spectra for Fe_3O_4 , $\text{Fe}_3\text{O}_4@\text{SiO}_2@\text{TiO}_2$, $\text{Fe}_3\text{O}_4@\text{SiO}_2@\text{TiO}_2\text{-WO}_3$, TiO_2 and $\text{TiO}_2\text{-WO}_3$ photocatalysts.

For the synthesized photocatalysts the BET surface area and the nitrogen adsorption–desorption isotherms were determined. The obtained isotherms (Fig. 3.5) were categorized as type IV with H3 hysteresis, employing the IUPAC classification, thus, the solids were classified as mesoporous. The surface area obtained for the commercial TiO₂ P25 photocatalyst was 56.5 m² g⁻¹, being consistent with the values reported in the literature (Lucas *et al.*, 2013; Ye *et al.*, 2010). The TiO₂, TiO₂-WO₃, Fe₃O₄@SiO₂@TiO₂ and Fe₃O₄@SiO₂@TiO₂-WO₃ samples showed a similar increase in the surface area with respect to the TiO₂ P25, with 130, 119, 135, and 116 m² g⁻¹, respectively. It is remarkable that the addition of the different coating layers resulted in the decrease in the BET surface area. This behavior could be due to blockage of the pores of the previous layer.

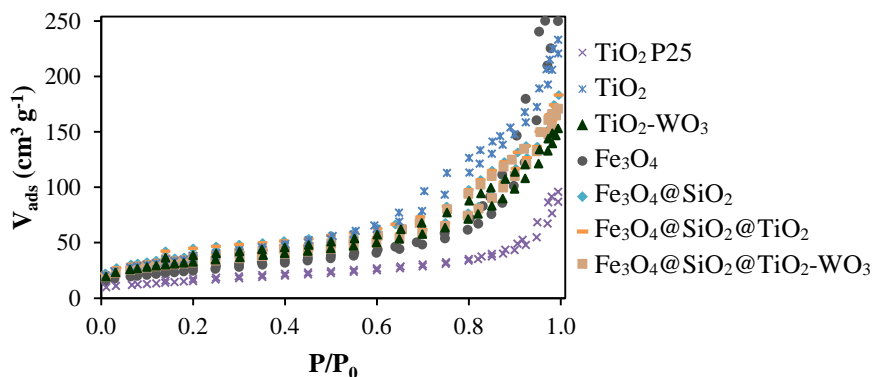


Fig. 3.5. Nitrogen adsorption–desorption isotherms.

The magnetization curves of the synthesized photocatalyst, which are shown in Fig. 3.6, were obtained in order to characterize the magnetic properties. The magnetization saturation (M_s) of the samples for the evaluation of the magnetic response to an external field (H) was determined at 26.9 °C. The values of M_s exhibited by the Fe₃O₄ and the

$\text{Fe}_3\text{O}_4@\text{SiO}_2@\text{TiO}_2$ were 68.1 and 16.0 emu g^{-1} , respectively. Hence, after the synthesis of the SiO_2 and TiO_2 layers a considerable reduction in the magnetic properties of the photocatalysts was observed. Chi *et al.* (2013), who prepared Fe_3O_4 and $\text{Fe}_3\text{O}_4@\text{SiO}_2@\text{TiO}_2$, also described this behavior with a M_s of 79.9 and 33.5 emu g^{-1} , respectively. Additionally, the $\text{Fe}_3\text{O}_4@\text{SiO}_2@\text{TiO}_2\text{-WO}_3$ showed smaller M_s , 8.54 emu g^{-1} , than the $\text{Fe}_3\text{O}_4@\text{SiO}_2@\text{TiO}_2$ photocatalyst, which could be attributed to an increase in the mass and size caused by the addition of WO_3 . Despite the reduction of M_s with the addition of the different layers, it has to be highlighted that the M_s values of the photocatalysts were still high enough to allow their recovery after the photocatalytic process applying a magnetic field. Furthermore, the coercivity and remanent magnetization values were close to zero, indicating that the photocatalyst had superparamagnetic properties (Fisli *et al.*, 2013).

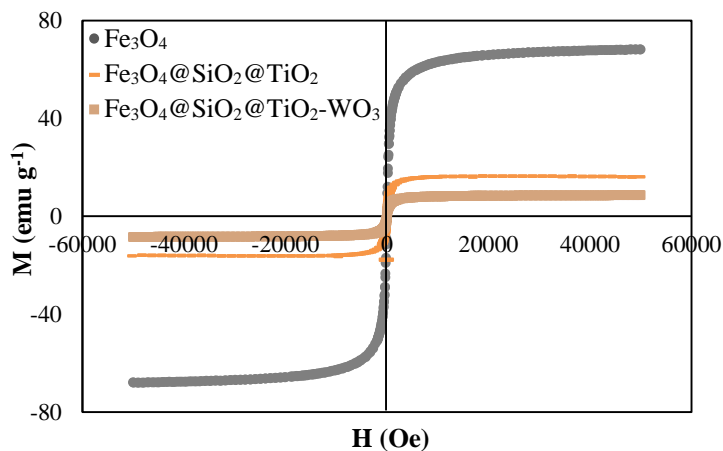


Fig. 3.6. Magnetization curves for magnetic photocatalysts.

3.2. Photocatalytic activity

The photocatalytic treatment under simulated solar light of 100 mL of a 10.0 mg L⁻¹ BPA solution was performed in the photoreactor 1 (Xe lamp) using the previously characterized photocatalysts (Fig. 3.7). BPA was solubilized in ultrapure (UP) water. It can be seen that in the absence of photocatalyst there was not BPA removal at all, which indicates that BPA was stable under simulated solar light irradiation. With the commercial TiO₂ Aeroxide® P25 (Evonik Industries), BPA was completely eliminated after 60.0 min of treatment, while when using the Fe₃O₄@SiO₂@TiO₂-WO₃ photocatalyst, the removal of BPA was only 17.5% after 120 min of treatment. This decrease of the effectiveness in the degradation of BPA when using the Fe₃O₄@SiO₂@TiO₂-WO₃ photocatalyst could be due to presence of an insufficient amount of TiO₂-WO₃ in the outer layer of the photocatalyst, which provided the photocatalytic capacity. Unfortunately, the amount of TiO₂-WO₃ deposited on the magnetic core could not be determined. Eventually, a minor amount of active photocatalyst was included within the magnetic composites, resulting in a much smaller BPA degradation rate than the one obtained when using the TiO₂ P25.

Despite the performance was increased when using the TiO₂-WO₃ photocatalyst, achieving a BPA removal of 27.9% after 120 min, this photocatalyst showed lower activity than the commercial photocatalyst. For the materials synthesized that do not include WO₃, the magnetic composite attained a removal of 40.9% of BPA at the end of the treatment while the as-prepared non-magnetic one degraded 38.3%.

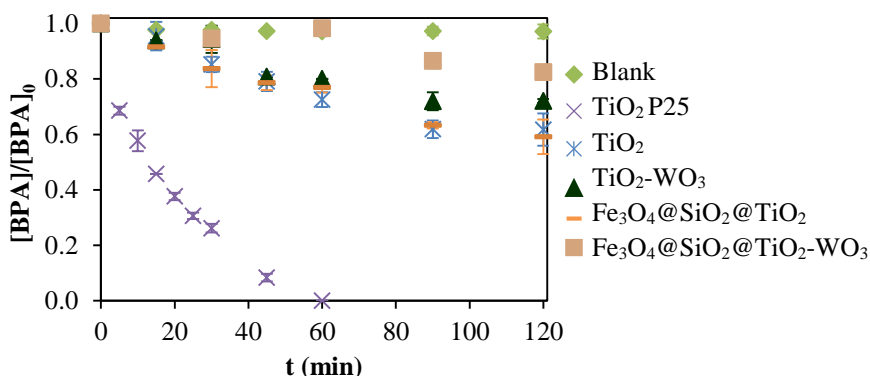


Fig. 3.7. Photocatalytic treatment of BPA in UP water with time in photoreactor 1 (Xe lamp). [BPA]₀ = 10.0 mg L⁻¹, [photocatalyst] = 5.00·10⁻¹ g L⁻¹.

It is remarkable that the Fe₃O₄@SiO₂@TiO₂-WO₃ was easily recovered by means of a neodymium magnet after the photocatalytic experiments (Fig. 3.8), corroborating the results displayed by the magnetization curves, and proving an efficient magnetic separation. Thus, the magnetic photocatalyst synthesized in this thesis showed important properties to result an adequate recyclable photocatalyst, containing a highly magnetic core that allowed its magnetic recovery, a silica layer that protected the core from dissolution, and an external layer that showed photocatalytic activity under simulated solar light.



Fig. 3.8. Separation process of the Fe₃O₄@SiO₂@TiO₂-WO₃ photocatalyst after the photocatalytic treatment of BPA in UP water in photoreactor 1 (Xe lamp).

[BPA]₀ = 10.0 mg L⁻¹, [photocatalyst] = 5.00·10⁻¹ g L⁻¹.

Next, the kinetics of BPA degradation were studied. The rate of the photocatalytic degradation of BPA could be fitted to a Langmuir-Hinshelwood kinetic equation, Eq. 3.1; nevertheless, since the initial concentration of BPA in the solution was low, this equation was simplified to the pseudo first-order kinetic expression showed in Eq. 3.2 (Li Puma *et al.*, 2004).

$$\frac{-d[\text{BPA}]}{dt} = \frac{K_{\text{ads}} \cdot k \cdot [\text{BPA}]}{1 + K_{\text{ads}} \cdot [\text{BPA}]} \quad (3.1)$$

where [BPA] is the concentration of bisphenol A (mg L^{-1}), t represents the reaction time (min), K_{ads} symbolizes the adsorption coefficient (L mg^{-1}), and k denotes the reaction-rate constant (min^{-1}).

$$\frac{-d[\text{BPA}]}{dt} = k_{\text{app}} \cdot [\text{BPA}] \quad (3.2)$$

where [BPA] is the concentration of bisphenol A (mg L^{-1}), t represents the reaction time (min) and k_{app} symbolizes the pseudo-first order kinetic constant (min^{-1}).

The pseudo-first order kinetic constants and regression coefficients (R^2) obtained from the fitting of the experimental data to the pseudo-first order kinetic model are collected in Table 3.1. As it can be observed, the removal of BPA with the commercial TiO_2 P25 fitted appropriately to the pseudo-first order kinetic model, with a k_{app} of $5.12 \times 10^{-2} \text{ min}^{-1}$ and R^2 of 0.976. However, when using the synthesized photocatalysts the regression coefficients were smaller; it is worth noticing that with these photocatalysts the degradation rates were significantly slower than with the commercial photocatalyst.

Table 3.1. Parameters obtained from the fitting of the experimental data of the photocatalytic treatment of BPA in UP water to a pseudo-first order kinetic model.

$$[\text{BPA}]_0 = 10.0 \text{ mg L}^{-1}, [\text{photocatalyst}] = 5.00 \cdot 10^{-1} \text{ g L}^{-1}.$$

	$k_{\text{app}} \text{ (min}^{-1}\text{)}$	R^2
TiO₂ P25	$5.12 \cdot 10^{-2}$	0.976
TiO₂	$3.90 \cdot 10^{-3}$	0.890
TiO₂-WO₃	$3.10 \cdot 10^{-3}$	0.924
Fe₃O₄@SiO₂@TiO₂	$3.90 \cdot 10^{-3}$	0.909
Fe₃O₄@SiO₂@TiO₂-WO₃	$1.40 \cdot 10^{-3}$	0.799

During the photocatalytic treatment it is important not only to check the degradation of the target contaminant but also to assess the likely appearance of different byproducts. The formation of several compounds was detected in the photocatalytic treatment of BPA in UP water. The concentration and rate of formation of these intermediate compounds could depend on the photocatalyst used. Thus, the change of the concentration of oxidation byproducts with time was followed by accurate mass measurement with the liquid chromatograph with quadrupole time of flight/mass spectrometer detailed in Chapter 2 and a degradation pathway was proposed (Fig. 3.9).

The signal corresponding to BPA decreased gradually with time, confirming its removal, while other peaks corresponding to the intermediate products appeared and disappeared, and some signals representing the final products showed up at the end of the treatment. The $\cdot\text{OH}$ generated during the photocatalytic treatment attacked the BPA (stage 1, Fig. 3.9), transforming it into compounds with different hydroxylation degrees.

Then, phenyl and isopropylphenol radicals were formed (stage 2, Fig. 3.9), degrading the BPA to intermediate compounds with one aromatic ring (Sin *et al.*, 2012; Thiruvengkatachari *et al.*, 2005). When using the commercial TiO₂ P25, 4-isopropylphenol (C₉H₁₂O), 4-hydroxyacetophenone (C₈H₈O₂) and 5-hydroxy-2-methylbenzoic acid (C₈H₈O₃) were detected within the first 5.00 min but remained at the end of the treatment, as it was previously reported by Maroga Mboula *et al.* (2013) and Sharma *et al.* (2016). Nonetheless, as it was stated by Da Silva *et al.* (2014), 4-isopropanol-1,2-benzenediol (C₉H₁₂O₃) appeared during the first minutes of treatment and then disappeared. Moreover, in the first 5.00 min, 2,4,5-trihydroxyacetophenone (C₈H₈O₄) was also detected and might derived from the hydroxylation of the 4-hydroxyacetophenone. However, in the treatment of BPA with any of the photocatalysts synthesized, the previously cited compounds were not identified. For these materials the only byproduct detected was 2-(4-hydroxyphenyl)-2-propanol (C₉H₁₂O₂), showing up after 30.0 min. Despite this compound was not found in this thesis when using the TiO₂ P25, it has been identified in literature during the photocatalytic oxidation of BPA with TiO₂ P25 (Tsai *et al.*, 2009; Watanabe *et al.*, 2003).

The oxidation of the aromatic ring (stage 3, Fig. 3.9) led to the generation of organic acids such as formic (CH₂O₂) and maleylacetic (C₆H₆O₅) (Ferro Orozco *et al.*, 2016; Thiruvengkatachari *et al.*, 2005; Watanabe *et al.*, 2003). It is worth noticing that acidic compounds with molecular weights of 114, 163, and 199 g mol⁻¹ were detected when using both the TiO₂ P25 and the synthesized photocatalysts, nevertheless, it was not possible to assign them to a specific structure. Finally, in an ultimate stage of the reaction (stage 4, Fig. 3.9), the organic acids were mineralized to carbon dioxide and water.

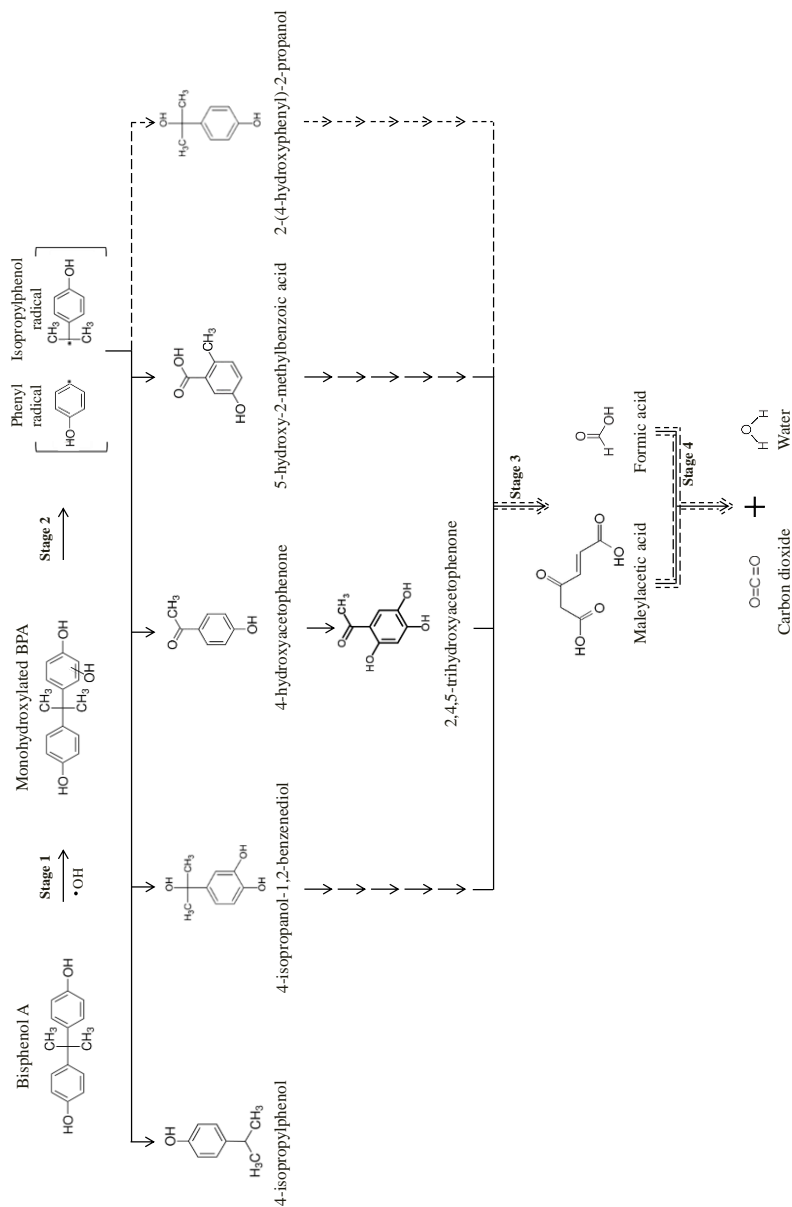


Fig. 3.9. Degradation route of BPA in UP water. Solid lines: TiO_2 P25, dashed lines: synthesized photocatalysts.

Since real wastewater is a much more complex matrix that contains numerous substances, the photocatalytic efficiency of the photocatalysts could be reduced with respect the values observed in UP water. Therefore, to check the photocatalysts performance in real wastewater, a sample of wastewater generated at the University of Cincinnati was spiked with BPA (Fig. 3.10). Wastewater was characterized, being the average alkalinity 292 mg CaCO₃ L⁻¹ and the average dissolved organic carbon was 23.6 mg L⁻¹. However, BPA was not detected, thus, 10.0 mg L⁻¹ of BPA were spiked into this water.

The results obtained showed that TiO₂ P25 removed 62.8% of BPA after 180 min of treatment, being the degradation rate lower than the value observed in UP water, where complete removal was attained after 60.0 min of treatment. This behavior was also detected in the case of the TiO₂-WO₃ composite, being the photocatalytic activity negligible. The decrease in the photocatalytic activity of both samples could be due to an inhibitory effect caused by the presence of inorganic ions, such as carbonates, or dissolved organic matter. These species could compete with BPA for the adsorption sites on the surface of the photocatalysts and/or behave as $\cdot\text{OH}/\text{h}^+$ scavengers (Carbajo *et al.*, 2014). Scavenging effects provoked by the presence of carbonates in the photocatalytic treatment of contaminants with TiO₂ have been also reported by Pelaez *et al.* (2011).

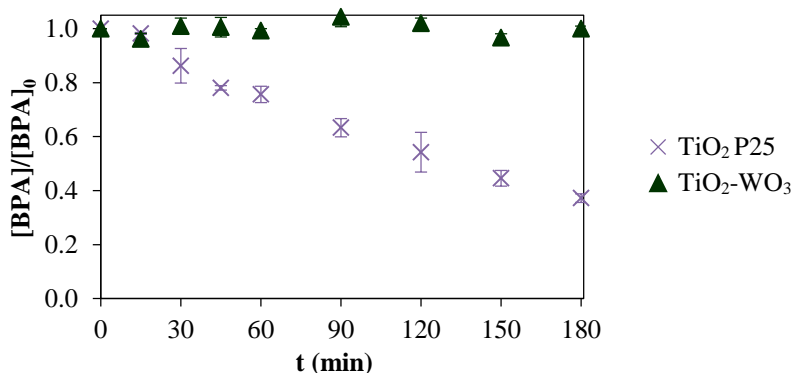


Fig. 3.10. Photocatalytic removal of BPA in wastewater with time in photoreactor 1 (Xe lamp). $[BPA]_0 = 10.0 \text{ mg L}^{-1}$, $[photocatalyst] = 5.00 \cdot 10^{-1} \text{ g L}^{-1}$.

The kinetics of the degradation were also studied for the treatment of the wastewater. In this case, the experimental data using TiO_2 P25 fitted well to a pseudo-first order kinetic model, obtaining a kinetic constant of $5.30 \times 10^{-3} \text{ min}^{-1}$ ($R^2 = 0.992$). Nevertheless, this value was approximately 10-fold smaller than the one got for BPA degradation in UP water.

3.3. Final remarks

A novel magnetically recoverable $\text{Fe}_3\text{O}_4@\text{SiO}_2@\text{TiO}_2$ photocatalyst was synthesized, characterized, and tested for the degradation of BPA under simulated solar light. To compare the obtained results, non-magnetic $\text{TiO}_2\text{-WO}_3$, $\text{Fe}_3\text{O}_4@\text{SiO}_2@\text{TiO}_2$ and pure TiO_2 were also synthesized and the commercial TiO_2 P25 photocatalyst was used.

Their photocatalytic activity was studied for the removal of BPA in UP water and in real wastewater, observing a decrease in the activity of the photocatalysts in the treatment of wastewater due to the high

complexity of its chemical composition. For the two water matrixes studied, TiO₂ P25 showed the best photocatalytic performance compared to the prepared photocatalysts.

A degradation pathway for the photocatalytic degradation of BPA in UP water was proposed. Hence, the identification of the reaction intermediates was performed. Intermediate compounds with one aromatic ring were formed at the beginning of the reaction. In the case of photocatalysis using any of the photocatalysts synthesized in this thesis, 2-(4-hydroxyphenyl)-2-propanol was the only intermediate compound that was identified, while when using TiO₂ P25 the compounds detected were different. In a further stage of the reaction, several organic acids were formed.

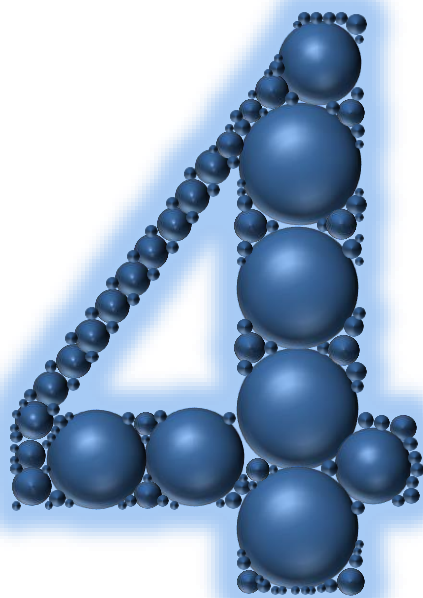
Finally, it has to be remarked that, an efficient and low cost magnetic separation of the photocatalyst results an attractive alternative for the scale-up and industrial implementation of photocatalysis for wastewater treatment. Anyway, further work is still essential to evaluate and increase the photocatalytic activity of the synthesized photocatalysts in order to improve the trade-off between loss of photocatalytic activity and photocatalyst recovery.

3.4. References

- [1] Bai, S., Liu, H., Sun, J., Tian, Y., Chen, S., Song, J., Luo, R., Li, D., Chen, A., Liu, C.C., 2015. Improvement of TiO₂ photocatalytic properties under visible light by WO₃/TiO₂ and MoO₃/TiO₂ composites. *Appl. Surf. Sci.* 338, 61–68.
- [2] Carbajo, J., García-Muñoz, P., Tolosana-Moranchel, A., Faraldos, M., Bahamonde, A., 2014. Effect of water composition on the photocatalytic removal of pesticides with different TiO₂ catalysts. *Environ. Sci. Pollut. Res.* 21, 12233–12240.
- [3] Chi, Y., Yuan, Q., Li, Y., Zhao, L., Li, N., Li, X., Yan, W., 2013. Magnetically separable Fe₃O₄@SiO₂@TiO₂-Ag microspheres with well-designed nanostructure and enhanced photocatalytic activity. *J. Hazard. Mater.* 262, 404–411.
- [4] Da Silva, J.C.C., Teodoro, J.A.R., De Cássia Franco Afonso, R.J., Aquino, S.F., Augusti, R., 2014. Photodegradation of bisphenol A in aqueous medium: monitoring and identification of by-products by liquid chromatography coupled to high-resolution mass spectrometry. *Rapid. Commun. Mass. Spectrom.* 28, 987–994.
- [5] Daghrir, R., Drogui, P., Robert, D., 2013. Modified TiO₂ for environmental photocatalytic applications: a review. *Ind. Eng. Chem. Res.* 52, 3581–3599.
- [6] Ferro Orozco, A.M., Contreras, E.M., Zaritzky, N.E., 2016. Biodegradation of bisphenol A and its metabolic intermediates by activated sludge: stoichiometry and kinetics analysis. *Int. Biodeter. Biodegr.* 106, 1–9.
- [7] Fisli, A., Saridewi, R., Dewi, S.H., Gunlazuardi, J., 2013. Preparation and characterization of Fe₃O₄/TiO₂ composites by heteroagglomeration. *Adv. Mat. Res.* 626, 131–137.

- [8] Jing, J., Li, J., Feng, J., Li, W., Yu, W.W., 2013. Photodegradation of quinoline in water over magnetically separable $\text{Fe}_3\text{O}_4/\text{TiO}_2$ composite photocatalysts. *Chem. Eng. J.* 219, 355–360.
- [9] Lipuma, G., Khor, J.N., Brucato, A., 2004. Modeling of an annular photocatalytic reactor for water purification: oxidation of pesticides. *Environ. Sci. Technol.* 38, 3737–3745.
- [10] Lucas, M.S., Tavares, P.B., Peres, J.A., Faria, J.L., Rocha, M., Pereira, C., Freire, C., 2013. Photocatalytic degradation of Reactive Black 5 with TiO_2 -coated magnetic nanoparticles. *Catal. Today* 209, 116–121.
- [11] Maroga Mboula, V., Héquet, V., Andrés, Y., Pastrana-Martínez, L.M., Doña-Rodríguez, J.M., Silva, A.M.T., Falaras, P., 2013. Photocatalytic degradation of endocrine disruptor compounds under simulated solar light. *Water. Res.* 47, 3997–4005.
- [12] Pelaez, M., De la Cruz, A.A., O'Shea, K., Falaras, P., Dionysiou, D.D., 2011. Effects of water parameters on the degradation of microcystin-LR under visible light-activated TiO_2 photocatalyst, *Water. Res.* 45, 3787–3796.
- [13] Ramos-Delgado, N.A., Gracia-Pinilla, M.A., Maya-Treviño, L., Hinojosa-Reyes, L., Guzman-Mar, J.L., Hernández-Ramírez, A., 2013. Solar photocatalytic activity of TiO_2 modified with WO_3 on the degradation of an organophosphorus pesticide. *J. Hazard. Mater.* 263, 36–44.
- [14] Sharma, J., Mishra, I.M., Kumar, V., 2016. Mechanistic study of photo-oxidation of Bisphenol-A (BPA) with hydrogen peroxide (H_2O_2) and sodium persulfate (SPS). *J. Environ. Manage.* 166, 12–22.

- [15] Sin, J.C., Lam, S.M., Mohamed, A.R., Lee, K.T., 2012. Degrading endocrine disrupting chemicals from wastewater by TiO₂ photocatalysis: a review. *Int. J. Photoenergy* 185159.
- [16] Thiruvengkatachari. R., Kwon, T.O., Moon, I.S., 2005. Application of slurry type photocatalytic oxidation-submerged hollow fiber microfiltration hybrid system for the degradation of bisphenol A (BPA). *Separ. Sci. Technol.* 40, 2871–2888.
- [17] Tsai, W.T., Lee, M.K., Su, T.Y., Chang, Y.M., 2009. Photodegradation of bisphenol-A in a batch TiO₂ suspension reactor. *J. Hazard. Mater.* 168, 269–275.
- [18] Watanabe, N., Horikoshi, S., Kawabe, H., Sugie, Y., Zhao, J., Hidaka, H., 2003. Photodegradation mechanism for bisphenol A at the TiO₂/H₂O interfaces. *Chemosphere* 52, 851–859.
- [19] Ye, M., Zhang, Q., Hu, Y., Ge, J., Lu, Z., He, L., Chen, Z., Yin, Y., 2010. Magnetically recoverable core–shell nanocomposites with enhanced photocatalytic activity. *Chem. Eur. J.* 16, 6243–6250.



PROGRESS ON REACTION

MECHANISMS

Chapter 4

Progress on reaction mechanisms

Abstract

The lack of suitable indexes that permit the comparison of the photocatalytic degradation results obtained in different experimental configurations and designs is one of the principal issues associated to the development of photocatalytic technology. Nevertheless, the rate of hydroxyl radicals ($\cdot\text{OH}$) generation seems to play a key role in the overall oxidation rate in photocatalysis and, thus it can be used for comparison purposes. Hence, the $\cdot\text{OH}$ generated were quantified, following the methodology shown in Chapter 2, and the kinetic modeling for the $\cdot\text{OH}$ generation as a function of the radiation intensity was proposed. Finally, an assessment of the energy efficiency was performed through the parameter electrical energy per order.

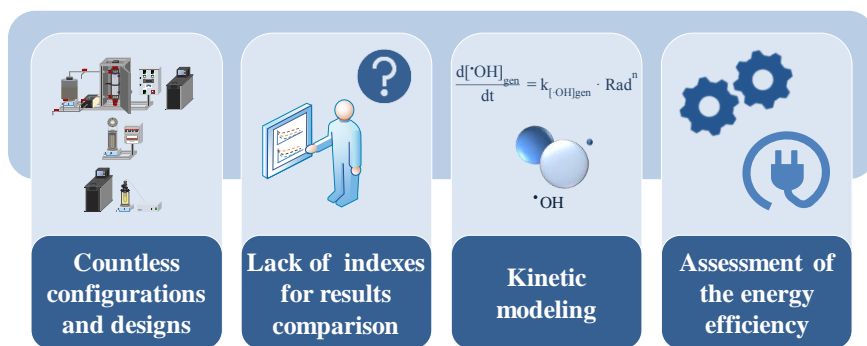


Fig. 4.1. Graphical abstract.

One of the key issues related to the development of photocatalysis is the design of adequate photoreactors with maximum illumination efficiency and minimum mass transfer limitations that allow the scale-up of the technology (Leblebici *et al.*, 2015). With this aim, several designs, such as slurry, annular or immersion photoreactors, have been proposed over the past years (Van Gerven *et al.*, 2007). However, the lack of suitable indexes for the comparison of the results obtained in the countless photoreactor configurations makes difficult the development of the photocatalytic technology. Therefore, contributing to the progress on reaction mechanisms is required to improve this stage.

In this chapter different photoreactor configurations and light sources were employed. The photocatalytic treatment of 50.0 mg L⁻¹ of sodium dodecylbenzenesulfonate (SDBS) in ultrapure (UP) water with titanium dioxide (TiO₂) Aeroxide[®] P25 (Evonik Industries) was performed in the photoreactor 2 (Hg lamp), photoreactor 3 (1st generation light emitting diodes (LEDs)), and photoreactor 4 (upgraded LEDs).

4.1. Hg lamp photoreactor

The photocatalytic degradation of SDBS was studied in photoreactor 2, which is illuminated by an Hg lamp immersed in a quartz sleeve in the center and has a fixed radiation intensity.

4.1.1. Influence of the photocatalyst dosage

The photocatalyst concentration has a strong influence in the overall photocatalytic reaction rate for any photoreactor configuration.

Specifically, it has been previously reported in literature that the overall photocatalytic reaction rate is directly proportional to the TiO_2 concentration up to a certain value known as saturation level (Ab Aziz *et al.*, 2016). Nevertheless, from this value on, due to the increase of the suspension opacity, a light screening effect reduces the penetration of the radiation reaching the surface area of TiO_2 and, thus, the available number of active sites for the photocatalytic process and the overall photocatalytic reaction (Ab Aziz *et al.*, 2016).

To evaluate the influence of the TiO_2 dosage, the initial SDBS was kept constant and the TiO_2 concentration was varied. Fig. 4.2 shows the change of SDBS concentration with time during the photocatalytic treatment. The highest SDBS removal was achieved when using $5.00 \cdot 10^{-1} \text{ g L}^{-1}$ of TiO_2 , reaching its total degradation after 360 min of treatment. However, when the TiO_2 concentration was increased over that value the removal obtained was smaller due to the screening effect previously mentioned.

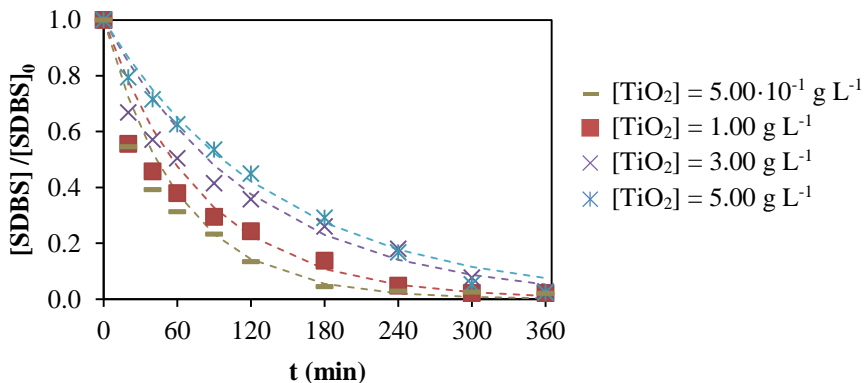


Fig. 4.2. Photocatalytic removal of SDBS in UP water with time in photoreactor 2 (Hg lamp). $[\text{SDBS}]_0 = 50.0 \text{ mg L}^{-1}$. Dash lines: pseudo-first order kinetics.

During the photocatalytic treatment the SDBS can disappear but form other intermediate organic compounds. Thus, it is important to follow its degree of mineralization by means of a global parameter such as dissolved organic carbon (DOC). Fig. 4.3 depicts the DOC change with time for the TiO_2 dosages under study. The results were similar to that obtained for the SDBS removal, showing a screening effect for TiO_2 dosages above 1.00 g L^{-1} . It has to be remarked that, for this amount of photocatalyst, 81.2% of DOC removal was attained after 360 min of treatment.

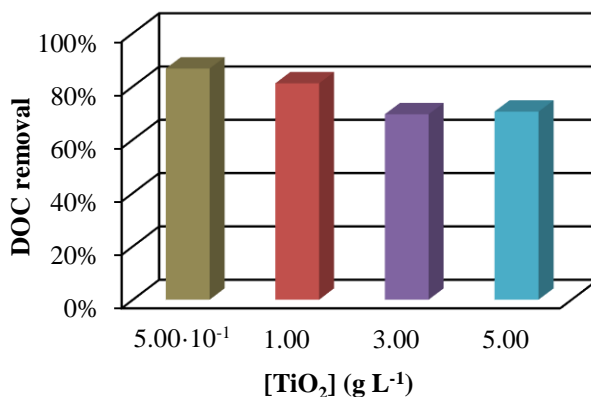


Fig. 4.3. Mineralization of SDBS in UP water after 360 min in photoreactor 2 (Hg lamp). $[\text{SDBS}]_0 = 50.0 \text{ mg L}^{-1}$.

4.1.2. Kinetic modeling

An optimal photocatalytic process design requires the availability of a robust kinetic model and its parameters. Hence, the kinetics of the photocatalytic removal of SDBS were fitted to a pseudo-first order kinetic model (Eq. 4.1).

$$\frac{-d[\text{SDBS}]}{dt} = k_{\text{app}} \cdot [\text{SDBS}] \quad (4.1)$$

where $[\text{SDBS}]$ is the concentration of sodium dodecylbenzenesulfonate (mg L^{-1}), t represents the reaction time (min), and k_{app} symbolizes the pseudo-first order kinetic constant (min^{-1}).

Table 4.1 contains the pseudo-first order kinetic constants obtained by applying a least-squares regression to the experimental data of SDBS concentration. As it can be seen, the removal of SDBS with the different TiO_2 concentrations fitted properly to the pseudo-first order kinetic model, with values of R^2 higher than 0.945. From the values of k_{app} obtained, it can be clearly corroborated that the reaction rate when using $5.00 \cdot 10^{-1} \text{ g L}^{-1}$ of TiO_2 was higher than when using the other dosages. It is remarkable that the value of k_{app} decreased more than 2-fold when the TiO_2 dosage was raised from $5.00 \cdot 10^{-1}$ to 5.00 g L^{-1} .

Table 4.1. Parameters got from the fitting of the experimental data of the SDBS photocatalytic treatment to pseudo-first order kinetics. $[\text{SDBS}]_0 = 50.0 \text{ mg L}^{-1}$.

$[\text{TiO}_2] (\text{g L}^{-1})$	$k_{\text{app}} (\text{min}^{-1})$	R^2
$5.00 \cdot 10^{-1}$	$1.62 \cdot 10^{-2}$	0.967
1.00	$1.24 \cdot 10^{-2}$	0.946
3.00	$8.17 \cdot 10^{-3}$	0.945
5.00	$7.20 \cdot 10^{-3}$	0.990

Although this photoreactor resulted adequate to attain the total removal of SDBS and a high degree of mineralization, especially when using low photocatalyst dosages, it was not able to evaluate the influence of the radiation intensity since it only allowed to work at a fixed intensity. Then, another set-up that allowed to modify the radiation intensity was required.

4.2. 1st generation light emitting diodes photoreactor

The photocatalytic degradation of SDBS was also evaluated in photoreactor 3. In this configuration 1st generation LEDs placed surrounding the reactor, which allowed to study the influence of the radiation intensity, were used as source of light.

The hydroxyl radicals ($\cdot\text{OH}$) generation rate is a key factor to determine the overall photocatalytic oxidation rate and compare the results obtained. Therefore, for a better understanding of the process, the quantitative determination of the hydroxyl radicals generated ($\cdot\text{OH}_{\text{gen}}$) results essential. Their quantification was performed following the methodology proposed by Tai *et al.* (2004) and described in Chapter 2.

4.2.1. Influence of the photocatalyst dosage

The influence of the TiO_2 concentration on the hydroxyl radicals generated ($[\cdot\text{OH}]_{\text{gen}}$) for a fixed value of radiation was evaluated. As it can be seen in Fig 4.3, for a given photocatalyst concentration, the $[\cdot\text{OH}]_{\text{gen}}$ evolved linearly with time, which was also observed by Schwarz *et al.* (1997). When the photocatalyst dosage was varied, the $[\cdot\text{OH}]_{\text{gen}}$ increased with TiO_2 dosage owing to the rise in the number of accessible active sites at the surface of the photocatalyst. Nonetheless, since an excess of photocatalyst could enhance the growing of the suspension opacity and the reduction of light penetration, the increase in the $\cdot\text{OH}$ generation was less pronounced for TiO_2 concentrations above 1.00 g L^{-1} . The highest $[\cdot\text{OH}]_{\text{gen}}$, 9.51 mg L^{-1} , was obtained for 2.00 g L^{-1} of TiO_2 after 180 min of treatment.

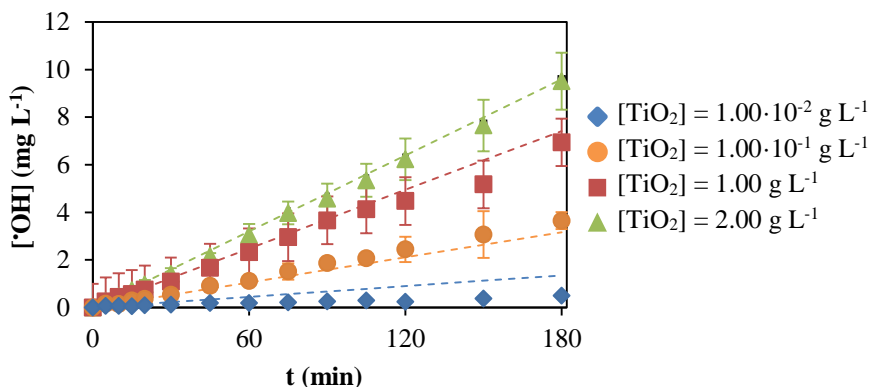


Fig. 4.4. Photocatalytic generation of $\cdot\text{OH}$ in UP water with time in photoreactor 3 (1st generation LEDs). $[\text{SDBS}]_0 = 50.0 \text{ mg L}^{-1}$, $\text{Rad} = 2.40 \cdot 10^{-2} \text{ mW cm}^{-2}$. Dash lines: proposed kinetics.

The influence of the photocatalyst dosage on the SDBS removal can be observed in Fig. 4.5. Higher SDBS removals were attained with an increment in the TiO_2 concentration. Thus, the highest removal of SDBS, 30.7%, was obtained for 2.00 g L^{-1} of TiO_2 after 180 min of treatment. It is remarkable that this removal was near 3-fold smaller than the one achieved in the photoreactor 2 (Hg lamp) with $5.00 \cdot 10^{-1} \text{ g L}^{-1}$ of TiO_2 after 180 min of treatment.

The mineralization attained was quantified through the determination of DOC (Fig. 4.6). For all the photocatalyst dosages used but for 2.00 g L^{-1} , its values were within 15.0% of the initial one. Thus, it was considered that most of the intermediate products that could be formed during the photocatalytic process remained in the oxidation medium at the same time that SDBS disappeared and that the $\cdot\text{OH}$ generated mainly attacked the SDBS.

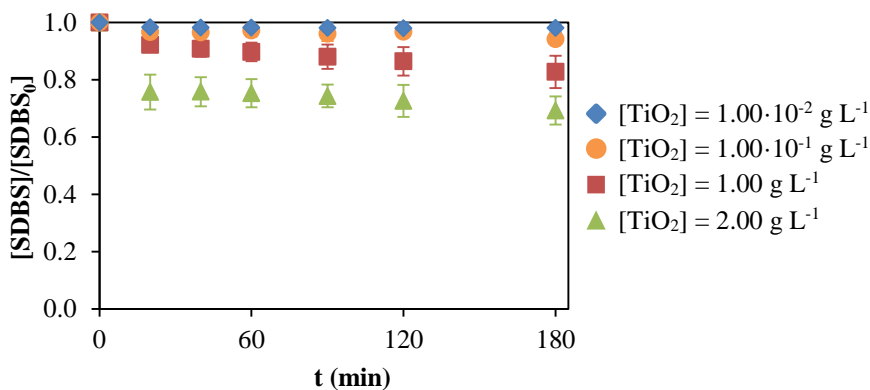


Fig. 4.5. Photocatalytic removal of SDBS in UP water with time in photoreactor 3 (1st generation LEDs). $[\text{SDBS}]_0 = 50.0 \text{ mg L}^{-1}$, $\text{Rad} = 2.40 \cdot 10^{-2} \text{ mW cm}^{-2}$.

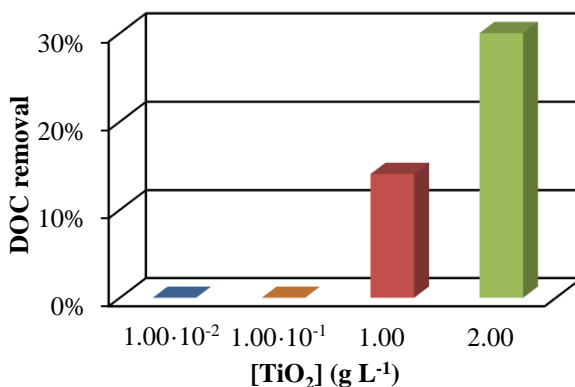


Fig. 4.6. Mineralization of SDBS in UP water after 180 min in photoreactor 3 (1st generation LEDs). $[\text{SDBS}]_0 = 50.0 \text{ mg L}^{-1}$, $\text{Rad} = 2.40 \cdot 10^{-2} \text{ mW cm}^{-2}$.

It is worth noticing that the screening effect observed in photoreactor 2 (Hg lamp) was not observed in this case, implying that the configuration of the photoreactor had a remarkable influence in the photocatalytic process.

4.2.2. Influence of the radiation intensity

In order to maximize the light efficiency and minimize the energy consumption, photoreactor 3 design, which had 1st generation LEDs, allowed to work with different radiation intensities (Rad).

The influence of the radiation intensity was evaluated for a fixed TiO₂ dosage of 1.00 g L⁻¹. Fig. 4.7 shows that, for all the Rad applied, the [·OH]_{gen} increased linearly with reaction time, which was also reported in literature (Schwarz *et al.*, 1997). The highest concentration of ·OH generated, 6.94 mg L⁻¹, was reached for the highest intensity applied, 2.40·10⁻² mW cm⁻². Furthermore, it can be checked that, for a fixed treatment time, [·OH]_{gen} increased linearly with Rad. This behavior was observed up to a value of 1.80·10⁻³ mW cm⁻² and then it remained almost constant for higher values.

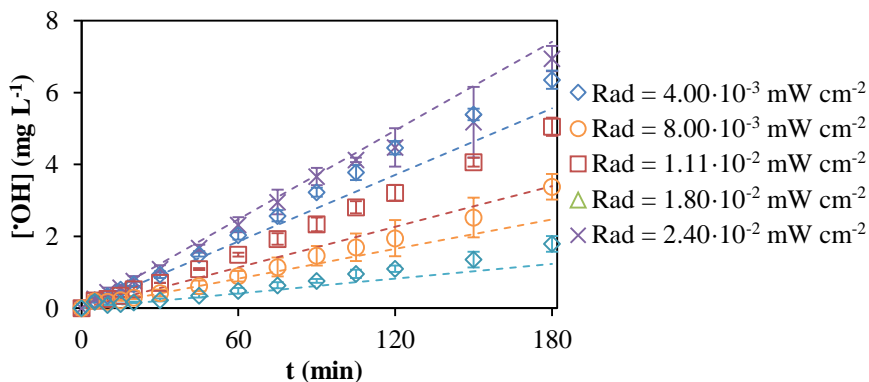


Fig. 4.7. Photocatalytic generation of ·OH in UP water with time in photoreactor 3 (1st generation LEDs). [SDBS]₀ = 50.0 mg L⁻¹, [TiO₂] = 1.00 g L⁻¹. Dash lines: proposed kinetics.

Fig. 4.8 shows that the influence of the radiation intensity applied on the SDBS degradation rate in this case was small due to the narrow range of radiation intensities used. However, for a fixed treatment time, higher SDBS removals were accomplished when the light intensity increased. Hence, the highest SDBS removal, which was 17.2% after 180 min, was achieved when working at $2.40 \cdot 10^{-2} \text{ mW cm}^{-2}$.

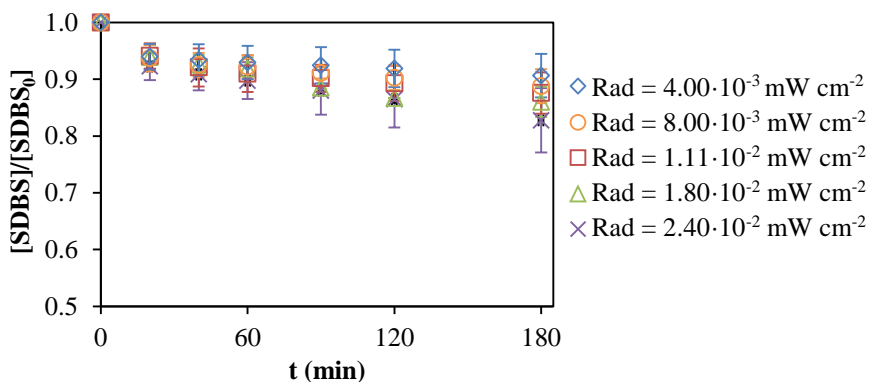


Fig. 4.8. Photocatalytic removal of SDBS in UP water with time in photoreactor 3 (1st generation LEDs). $[\text{SDBS}]_0 = 50.0 \text{ mg L}^{-1}$, $[\text{TiO}_2] = 1.00 \text{ g L}^{-1}$.

The mineralization of SDBS is shown in Fig. 4.9. For all the radiation intensities used, DOC values were within 15.0% of the initial one. Therefore, it was assumed that the $\cdot\text{OH}$ generated mainly attacked the SDBS. Taking this into account, the removal of SDBS could be directly correlated to the radiation intensity and, thus, to the $\cdot\text{OH}$ generated.

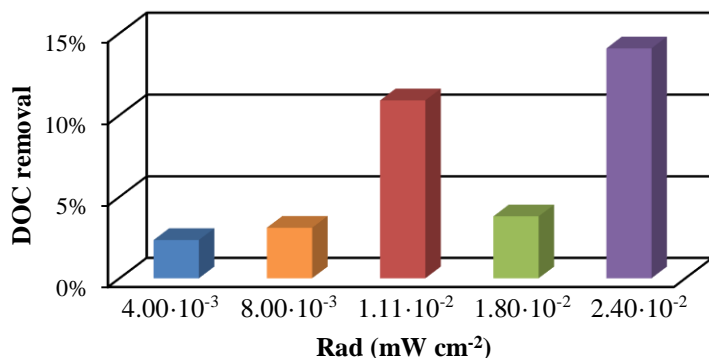


Fig. 4.9. Mineralization of SDBS in UP water after 180 min in photoreactor 3 (1st generation LEDs). $[\text{SDBS}]_0 = 50.0 \text{ mg L}^{-1}$, $[\text{TiO}_2] = 1.00 \text{ g L}^{-1}$.

Hence, using the data from Fig. 4.7 and Fig. 4.8, a correlation for the concentration of SDBS removed, ($[\text{SDBS}]_{\text{rem}}$), at defined treatment times as a function of the $[\cdot\text{OH}]_{\text{gen}}$ (for the same times) could be established (Fig. 4.10). It can be observed that the influence of both variables was lumped in the $[\cdot\text{OH}]_{\text{gen}}$, concluding that this variable represented a suitable index to describe properly the kinetics of photocatalytic processes.

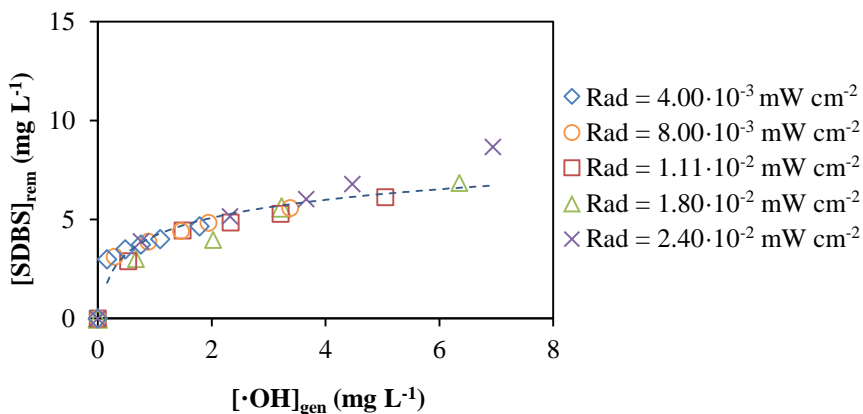


Fig. 4.10. SDBS removed vs. $\cdot\text{OH}$ generated in photoreactor 3 (1st generation LEDs) after 180 min of treatment. $[\text{SDBS}]_0 = 50.0 \text{ mg L}^{-1}$, $[\text{TiO}_2] = 1.00 \text{ g L}^{-1}$.

4.2.3. Kinetic modeling

The availability of robust kinetic models including specific parameters related to the radiation is fundamental to the photocatalysis optimization. Therefore, the development of a kinetic model for the $\cdot\text{OH}$ generation including the influence of the radiation intensity was proposed next (Eq. 4.2). This model described the $\cdot\text{OH}$ generation considering not only the influence of the radiation intensity but also the photocatalyst dosage.

$$\frac{d[\cdot\text{OH}]_{\text{gen}}}{dt} = k_{[\cdot\text{OH}]_{\text{gen}}} \cdot [\text{TiO}_2]^m \cdot \text{Rad}^n \quad (4.2)$$

where $[\cdot\text{OH}]_{\text{gen}}$ is the concentration of $\cdot\text{OH}$ generated (mg L^{-1}), t represents the reaction time (min), $k_{[\cdot\text{OH}]_{\text{gen}}}$ symbolizes the kinetic constant ($\text{mg L}^{-1} \cdot\text{OH cm}^{2n} \text{min}^{-1} \text{mW}^{-n} \text{mg L}^{-1} \text{TiO}_2^{-m}$), $[\text{TiO}_2]$ denotes the photocatalyst dosage (mg L^{-1}), m and n depict experimental fitted parameters (-), and Rad designates the radiation applied (mW cm^{-2}).

The kinetic parameters, $k_{[\cdot\text{OH}]_{\text{gen}}} = 1.72 \text{ mg L}^{-1} \cdot\text{OH cm}^2 \text{min}^{-1} \text{mW}^{-1} \text{mg L}^{-1} \text{TiO}_2^{-0.370}$, $m = 0.370$ and $n = 1.00$, were obtained from regression of the experimental data to Eq. 4.2 using the Excel tool Solver. Including these values in Eq. 4.2, the generation of hydroxyl radicals can be described by Eq. 4.3.

$$\frac{d[\cdot\text{OH}]_{\text{gen}}}{dt} = 1.72 \cdot [\text{TiO}_2]^{0.370} \cdot \text{Rad}^{1.00} \quad (4.3)$$

The relationship between the measured and simulated $\cdot\text{OH}$ data is shown in Fig. 4.11 by means of a parity graph. The $\cdot\text{OH}$ generation was adequately described by the proposed model, with 68.0% of the simulated results falling within the interval $[\cdot\text{OH}]_{\text{gen}} \pm 15.0\% [\cdot\text{OH}]_{\text{gen}}$.

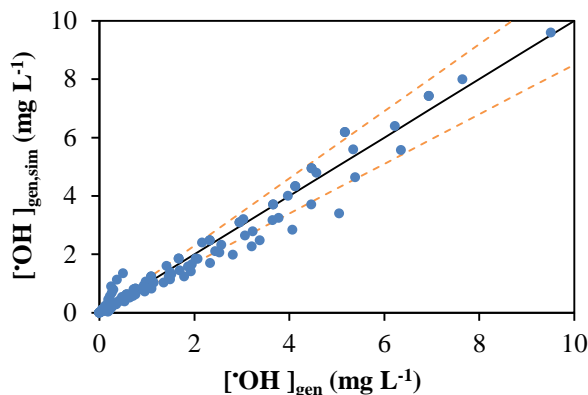


Fig. 4.11. Fitting of the experimental $[\text{OH}]_{\text{gen}}$ data in photoreactor 3 (1st generation LEDs) to the kinetic model proposed by Eq. 4.3. $[\text{SDBS}]_0 = 50.0 \text{ mg L}^{-1}$, $[\text{TiO}_2] = 1.00 \cdot 10^{-2} - 2.00 \text{ g L}^{-1}$, $\text{Rad} = 4.00 \cdot 10^{-3} - 2.40 \cdot 10^{-2} \text{ mW cm}^{-2}$.

It is well established that, depending on the radiation intensity applied, photocatalytic reactions mostly occur in three different kinetic regimes (Domènech *et al.*, 2004; Tanveer and Guyer, 2013; Xiang *et al.*, 2011; Yu *et al.*, 2007). The first one is for low radiation intensities and appears when the consumption of the electron-hole pairs (e^-/h^+) generated is faster than their recombination. Within this regime, there is a linear relationship between the radiation intensity and the reaction rate of the photocatalytic reaction (Yu *et al.*, 2007). Daneshvar *et al.* (2004) and Wang *et al.* (2011) found this regime for values below 1.00 mW cm^{-2} . At higher intensities, there is a second regime where the recombination of the e^-/h^+ generated is the dominant stage and the photocatalytic reaction rate depends on the square root of the radiation intensity (Daneshvar *et al.* 2004; Domènech *et al.*, 2004). Li *et al.* (2008) and Meng *et al.* (2002) detected this behavior up to values of 60.0 mW cm^{-2} . The last regime can be found working at higher intensities where there is no further generation of e^-/h^+ . Here, the reaction rate is limited only by the mass transfer rate and does not depend on the radiation intensity (Daneshvar *et al.* 2004; Domènech *et al.*, 2004).

The model proposed for the generation of hydroxyl radicals corroborated that the 1st generation light emitting diodes only allowed to work in the first regime for low radiation intensities. Thus, this system provided information regarding the reaction mechanisms for a low range of radiation intensity and small amount of $\cdot\text{OH}$ generated. However, this configuration did not result adequate for the SDBS removal since low removals of SDBS and DOC were attained.

4.3. Upgraded light emitting diodes photoreactor

Since the available range of radiation intensities when working with the 1st generation LEDs was narrow, it did not allow to evaluate properly the influence of the radiation intensity in the photocatalytic process. Hence, upgraded LEDs were used in photoreactor 4, which had a tubular configuration, in order to study the influence of the radiation intensity in a wider range.

4.3.1. Influence of the radiation intensity

The concentration of $\cdot\text{OH}$ generated was quantified for different radiation intensities and a fixed TiO_2 concentration of 1.00 g L^{-1} (Fig. 4.12). There was a linear increase with the treatment time, confirming the behavior also observed in photoreactor 3 (1st generation LEDs). Moreover, the $[\cdot\text{OH}]_{\text{gen}}$ rose with the radiation applied, obtaining a maximum of 158 mg L^{-1} for 27.5 mW cm^{-2} . It is remarkable that for a fixed time of 180 min, the highest $[\cdot\text{OH}]_{\text{gen}}$ obtained for this Rad was 70.9 mg L^{-1} , being this value near 10-fold than the highest $[\cdot\text{OH}]_{\text{gen}}$ attained in the photoreactor 3 (1st generation LEDs) for the same TiO_2 dosage and treatment time.

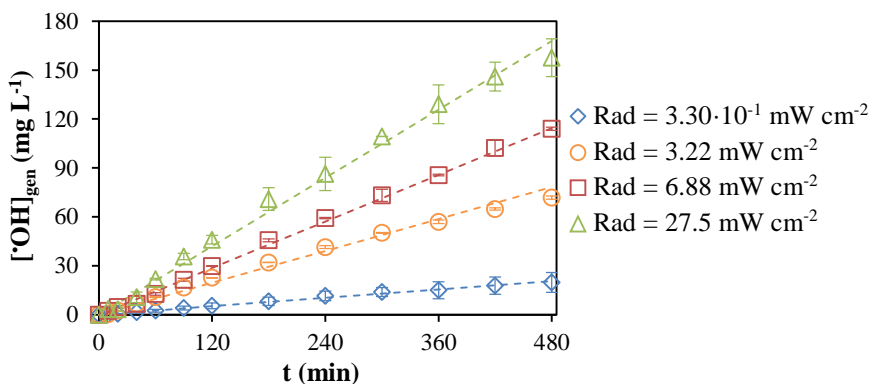


Fig. 4.12. Photocatalytic generation of $\cdot\text{OH}$ in UP water with time in photoreactor 4 (upgraded LEDs). $[\text{SDBS}]_0 = 50.0 \text{ mg L}^{-1}$, $[\text{TiO}_2] = 1.00 \text{ g L}^{-1}$. Dash lines: proposed kinetics.

Fig. 4.13 shows the photocatalytic removal of SDBS in photoreactor 4 (upgraded LEDs) when different radiation intensities were applied. It can be appreciated that its degradation was small for the lowest intensity applied, $3.30 \cdot 10^{-1} \text{ mW} \cdot \text{cm}^{-2}$, eliminating only 12.1% after 480 min of treatment. Nevertheless, an increase in the radiation intensity led to higher degradations, attaining the highest SDBS removal, 93.5%, with $27.5 \text{ mW} \cdot \text{cm}^{-2}$. For this radiation, the SDBS removal achieved after 180 min of treatment was 52.0%, which was about 3-fold higher than the highest removal obtained working with the same TiO_2 concentration in photoreactor 3 (1st generation LEDs) after the same treatment time.

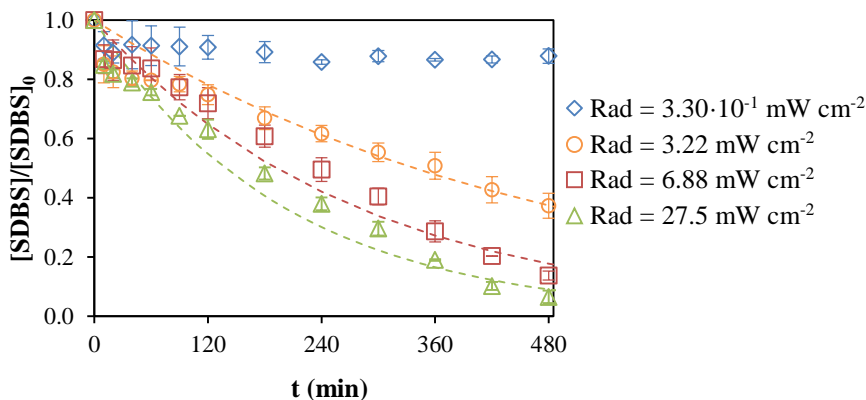


Fig. 4.13. Photocatalytic removal of SDBS in UP water with time in photoreactor 4 (upgraded LEDs). $[SDBS]_0 = 50.0 \text{ mg L}^{-1}$, $[TiO_2] = 1.00 \text{ g L}^{-1}$. Dash lines: pseudo-first kinetics.

The mineralization of SDBS is depicted in Fig. 4.14. The maximum DOC removal, 39.8%, was obtained for the highest radiation intensity, 27.5 mW cm^{-2} . Then, the mineralization attained with this photoreactor was higher than with photoreactor 3 (1st generation LEDs).

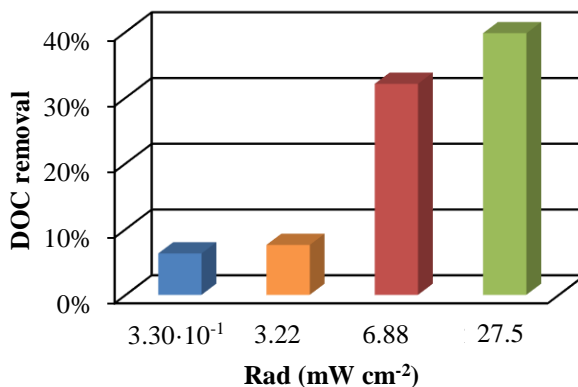


Fig. 4.14. Mineralization of SDBS in UP water after 480 min in photoreactor 4 (upgraded LEDs). $[SDBS]_0 = 50.0 \text{ mg L}^{-1}$, $[TiO_2] = 1.00 \text{ g L}^{-1}$.

4.3.2. Kinetic modeling

The kinetics of the SDBS removal were also described by the pseudo-first order kinetic model proposed in Eq. 4.1, except when the radiation was too low. As it can be seen in Fig. 4.12, the fitting of the model was appropriate for all the radiation intensity. Table 4.2 contains the kinetic parameters obtained. It can be observed that the k_{app} increased more than 2-fold for an increment in the Rad from 3.22 to 27.5 $\text{mW}\cdot\text{cm}^{-2}$.

Table 4.2. Parameters obtained from the fitting of the experimental data of the SDBS photocatalytic treatment to a pseudo-first order kinetic model.

$[\text{SDBS}]_0 = 50.0 \text{ mg L}^{-1}$, $[\text{TiO}_2] = 1.00 \text{ g L}^{-1}$.

Rad (mW cm^{-2})	k_{app} (min^{-1})	R^2
3.22	$2.05 \cdot 10^{-3}$	0.934
6.88	$3.61 \cdot 10^{-3}$	0.961
27.5	$5.00 \cdot 10^{-3}$	0.959

As it was previously stated in section 4.2.3, it is known that the photocatalytic process can occur in three different kinetic regimes depending on the radiation intensity applied. In order to show these regimes, a kinetic model to relate the radiation intensities to the concentration of $\cdot\text{OH}$ generated was desired for photoreactor 4 (upgraded LEDs). Then, for the estimation of the $[\cdot\text{OH}]_{gen}$, following the methodology used to get Eq. 4.2, Eq. 4.4 was obtained. Therefore, the estimation of the corresponding $k_{[\cdot\text{OH}]_{gen}}$ was performed with the Excel tool Solver, obtaining Eq. 4.5, Eq. 4.6, and Eq. 4.7.

$$\frac{d[\cdot\text{OH}]_{\text{gen}}}{dt} = k_{[\cdot\text{OH}]_{\text{gen}}} \cdot \text{Rad}^n \quad (4.4)$$

where $[\cdot\text{OH}]_{\text{gen}}$ is the concentration of $\cdot\text{OH}$ generated (mg L^{-1}), t represents the reaction time (min), $k_{[\cdot\text{OH}]_{\text{gen}}}$ symbolizes the kinetic constant ($\text{mg L}^{-1} \cdot \text{OH cm}^{2n} \text{ min}^{-1} \text{ mW}^{-n} \text{ mg L}^{-1}$), n denotes an experimental fitted parameter (-), and Rad depicts the radiation applied (mW cm^{-2}).

$$\frac{d[\cdot\text{OH}]_{\text{gen}}}{dt} = 1.30 \cdot 10^{-1} \cdot \text{Rad}^{1.00} \quad (\text{Rad} \leq 3.30 \cdot 10^{-1} \text{ mW cm}^{-2}) \quad (4.5)$$

$$\frac{d[\cdot\text{OH}]_{\text{gen}}}{dt} = 9.08 \cdot 10^{-2} \cdot \text{Rad}^{0.500} \quad (\text{Rad} = 3.30 \cdot 10^{-1} - 15.0 \text{ mW cm}^{-2}) \quad (4.6)$$

$$\frac{d[\cdot\text{OH}]_{\text{gen}}}{dt} = 3.50 \cdot 10^{-1} \cdot \text{Rad}^0 \quad (\text{Rad} \geq 15.0 \text{ mW cm}^{-2}) \quad (4.7)$$

Eq. 4.5 demonstrates that for radiation intensities below $3.30 \cdot 10^{-1} \text{ mW} \cdot \text{cm}^{-2}$, the $\cdot\text{OH}$ generation reaction rate depended linearly on the radiation intensity. For values between $3.30 \cdot 10^{-1}$ and $15.0 \text{ mW} \cdot \text{cm}^{-2}$, Eq. 4.6 shows that the reaction rate depended on the square root of the radiation intensity. Finally, for intensities above $15.0 \text{ mW} \cdot \text{cm}^{-2}$, Eq. 4.7 confirms that the $\cdot\text{OH}$ generation was independent of the radiation intensity applied. Representing the rate of $\cdot\text{OH}$ generation ($r_{[\cdot\text{OH}]_{\text{gen}}}$) vs. the radiation intensities (Fig. 4.15), these trends could be appreciated, confirming that photoreactor 4 (upgraded LEDs) showed the three existing kinetic regimes for photocatalysis.

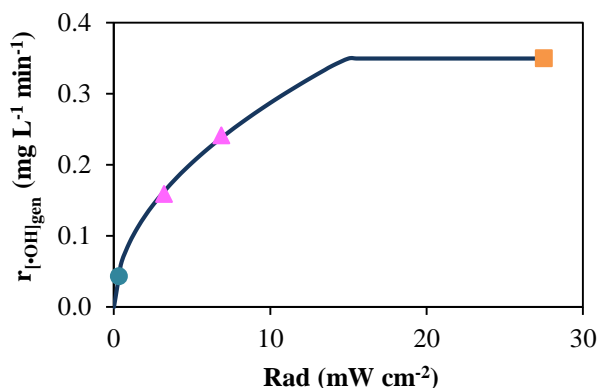


Fig. 4.15. $\cdot\text{OH}$ generation reaction rate versus the radiation intensity in photoreactor 4 (upgraded LEDs). $[\text{SDBS}]_0 = 50.0 \text{ mg L}^{-1}$, $[\text{TiO}_2] = 1.00 \text{ g L}^{-1}$, $\text{Rad} = 3.30 \cdot 10^{-1} - 27.5 \text{ mW} \cdot \text{cm}^{-2}$.

Furthermore, the model proposed allowed to determine the lowest intensity that would have to be applied to achieve the highest $r_{[\cdot\text{OH}]_{\text{gen}}}$, $15.0 \text{ mW} \cdot \text{cm}^{-2}$. Thus, it contributed to the optimization of photocatalysis as a function of the radiation intensity applied. Nevertheless, it is remarkable that the value obtained did not automatically represent the energy optimum for the SDBS removal. In spite of the $\cdot\text{OH}$ generation rate would diminish and the reaction time would growth, the energy consumption of the treatment could be smaller using lower radiation intensities. Hence, a parameter that considers both, the energy required and the kinetics, was evaluated in the following section to contribute to a better understanding of photocatalysis and, therefore, to the design of photocatalytic reactors.

There was a satisfactory fitting of the simulated results obtained by the kinetic model proposed to the experimental results for the three regions, with 92.0% of the simulated results falling within the interval $[\cdot\text{OH}]_{\text{gen}} \pm 15.0\% \cdot [\cdot\text{OH}]_{\text{gen}}$, as it can be observed in the parity graph shown in Fig. 4.16.

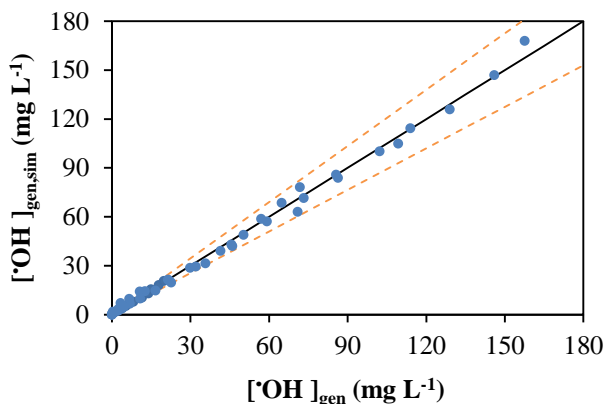


Fig. 4.16. Fitting of the experimental $[\cdot\text{OH}]_{\text{gen}}$ data in photoreactor 4 (upgraded LEDs) to the kinetic model proposed by Eq. 4.5, Eq. 4.6, and Eq. 4.7.
 $[\text{SDBS}]_0 = 50.0 \text{ mg L}^{-1}$, $[\text{TiO}_2] = 1.00 \text{ g L}^{-1}$, $\text{Rad} = 3.30 \cdot 10^{-1} - 27.5 \text{ mW cm}^{-2}$.

It is remarkable that photoreactor 4 (upgraded LEDs) obtained higher removal and mineralization of SDBS and allowed to evaluate the influence of the radiation intensity in a wider range than photoreactor 3 (1st generation LEDs). However, since the removal and mineralization attained were still smaller than in photoreactor 2 (Hg lamp), a study considering the energy required and the kinetics became crucial to select the optimum configuration for the development of an adequate photocatalytic process.

4.4. Assessment of the energy efficiency

Since the photocatalytic overall reaction rate depends on the radiation intensity, the optimization of the radiation intensity and, therefore, of the energy intake results crucial for an adequate photoreactor design. Nonetheless, energy optimization remains as one of the main challenges for the industrial implementation of photocatalysis.

The average radiation intensity quantified for photoreactor 3 (1st generation LEDs) and photoreactor 4 (upgraded LEDs) as a function of the electric power (P_{el}) is shown in Fig. 4.17. It is observed that for the same electricity intake upgraded LEDs were more efficient than the 1st generation ones. For instance, for 10 W, photoreactor 3 emitted almost $4.00 \text{ mW}\cdot\text{cm}^{-2}$ while photoreactor 4 decreased the emission to $2.00\cdot 10^{-2} \text{ mW}\cdot\text{cm}^{-2}$. However, since photoreactor 2 (Hg lamp) had a fixed electricity demand (150 W) and emitted only one fixed Rad, a specific parameter that allows the comparison of the energy intake of the systems was required.

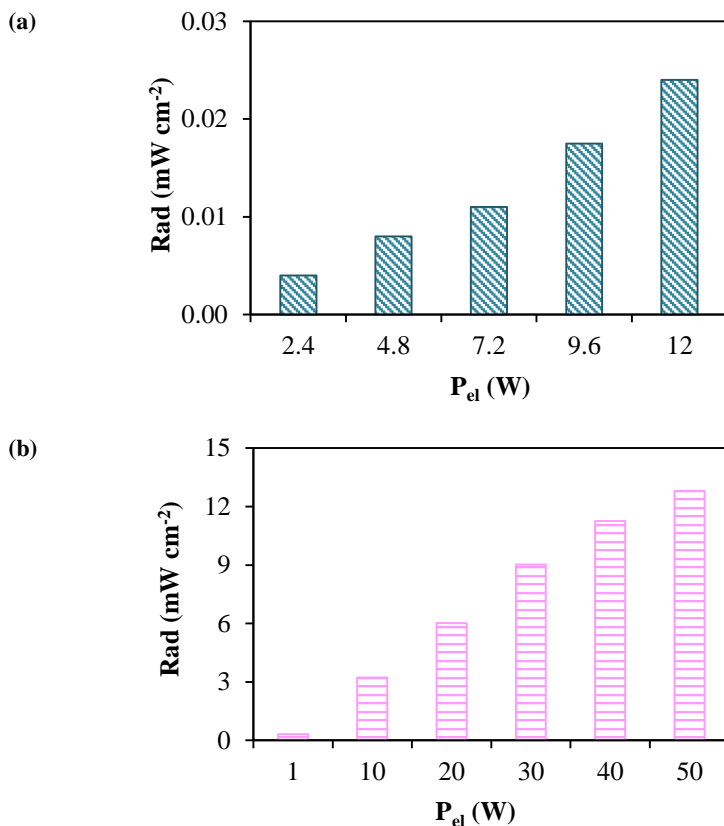


Fig. 4.17. Relationship between the electric power and the radiation intensity in (a) photoreactor 3 (1st generation LEDs) and (b) photoreactor 4 (upgraded LEDs).

Bolton *et al.* (1996) defined a parameter named electrical energy per order (E_{EO}) with the purpose of comparing the energy intake of different water treatment processes. As shown in Eq. 4.8, the E_{EO} denotes the electrical energy necessary to degrade a contaminant with low initial concentration by one order of magnitude (90.0%) in a fixed volume of wastewater.

$$E_{EO} = \frac{P_{el} \cdot t}{V \cdot \lg\left(\frac{c_i}{c_f}\right)} = \frac{P_{el} \cdot t}{V \cdot 4.34 \cdot 10^{-1} \cdot \ln\left(\frac{c_i}{c_f}\right)} \quad (4.8)$$

where P_{el} is the electric power (kW), t represents the time (h), V symbolizes the reaction volume (m^3), \lg denotes the decadic logarithm, \ln depicts the natural logarithm, and c_i and c_f designate the initial and final compound concentrations, respectively ($mg L^{-1}$).

The E_{EO} allows the comparison of the electrical efficiency independently of the system under investigation (Arslan-Alaton *et al.*, 2002; Bolton *et al.*, 1996). Moreover, since smaller values of E_{EO} indicate higher efficiency, this parameter can be particularly helpful in the optimization of the photocatalytic treatment of wastewater by helping to minimize the costs related to energy consumption.

Since the photocatalytic SDBS degradation could be described by the pseudo-first order kinetic expression showed in Eq. 4.1, when the radiation intensity was high enough, substituting the pseudo-first order kinetic constant into Eq. 4.8 the expression depicted in Eq. 4.9 was obtained, which allowed the estimation of the electricity demanded by the light source to remove the 90.0% of SDBS.

$$E_{EO} = \frac{P_{el}}{V \cdot 4.34 \cdot 10^{-1} \cdot k \cdot 60.0} = \frac{P_{el} \cdot 3.84 \cdot 10^{-2}}{V \cdot k} \quad (4.9)$$

where P_{el} is the electric power (kW), V represents the reaction volume (m^3), and k symbolizes the pseudo-first order kinetic constant (min^{-1}).

The results obtained are summarized in Table 4.3. In the case of photoreactor 2, since the Hg lamp had only one fixed radiation intensity, only one E_{EO} was estimated. Although the kinetics were faster than for the other photoreactors, the k_{app} was about 13-fold higher than in photoreactor 3 (1st generation LEDs) and 2-fold higher than in photoreactor 4 (upgraded LEDs), the E_{EO} was high, $595 \text{ kW h m}^{-3} \text{ order}^{-1}$, due to the high electricity requirement of the Hg lamp (150 W).

For photoreactor 3, in spite of the 1st generation LEDs had several radiation intensities available, only one E_{EO} was considered. This was because the working intensities were so low that the SDBS removal could not be properly fitted to a pseudo-first kinetic model and, hence, the E_{EO} could not be calculated for the smaller radiation intensities used. Although the power consumed with the 1st generation LED was low, 11.9 W, it showed the highest E_{EO} value, $640 \text{ kW h m}^{-3} \text{ order}^{-1}$. This was because the k_{app} was extremely low and, therefore, the time required for the SDBS removal was considerably long.

Photoreactor 4 (upgraded LEDs) had several E_{EO} because the upgraded LEDs could work at different radiation intensities. The E_{EO} obtained for $3.22 \text{ mW} \cdot \text{cm}^{-2}$ was $47.5 \text{ kW} \cdot \text{h} \cdot \text{m}^{-3} \cdot \text{order}^{-1}$, resulting the optimal working radiation from an energetic point of view. For higher radiations, due to the increase of the electricity demand of LEDs, the E_{EO} increased, being 67.5 and $196 \text{ kW} \cdot \text{h} \cdot \text{m}^{-3} \cdot \text{order}^{-1}$ for 6.88 and $27.5 \text{ mW} \cdot \text{cm}^{-2}$, respectively.

Table 4.3. Design parameters and E_{EO} values for all the photoreactors.

$[SDBS]_0 = 50.0 \text{ mg L}^{-1}$, $[TiO_2] = 1.00 \text{ g L}^{-1}$.

Photoreactor	Rad (mW cm^{-2})	k_{app} (min^{-1})	R^2	E_{EO} ($\text{kW h m}^{-3} \text{ order}^{-1}$)
2 (Hg lamp)	281	$1.24 \cdot 10^{-2}$	0.946	595
3 (1 st generation LEDs)	$2.40 \cdot 10^{-2}$	$9.22 \cdot 10^{-4}$	0.922	640
	3.22	$2.05 \cdot 10^{-3}$	0.934	47.5
4 (upgraded LEDs)	6.88	$3.61 \cdot 10^{-3}$	0.961	67.5
	27.5	$5.00 \cdot 10^{-3}$	0.959	196

Photoreactor 4 (upgraded LEDs) showed the lowest energy consumption among the three alternatives studied. If its optimum E_{EO} , $47.5 \text{ kW} \cdot \text{h} \cdot \text{m}^{-3} \cdot \text{order}^{-1}$, is compared with literature values, upgraded LEDs have high competitiveness as light source in terms of energy. For instance, Urkude *et al.* (2004) obtained an E_{EO} of $80.0 \text{ kW} \cdot \text{h} \cdot \text{m}^{-3} \cdot \text{order}^{-1}$ for the photocatalytic removal of 1.39 mg L^{-1} of 4-nitrophenol with 1.00 g L^{-1} of a TiO_2 -polyaniline composite and a 40.0 W commercial lamp. E_{EO} values of 790, 1500, and $3000 \text{ kW} \cdot \text{h} \cdot \text{m}^{-3} \cdot \text{order}^{-1}$ were reported by Natarajan *et al.* (2011) for the degradation of malachite green, rhodamine B, and methylene blue dyes, respectively, using a photoreactor based on UV-LEDs and TiO_2 coated quartz tube. Ung-Meding *et al.* (2017) found E_{EO} values between 17.1 and $111 \text{ kW} \cdot \text{h} \cdot \text{m}^{-3} \cdot \text{order}^{-1}$ for the degradation of the acid blue 9 dye working at different temperatures and employing 1.00 g L^{-1} of TiO_2 P25 and a 8.00 W blacklight blue lamp.

Considering that the electricity price for industrial consumers in Europe is $1.19 \cdot 10^{-1} \text{ €}$ per each kWh (European Commission, 2017), the cost attributed to energy consumed by the light source for attaining a 90.0% SDBS removal in this photoreactor was 5.65 € m^{-3} . Although this cost is slightly higher than the cost of conventional treatments, it should be highlighted that SDBS cannot be degraded by those treatments.

The kinetics of SDBS degradation obtained for the three photoreactors when working with the radiation intensity that allowed to achieve the energy optimum and the same TiO_2 dosage, 1.00 g L^{-1} , are shown in Fig. 4.18. When using photoreactor 2 (Hg lamp), complete SDBS removal was obtained after 360 min of treatment, while when using the photoreactors with LEDs, longer times were required for attaining lower SDBS degradations. With photoreactor 3 (1st generation LEDs), only 33.9% of SDBS was removed after 600 min of reaction working with a radiation intensity of $2.40 \cdot 10^{-2} \text{ mW cm}^{-2}$, while with photoreactor 4 (upgraded LEDs) the removal increased up to 62.7% after 480 min of treatment. Thus, it can be concluded that, although the degradation kinetics were faster in the photoreactor 2 (Hg lamp) than in photoreactor 4 (upgraded LEDs), the best alternative for the photocatalytic treatment of SBDS among the configurations studied was photoreactor 4 (upgraded LEDs), since it was the most efficient process from a kinetic and energy consumption coupled point of view.

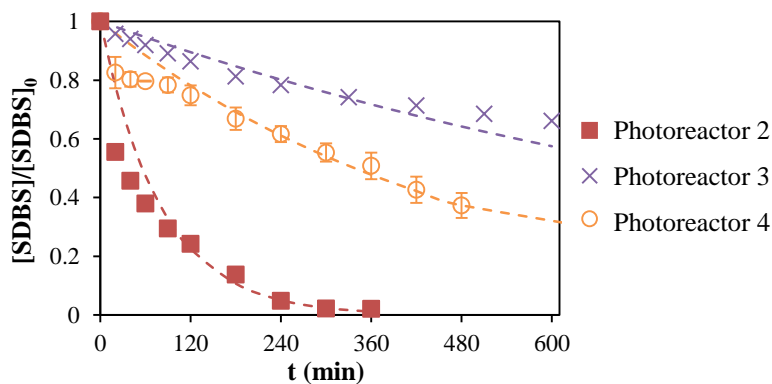


Fig. 4.18. Photocatalytic removal of SDBS in UP water with time.
 $[\text{SDBS}]_0 = 50.0 \text{ mg L}^{-1}$, $[\text{TiO}_2] = 1.00 \text{ g L}^{-1}$. Dash lines: pseudo-first kinetics.

4.5. Final remarks

The viability of using several light sources and photoreactor configurations for the photocatalytic degradation of SDBS was shown. Photoreactor 2 (Hg lamp) provided high removal and mineralization rates of SDBS, however, it only permitted operation at fixed radiation intensity. Hence, LEDs resulted a promising alternative to promote the development of the photocatalytic process via the design of photoreactors of adjustable radiation intensity.

For both LEDs configurations, the $\cdot\text{OH}$ generated were quantified and related to the radiation intensity applied. Therefore, two satisfactory kinetic models were proposed as a function of the applied radiation intensity. Although kinetic models for photocatalysis including the radiation intensity have already been proposed in literature, a unified kinetic model has not been concluded yet. Thus, this thesis contributes to the state of the art by proposing a methodology for kinetic models that consider the $\cdot\text{OH}$ generated. It is worth noticing that photoreactor 4 (upgraded LEDs) allowed the change of radiation intensity in a wider range than photoreactor 3 (1st generation LEDs), permitting to accomplish higher removal and mineralization of SDBS.

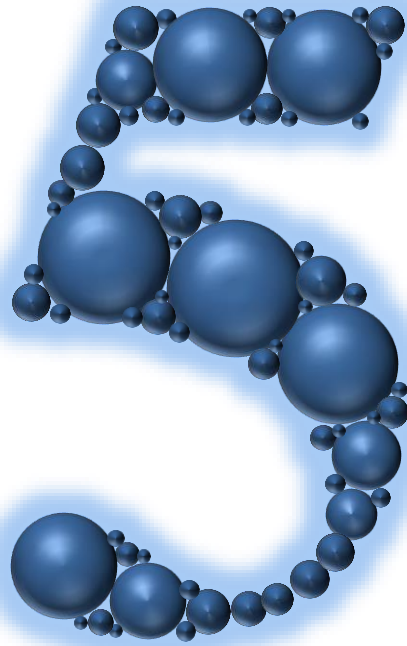
Finally, a study for the SDBS photocatalytic removal considering both energy consumption and kinetics was performed by estimating the electrical energy per order. Photoreactor 4 (upgraded LEDs) showed the minimum value of this parameter. Hence, it can be concluded that, although photoreactor 2 (Hg lamp) resulted the best alternative from a kinetic point of view, photoreactor 4 (upgraded LEDs) resulted the best global option from a kinetic and energy consumption coupled perspective.

4.6. References

- [1] Ab Aziz, N.A., Palaniandy, P., Abdul Aziz, H., Dahlan, I., 2016. Review of the mechanism and operational factors influencing the degradation process of contaminants in heterogenous photocatalysis. *J. Chem. Res.* 40, 704–712.
- [2] Arslan-Alaton, I.A., Balcioglu, I.A., Bahnemann, D.W., 2002. Advanced oxidation of a reactive dyebath effluent: comparison of O₃, H₂O₂/UV-C and TiO₂/UV-A processes. *Water Res.* 36, 1143–1154.
- [3] Bolton, J.R., Bircher, K.G., Tumas, W., Tolman, C.A., 1996. Figures-of-merit for the technical development and application of advanced oxidation processes. *J. Adv. Oxid. Technol.* 1, 13–17.
- [4] Daneshvar, N., Rabbani, M., Modirshahla, N., Behnajady, M.A., 2004. Kinetic modeling of photocatalytic degradation of Acid Red 27 in UV/TiO₂ process. *J. Photochem. Photobiol. A* 168, 39–45.
- [5] Domènech, X., Jardim, W.F., Litter, M.I., 2004. Procesos avanzados de oxidación para la eliminación de contaminantes. Eliminación de contaminantes por fotocátalisis heterogénea, 3–26. Blesa, M. A., Sánchez, B., CIEMAT, Madrid, Spain.
- [6] European Commission 2017. http://ec.europa.eu/eurostat/statistics-explained/index.php/Energy_price_statistics (accessed 10.09.2017).
- [7] Leblebici, M.E., Stefanidis, G.D., Van Gerven, T., 2015. Comparison of photocatalytic space-time yields of 12 reactor designs for wastewater treatment. *Chem. Eng. Process.* 97, 106–111.
- [8] Li, Y., Sun, S., Ma, M., Ouyang, Y., Yan, W., 2008. Kinetic study and model of the photocatalytic degradation of rhodamine B (RhB) by a TiO₂-coated activated carbon catalyst: effects of initial RhB

- content, light intensity and TiO₂ content in the catalyst. *Chem. Eng. J.* 142, 147–155.
- [9] Meng, Y., Huang, X., Wu, Y., Wang, X., Qian, Y., 2002. Kinetic study and modeling on photocatalytic degradation of parachlorobenzoate at different light intensities. *Environ. Pollut.* 117, 307–313.
- [10] Natarajan, K., Natarajan, T.S., Bajaj, H.C., Tayade, R.J., 2011. Photocatalytic reactor based on UV-LED/TiO₂ coated quartz tube for degradation of dyes. *Chem. Eng. J.* 178, 40–49.
- [11] Schwarz, P.F., Turro, N.J., Bossmann, S.H., Braun, A.M., Abdel Wahaband, A.M.A., Dürr, H., 1997. *J. Phys. Chem. B* 101, 7127–7134.
- [12] Tai, C., Peng, J., Liu, J., Jiang, G., Zou, H., 2004. Determination of hydroxyl radicals in advanced oxidation processes with dimethyl sulfoxide trapping and liquid chromatography. *Anal. Chim. Acta* 527, 73–80.
- [13] Tanveer, M., Guyer, G.T., 2013. Solar assisted photo degradation of wastewater by compound parabolic collectors: review of design and operational parameters. *Renew. Sust. Energ. Rev.* 24, 534–543.
- [14] Ung-Medina, F., Caudillo-Flores, U., Correa-González, J.C., Maya-Yescas, R., Chávez-Parga, Ma. del C., Cortés, J.A., 2017. Use of an annular non-sleeve photoreactor for photocatalytic dye degradation: study of temperature and light intensity effects. *Environ. Prog. Sustain.* 36(4), 1083–1088.
- [15] Urkude, K., Thakare, S.R., Gawande, S., 2014. An energy efficient photocatalytic reduction of 4-nitrophenol. *J. Environ. Chem. Eng.* 2, 759–764.

- [16] Van Gerven, T., Mul, G., Moulijn, J., Stankiewicz, A., 2007. A review of intensification of photocatalytic processes. *Chem. Eng. Process.* 46,781–789
- [17] Wang, Z., Liu, J., Dai, Y., Dong, W., Zhang, S., Chen, J., 2011. Dimethyl sulfide photocatalytic degradation in a light-emitting-diode continuous reactor: kinetic and mechanistic study. *Ind. Eng. Chem. Res.* 50, 7977–7984.
- [18] Xiang, Q., Jiaguo, Y., Wong, P.K., 2011. Quantitative characterization of hydroxyl radicals produced by various photocatalysts. *J. Colloid Interf. Sci.* 357, 163–167.
- [19] Yu, H., Zhang, K., Rossi, C., 2007. Theoretical study on photocatalytic oxidation of VOCs using nano-TiO₂ photocatalyst. *J. Photochem. Photobiol. A* 188, 65–73.



ENVIRONMENTAL ASSESSMENT

Chapter 5

Environmental assessment

Abstract

For the final implementation of the photocatalysis, the application should consider not only the degradation and mineralization achieved during the treatment but also the environmental impacts generated. Thus, a complete environmental assessment by means of the life cycle assessment (LCA) tool was performed for the photocatalytic treatment of greywater generated in a hotel laundry facility. Additionally, the LCA results were compared to those attained with two alternative treatments i) photovoltaic solar-driven photocatalysis and ii) membrane biological reactor.

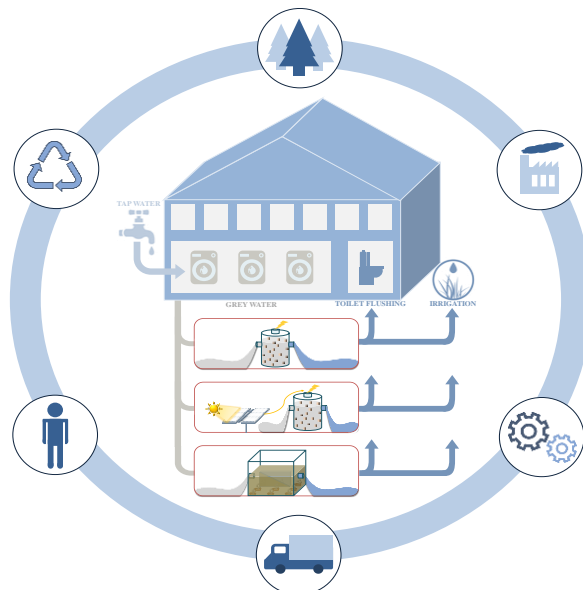


Fig. 5.1. Graphical abstract.

For the scale-up and industrial implementation of the photocatalysis it is necessary to perform a complete environmental assessment. In this sense, the life cycle assessment (LCA) approach appears as a robust tool to define, evaluate, quantify, and reduce the potential impacts of the lifecycle stages of this technology. Furthermore, LCA provides an appropriate framework to allow the identification of the main hot-spots of photocatalysis.

Under water scarcity circumstances, one attractive alternative for the sustainable management of water within a water circular economy restorative thinking framework is the possible treatment and on-site recycling of wastewater. The Spanish law regulates the reuse of treated wastewater for several applications, such as car and window washing, irrigation, laundry or toilet flushing (Real Decreto 1620/2007, 2007).

The reuse of greywater, a domestic wastewater originated in hand basins, kitchen sinks, showers, and washing machines, appears as a promising option in hotel facilities, households, and sport centers (Gabarró *et al.*, 2013; Sanchez *et al.*, 2010). Hence, the LCA of the photocatalytic treatment of greywater generated in a hotel laundry was performed. The aim of the greywater treatment proposed was to allow its reuse on-site for toilet flushing in the hotel rooms and garden irrigation. According to the Spanish law (Real Decreto 1620/2007, 2007), the recycling of treated wastewater for these purposes is included within the category “residential reuse”, that should meet certain quality parameters regarding intestinal nematodes, *Escherichia coli*, suspended solids, and turbidity. However, it was assumed that these requirements were met with the treatment proposed and, therefore, considering the current concern about the presence of emerging pollutants, the scale-up of the treatment was made considering

sodium dodecylbenzenesulfonate (SDBS) as target pollutant. Moreover, this contaminant is a key component in hotel laundry greywater due to its presence in detergents, and it is accompanied of high persistence in the environment, as a result of its low biodegradability.

Thus, the functional unit selected was defined fixing the same greywater treated volume and the same amount of SDBS removed. In order to specify the amount of SDBS that was removed, a minimum threshold that should be accomplished by the scenarios under study had to be selected (Muñoz *et al.*, 2005). Hence, 1.00 m³ of treated greywater with 90.0% reduction of the SDBS initial concentration was established as the functional unit and all the energy and mass flows was referred to this unit. A similar functional unit, considering the same treated water volume and the same pollutant removal, has been previously reported in literature. Muñoz *et al.* (2005) defined the removal of 15.0% DOC from 1.00 m³ kraft pulp mill wastewater as functional unit. In the study conducted by Serra *et al.* (2011) the removal of 93.0% TOC from 250 mL of water with 500 mg L⁻¹ of α -methyl-phenylglycine was established as functional unit.

LCA was applied using the Environmental Sustainability Assessment methodology developed by Irabien *et al.* (2009) and carried out according to the requirements of the ISO 14040 and ISO 14044 international standards (ISO, 2006a; ISO, 2006b). The LCA software GaBi 6.0 and the database of PE International (PE International, 2016) were used. The following stages were applied: definition of the goal and scope of the study, development of the life cycle inventory (LCI), which collected data regarding the energy and mass flows and recorded in separate unit processes the most important input and output data for the scenarios under study, life cycle impact assessment (LCIA), and results analysis. The

assessment in this thesis was carried out following the ‘cradle to gate’ pathway, taking into account the extraction, production, and transportation of the raw materials, the greywater treatment, and the management of the waste generated during all processes.

The two main indicators considered were natural resources (NRs) and environmental burdens (EBs), which were based on the environmental sustainability metrics established by the Institution of Chemical Engineers (IChemE, 2002). The consumption of energy ($X_{1,1}$), materials ($X_{1,2}$), and water ($X_{1,3}$) were considered within the NRs. The EBs included the primary burdens to air ($X_{2,1}$), water ($X_{2,2}$), and land ($X_{2,3}$) and were organized in 12 impact categories. For the atmospheric burdens, the categories were atmospheric acidification (AA), global warming (GW), human health effects (HHE), photochemical ozone formation (POF), and stratospheric ozone depletion (SOD). For water burdens, the categories were aquatic acidification (AqA), aquatic oxygen demand (AOD), ecotoxicity to aquatic life (metals to seawater) (MEco), ecotoxicity to aquatic life (other substances) (NMEco), and eutrophication (EU) (García *et al.*, 2013). The impact categories within the land burdens were given by the quantity of hazardous and non-hazardous waste generated (Margallo *et al.*, 2014a). Nonetheless, they were not considered in this study because the amount of waste generated was minimal and because its management was included in the assessment.

Since the indicators employed had different units depending on the environmental impact category considered, to conduct a comparison in a common basis a normalization process to obtain dimensionless impacts indicators was proposed (Garcia-Herrero *et al.*, 2017a). Therefore, the normalization of both kind of indicators was performed. As it can be seen

observed in Eq. 5.1, in the case of the NRs it was done regarding the natural resource that had the highest impact, while Eq. 5.2 shows that the EBs were normalized considering the threshold values specified in the European Pollutant Release and Transfer Register (E-PRTR, 2006).

$$X_{1,i}^* = \frac{X_{1,i}}{X_{1,i}^{\text{ref}}} \quad (5.1)$$

$$X_{2,j,k}^* = \frac{X_{2,j,k}}{X_{2,j,k}^{\text{ref}}} \quad (5.2)$$

where “i” represents the NRs indicators (energy, materials, and water), “j” is the environmental compartments (air, water, and land), and “k” symbolizes the environmental impacts to the corresponding compartment.

Therefore, $X_{1,i}$ denotes the consumption of each NRs, $X_{1,i}^*$ depicts the normalized $X_{1,i}$, $X_{1,i}^{\text{ref}}$ designates the reference NR, $X_{2,j,k}$ represents the EBs to the corresponding compartment, $X_{2,j,k}^*$ is the normalized $X_{2,j,k}$, and $X_{2,j,k}^{\text{ref}}$ symbolizes the reference environmental burden.

After the normalization stage an additional weighting procedure was also developed to rank the impact categories considering their relative importance (EC JCR, 2010). Thus, the normalized NRs and EBs were aggregated according to Eq. 5.3 and Eq. 5.4.

$$X_1 = \sum_{i=1}^{i=n} \alpha_{1,i} \cdot X_{1,i}^* \quad n \in [1, 3] \quad (5.3)$$

$$X_{2,j} = \sum_{k=1}^{k=m} \beta_{2,j,k} \cdot X_{2,j,k}^* \quad m \in [1, 5] \text{ if } 1 \leq j \leq 2 \wedge m \in [1, 2] \text{ if } j = 3 \quad (5.4)$$

where $\alpha_{1,i}$ is the weighting factor for the NRs and $\beta_{2,j,k}$ represents the one for the EBs.

It was assumed that the three natural resources were equally important, then $\alpha_{1,i}$ resulted 1/3 for each i . This assumption was taken as it was the best option for obtaining a single indicator that allows the comparison of the scenarios evaluated (Margallo *et al.*, 2014a).

5.1. Life cycle assessment of two photocatalytic alternatives for the treatment of greywater

To study the influence of using renewable energy, two photocatalytic scenarios were considered, photocatalysis (Sc. 1) and photovoltaic solar-driven photocatalysis (Sc. 2). It is remarkable that a solar-driven photocatalysis scenario would be desirable, however, it was not considered because several barriers have to be overcome for its full implementation (Spasiano *et al.*, 2015). The most important are that the sunlight reaching the Earth's surface is not homogeneous, the TiO_2 is only active in the ultraviolet region and large land areas are necessary for the treatment (Muñoz *et al.*, 2006; Spasiano *et al.*, 2015).

Data from laboratory experiments with 50.0 mg L⁻¹ of SDBS and 1.00 g L⁻¹ of titanium dioxide (TiO₂) Aeroxide® P25 (Evonik Industries) in the photoreactor 4 (upgraded light emitting diodes (LEDs)) were considered to obtain information for the process scale-up for both scenarios (Fig. 5.2). For the Sc. 2 it had to be considered that each kind of photovoltaic panels, which were made with different materials and had distinct processing requirements, led to different emission profiles. Hence, a global average share of different photovoltaic panels was contemplated: mono-silicon (47.7%), multi-silicon (38.3%), cadmium-telluride (6.40%), amorphous-silicon (5.10%), ribbon-silicon (1.50%), and copper-indium-gallium-diselenide (1.00%).

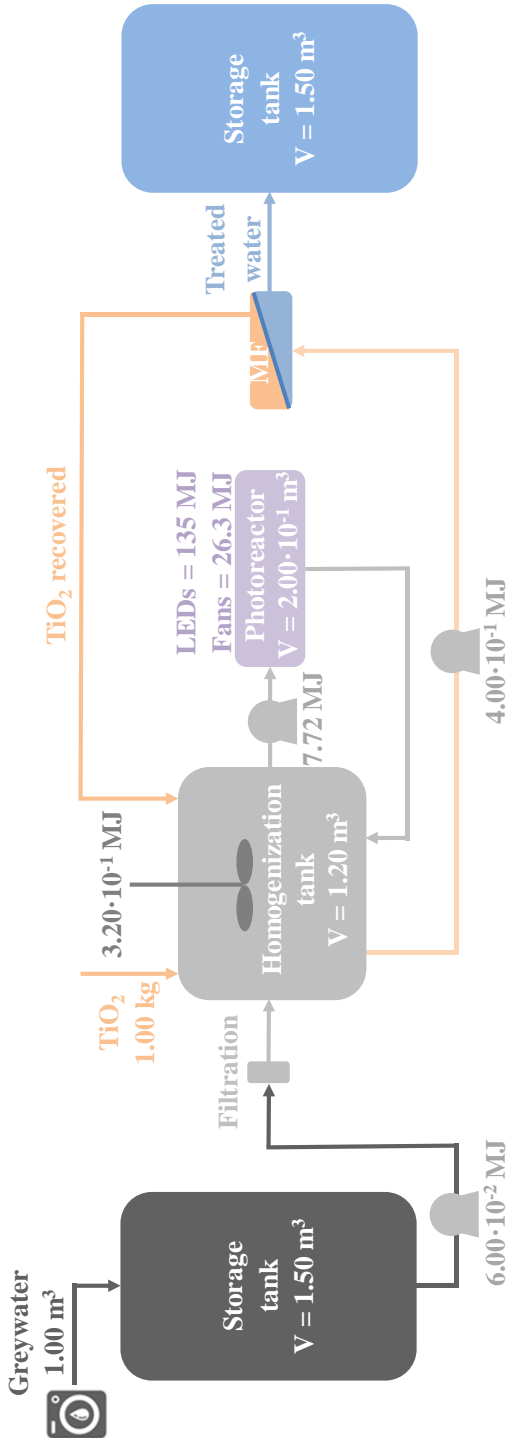


Fig. 5.2. Scale-up of the photocatalytic treatment for 1.00 m³ of hotel laundry greywater.

The main hypothesis assumed in the LCA can be summarized as follows:

- For process scale-up, estimation of energy consumption, reagents expenditure, and waste generation, both scenarios were assumed to be implemented in the facilities of a hotel laundry in Santander (Cantabria, Spain) to treat greywater with 50.0 mg L⁻¹ of SDBS.
- It was supposed that the hotel had a capacity of 75 guests, each one produced 1.00 kg of laundry per day (2 bed sheets, 1 pillow slip and 1 towel), and 13.0 L of fresh water were required per kg of laundry in the washing process (Filimonau *et al.*, 2011; Máša *et al.*, 2013).
- The photocatalytic treatment worked in batch mode during 20.6 h each day and all the year round. This time was calculated from extrapolation of the results previously obtained at laboratory scale in Chapter 4.
- The energy used in Sc. 1 was delivered by the Spanish grid of 2016.
- Sc. 2 employed the energy taken from photovoltaic solar panels.
- The electricity consumption was calculated taking into account the time required to remove 90.0% of the initial SDBS concentration, which in this case was 19.5 h for both scenarios. Furthermore, an extra time of 30.0 min was considered for dark adsorption of the photocatalyst, 9.00 min for pumping the greywater to the system and 1.00 h for pumping the treated water during the TiO₂ separation step.
- A photocatalyst recovery stage by means of microfiltration membranes was considered (Rivero *et al.*, 2006), assuming that the

TiO₂ was totally recovered and that it could be reused ten times in a closed cycle (Muñoz *et al.*, 2006).

- It was considered that waste TiO₂ was disposed of in landfill, being transported 32.8 km by a Euro 4 truck with a maximum total capacity of 28.0 tones along.
- The TiO₂ was transported 1596 km from the production plant of Evonik Industries in Frankfurt, Germany, to the hotel facilities in Santander, Spain, by a 28.0 tones Euro 4 truck (Evonik Industries, 2017; Muñoz *et al.*, 2005).
- To simplify the LCA application the infrastructure related to both cases was not considered. The contribution of the infrastructure to the impacts of these kind of processes is generally negligible owing to the long lifetime of the considered installations (Garcia-Herrero *et al.*, 2017a).

Fig. 5.3 shows the flow diagram and the system boundaries considered for both scenarios. The main system flows were the energy input, water input, production of reagents used (extraction of resources, manufacture, and transport), and their outputs to the environment. The boundaries for Sc. 1 and Sc. 2 were the same because the only difference between both scenarios was the method employed to obtain the energy required for the treatment, being the Spanish grid in Sc. 1 and renewable solar energy in Sc. 2.

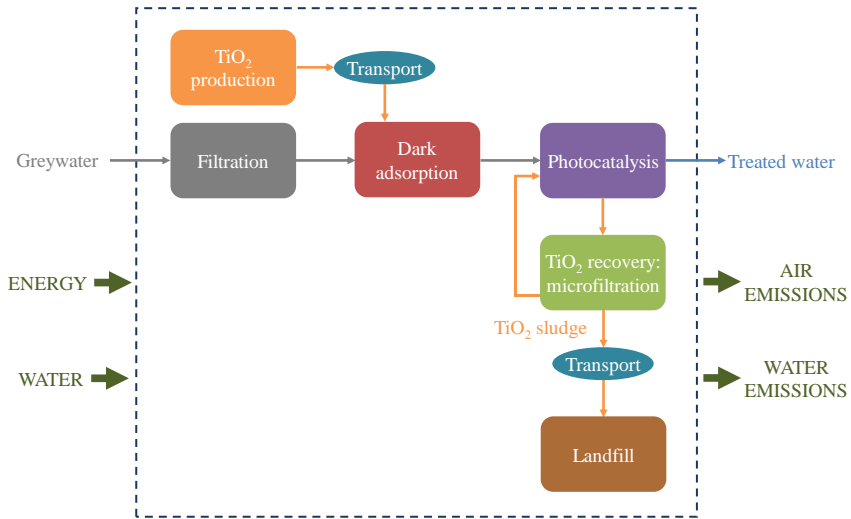


Fig. 5.3. System boundaries for the greywater treatment in Sc. 1 (photocatalysis) and Sc 2. (photovoltaic solar-driven photocatalysis).

The data for the LCI were taken either from experimental results of Chapter 4 or from literature. The sources and quality of the LCI are depicted in Table 5.1, and Table 5.2 shows the LCI data per functional unit. Using these values, the natural resources consumption and the environmental burdens generation associated to both scenarios were estimated.

Table 5.1. Summary of data sources used in the LCI for Sc. 1 (photocatalysis) and Sc. 2 (photovoltaic solar-driven photocatalysis).

Topic	Geographical area	Period	Data source
ENERGY			
Electricity in Sc. 1	Spain	2016	PE database adapted to the characteristics of the Spanish electricity mix of 2016 (PE International, 2016) and extrapolation from experimental data
Electricity in Sc. 2	Spain	2016	PE database (PE International, 2016) and extrapolation from experimental data
REAGENTS			
TiO ₂			Literature (Muñoz, 2003)
Sc. 1	Spain	2016	Extrapolation from experimental data
Sc. 2	Spain	2016	Extrapolation from experimental data
TRANSPORT			
Truck	Europe	2016	PE database (PE International, 2016)
Distances	Europe	2016	Assumptions
END OF LIFE			
Landfilling	Europe	2016	PE database (PE International, 2016)

Table 5.2. LCI for Sc. 1 (photocatalysis) and Sc. 2 (photovoltaic solar-driven photocatalysis).

Input / output data	Unit	Sc. 1 and Sc. 2
INPUTS		
Greywater	m ³	1.00
Reagents		
Cleaning water	m ³ FU ⁻¹	2.00·10 ⁻¹
TiO ₂	kg FU ⁻¹	1.00/10*
Energy		
Aeration	MJ FU ⁻¹	26.3
Light source	MJ FU ⁻¹	135
Pumping	MJ FU ⁻¹	8.17
Stirring	MJ FU ⁻¹	3.20·10 ⁻¹
OUTPUTS		
Exhausted TiO ₂	kg FU ⁻¹	1.00/10*
Treated water (90.0% SDBS removal)	m ³ FU ⁻¹	1.00

* Value divided by 10 because the TiO₂ was used 10 cycles

5.1.1. Estimation of the natural resources consumption

The analysis of the consumption of NRs, including energy, materials, and water, was performed for the two scenarios. The results obtained were normalized using water as reference, which was the natural resource with the highest impact in both scenarios (Table 5.3).

The energy accounted for the consumption of electricity, diesel, natural gas, and steam. Sc. 2 resulted the most energy intensive, being the total energy demand close to 1304 MJ, while in Sc. 1 it was 450 MJ. Table 5.4 shows that the energy consumption demanded by the photocatalytic reaction in Sc. 1 was 99.5% while in Sc. 2 was 99.8%. This behavior was

a result of the intensive energy requirements of the light source employed and represented the principal hot spot of the system. Therefore, the contribution of the cleaning water and the production, transport, consumption, and end of life of the TiO_2 to $X_{1,1}$ were considered negligible in both scenarios.

Table 5.3. Normalized NRs (dimensionless) for Sc. 1 (photocatalysis) and Sc. 2 (photovoltaic solar-driven photocatalysis).

	Sc. 1	Sc. 2
Energy: $X_{1,1}^*$	$4.00 \cdot 10^{-2}$	$1.60 \cdot 10^{-2}$
Materials: $X_{1,2}^*$	$7.40 \cdot 10^{-3}$	$2.90 \cdot 10^{-3}$
Water: $X_{1,3}^*$	1.00	1.00
Total: X_1	$3.50 \cdot 10^{-1}$	$3.90 \cdot 10^{-1}$

Within the materials, TiO_2 was the only element considered for both scenarios. The results showed that the materials associated to the primary energy transformation had the major contribution to $X_{1,2}$. Sc. 2 had lower consumption of material resources, 24.1 kg, than Sc. 1, 77.1 kg, because it used renewable energy and the amount of materials required to produce this kind of energy was smaller. In Sc. 1, the intake of materials during the photocatalytic reaction represented 92.4% of the indicator while the cleaning water and TiO_2 production only had contributions of 6.66% and $7.90 \cdot 10^{-1}\%$, respectively. For Sc. 2, the demand of materials during the photocatalysis decreased to 69.2%, however, the TiO_2 production and the cleaning water increased to 11.0% and 19.5%, respectively. It has to be remarked that it was necessary to assess not only the amount of materials consumed but also the environmental impacts and toxicity of their production and consumption. This point was studied by means of the analysis of the environmental burdens.

Although the intake of water for cleaning and for the reagents production was contained within the indicator $X_{1,3}$, the hot spot in both scenarios was the water needed for the primary energy transformation. According to Table 5.4, this value varied from 96.8% for Sc. 2 to 97.4% for Sc. 1.

Regarding the global consumption of NRs, Sc. 2 showed the highest demand ($X_1 = 3.90 \cdot 10^{-1}$), displaying a value slightly higher than Sc. 1 ($X_1 = 3.50 \cdot 10^{-1}$).

Table 5.4. Contribution of the main stages in Sc. 1 (photocatalysis) and Sc. 2 (photovoltaic solar-driven photocatalysis) to their NRs.

	Contribution to Sc. 1 (%)			Contribution to Sc. 2 (%)		
	Energy	Materials	Water	Energy	Materials	Water
Cleaning water	$2.80 \cdot 10^{-1}$	6.66	2.52	$1.00 \cdot 10^{-1}$	19.5	3.13
Photocatalytic treatment	99.5	92.4	97.4	99.8	69.2	96.8
TiO₂ production	$1.40 \cdot 10^{-1}$	$7.90 \cdot 10^{-1}$	$2.00 \cdot 10^{-2}$	$5.00 \cdot 10^{-2}$	11.0	$3.00 \cdot 10^{-2}$
TiO₂ landfill	$1.00 \cdot 10^{-2}$	$1.00 \cdot 10^{-1}$	$2.00 \cdot 10^{-2}$	0.00	$2.90 \cdot 10^{-1}$	$3.00 \cdot 10^{-2}$
Transport	$3.00 \cdot 10^{-2}$	0.00	$1.00 \cdot 10^{-2}$	$1.00 \cdot 10^{-2}$	$1.00 \cdot 10^{-2}$	$1.00 \cdot 10^{-2}$

5.1.2. Determination of the environmental burdens

The environmental burdens to air and water were estimated according to the procedure previously explained. It is worth noticing that before the normalization process, global warming had the highest impact in both scenarios. The main cause was the greenhouse gases emitted during the energy production process, the consumption of coke and energy during the reagents production (CH_4 , CO , CO_2 , NO_x , N_2O), consumption of diesel and its production, landfill emissions (NO_x , N_2O), and transport of

reagents and waste. It has to be remarked that in the case of Sc. 1, the electricity grid mix selected had a significant impact on the amount of greenhouse gases emitted and, thus, in the results regarding the energy consumption obtained. Hence, as it was detailed before, the Spanish electricity mix of 2016 was selected for this scenario. The lowest score for the GW was obtained in Sc. 2 (2.14 kg CO₂ eq.) being approximately 6-fold smaller than in Sc. 1 (12.69 kg CO₂ eq.). Regarding the aquatic indicators obtained before the normalization, the EU had the highest impact in the two scenarios owing to the emissions of ammonia, chemical oxygen demand, nitrogen, and phosphate during the energy production.

As it is shown in Table 5.5, the normalization of the EBs was carried out employing the European threshold values (E-PRTR, 2006). In spite of GW had the highest air impact for both scenarios without normalization, the HHE and POF resulted the most important categories among air metrics after the normalization process. This was due to the fact that when GW was referenced to its threshold value ($1.00 \cdot 10^8$ kg CO₂ eq.) the normalized results were reduced by 8 orders of magnitude. Nevertheless, in the case of the normalization of HHE and POF the thresholds used as reference were much lower (1000 kg benzene eq. and 1000 kg. ethylene eq., respectively). For water impacts, there were no substantial differences before and after the normalization procedure because the threshold values were lower than those for the air metrics. All the indicators of the EBs to water were slightly smaller in Sc. 2 than in Sc. 1.

Table 5.5. EBs dimensionless variables for Sc. 1 (photocatalysis) and Sc. 2 (photovoltaic solar-driven photocatalysis).

Environmental burden	Unit	Threshold values		
		(kg year ⁻¹) (E-PRTR, 2006)	Sc. 1	Sc. 2
To air: X*_{2,1}			6.50·10⁻⁶	1.89·10⁻⁵
AA: X* _{2,1,1}	kg SO ₂ eq.	150000	2.94·10 ⁻⁷	3.01·10 ⁻⁸
GW: X* _{2,1,2}	kg CO ₂ eq.	100000000	1.27·10 ⁻⁷	2.14·10 ⁻⁸
HHE: X* _{2,1,3}	kg benzene eq.	1000	1.52·10 ⁻⁶	1.81·10 ⁻⁵
POF: X* _{2,1,4}	kg ethylene eq.	1000	4.55·10 ⁻⁶	6.79·10 ⁻⁷
SOD: X* _{2,1,5}	kg CFC-11eq.	1.00	7.64·10 ⁻⁹	5.36·10 ⁻¹⁰
To water: X*_{2,2}			8.74·10⁻⁸	1.46·10⁻⁸
AOD: X* _{2,2,1}	kg O ₂ eq.	50000	1.92·10 ⁻¹⁰	1.24·10 ⁻¹⁰
AqA: X* _{2,2,2}	kg H ⁺ eq.	100	7.92·10 ⁻¹¹	1.10·10 ⁻⁹
MEco: X* _{2,2,3,1}	kg Cu eq.	50.0	4.45·10 ⁻⁹	3.19·10 ⁻⁹
NMEco: X* _{2,2,3,2}	kg formaldehyde eq.	50.0	1.39·10 ⁻⁹	1.04·10 ⁻⁹
EU: X* _{2,2,4}	kg phosphate eq.	5000	8.12·10 ⁻⁸	9.15·10 ⁻⁹

The EBs to air in Sc. 2 were smaller than Sc. 1 for all the indicators with the exception of the HHE. This high contribution to human toxicity in Sc. 2 came mainly from the extraction of raw materials and the production of components necessary for the photovoltaic solar panels fabrication. For example, during the development of the copper part of cables, electric components, and electronic devices, the toxicity comes from the mining and processing of the raw metal, particularly due to the disposal of sulfidic ore tailings (Corona *et al.*, 2017). It is remarkable that, although Sc. 2 had the lowest values for all the air metrics but the human toxicity, this indicator made Sc. 2 the one with the highest X*_{2,1}. However,

over the last few years the development of new photovoltaic panels that do not require toxic elements like cadmium has been evaluated and their use in the future might reduce the influence of the HHE in the photovoltaic solar-driven photocatalysis scenario, making it an extremely attractive option for the treatment of greywater. Furthermore, since LEDs technology is evolving fast (Song *et al.*, 2016), the change to most energy efficient LEDs with the same intensity of radiation but less electricity demand seems feasible. Therefore, an extraordinary environmental progress of the photocatalytic treatments proposed seems feasible in the following years. Regarding EBs to water, it could be observed that all the indicators, excluding the AqA, were slightly smaller in Sc. 2 than in Sc. 1.

5.2. Comparison to the alternative treatment of greywater with a membrane biological reactor

To confirm whether photocatalysis is a sustainable technology for greywater treatment, it is important to consider the technologies that can potentially be competitive. The use of membrane biological reactors (MBR), which combine activated sludge biological treatment with membrane filtration, is a feasible alternative to treat greywater (Fountoulakis *et al.*, 2016; Gander *et al.*, 2000; Merz *et al.*, 2007). This treatment offers high efficiency in surfactants elimination, good effluent quality, high mixed liquor suspended solids concentration, small space requirements and reduced sludge production (Chai *et al.*, 2013; De Gisi *et al.*, 2016; Dhouib *et al.*, 2005). Thus, the environmental assessment of a new scenario including the treatment of greywater with an MBR, Sc. 3, was evaluated using LCA and compared with the results obtained in Sc. 1 and Sc. 2.

Data necessary to scale-up the process (Fig. 5.4), were obtained from literature. The MBR had submerged configuration to decrease energy consumption (Khan *et al.*, 2016). The selected flat sheet ultrafiltration membrane was made of polyethersulfone and had a permeate flux of $19.2 \text{ L m}^{-2} \text{ h}^{-1}$ (Santasmás *et al.*, 2013). It was assumed that the sludge retention time was 35 days (Gori *et al.*, 2010) because high values of this parameter origin endogenous respiration in the biomass dropping the sludge production (Gander *et al.*, 2000). An average mixed liquor total suspended solids of 8.00 g L^{-1} was assumed for the biomass (Gori *et al.*, 2010). The sludge was incinerated and deposited in a municipal landfill, which is one of the most common processes in the wastewater area.

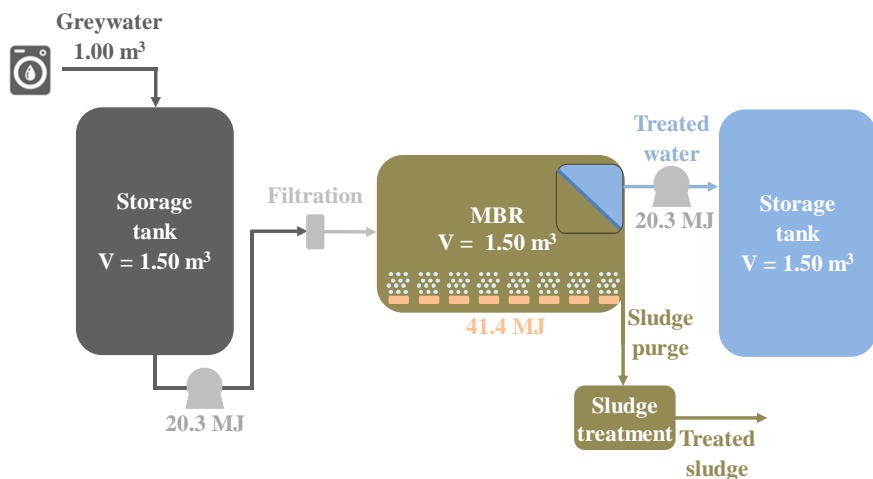


Fig. 5.4. Scale-up of the MBR treatment for 1.00 m^3 of hotel laundry greywater treated.

The main hypothesis that were considered for the LCA are summarized below:

- The treatment was also performed in the facilities of the same hotel that the one for Sc.1 and Sc. 2.
- The MBR worked in a continuous mode, having a hydraulic retention time of 25.6 h (Santasmás *et al.*, 2013).
- The energy employed was delivered by the Spanish grid of 2016.
- The electricity consumption was estimated for the specific time necessary to remove 90.0% of the initial SDBS concentration, being, 25.6 h.
- It was assumed that in the cleaning step of the MBR treatment air scouring was applied to avoid backwashing cycles or the use of chemicals (Lieberman *et al.*, 2016).
- The data used for the sludge treatment were taken from literature (Hospido *et al.*, 2005; Suh and Rousseaux, 2002). The sludge was thickened and dewatered on-site, being the addition of polyacrylamide required in these two stages. Then, it was transported 32.8 km by a 28.0 tones Euro 4 truck to an incineration plant situated in a landfill site in Meruelo, Cantabria, Spain, where it was treated and dispose of (Suh and Rousseaux, 2002).
- After its production in a plant of Derypol, S.A. in Les Franqueses del Vallés, Spain, the polyacrylamide was transported 722 km by a 28.0 tones Euro 4 truck (Derypol, 2017).
- The infrastructure related to the treatment was not considered (Giménez *et al.*, 2015) in order to simplify the LCA application.

Fig. 5.5 depicts the flow diagram and the system boundaries considered for Sc. 3. The main system flows were energy input, water input, manufacture of the reagents used (extraction of resources, manufacture, and transport), and their outputs to the environment.

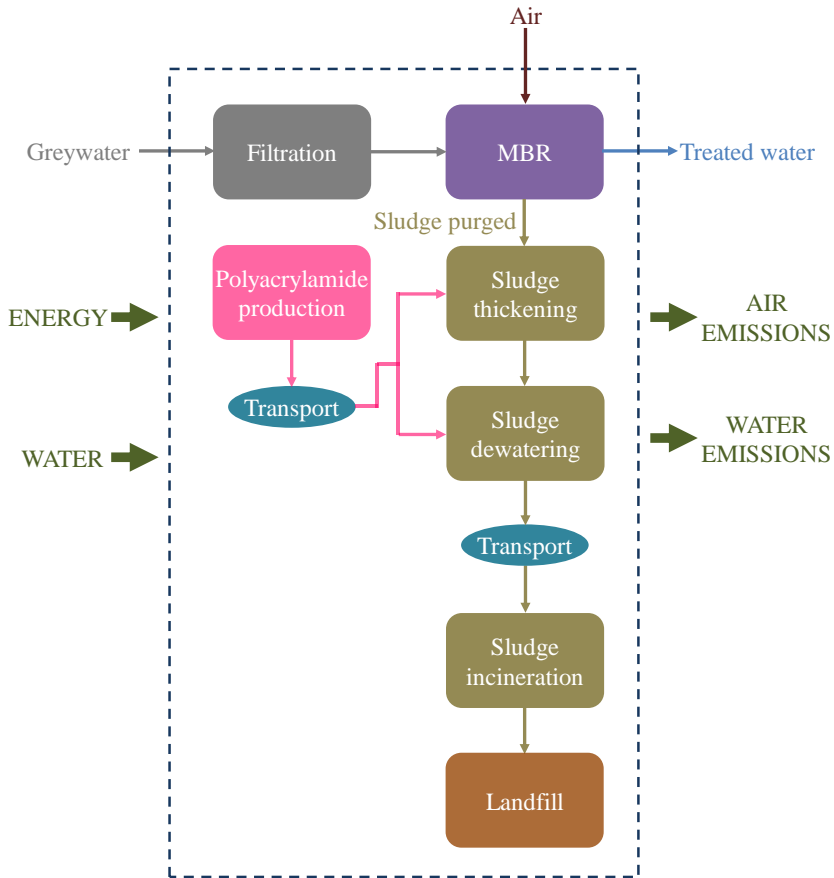


Fig. 5.5. System boundaries for the greywater treatment in Sc. 3 (MBR with sludge incineration).

The sources and quality of the LCI are recorded in Table 5.6 and the energy and mass flows are depicted in the LCI data per functional unit are presented in Table 5.7. Using these values, the natural resources demand and the environmental burdens production associated to the treatment were calculated.

Table 5.6. Summary of data sources used in the LCI for Sc. 3 (MBR with sludge incineration).

Topic	Geographical area	Period	Data source
ENERGY			
Electricity	Spain	2016	Conversion: PE database adapted to the characteristics of the Spanish electricity mix of 2016 (PE International, 2016) Consumption: extrapolation from Literature (Santasmás <i>et al.</i> , 2013)
REAGENTS			
Air	Global	2016	PE database (PE International, 2016)
Polyacrylamide	Global	2012-2014	Ecoinvent database (Frischknecht <i>et al.</i> , 2007)
Reagents consumption	France, Spain	2002-2005	Literature (Hospido <i>et al.</i> , 2005; Suh and Rousseaux, 2002)
TRANSPORT			
Truck	Europe	2016	PE database (PE International, 2016)
Distances	Europe	2016	Assumptions
END OF LIFE			
Incineration	Spain	2014-2015	Literature (Margallo <i>et al.</i> , 2014b; Margallo <i>et al.</i> , 2015)

Table 5.7. LCI for Sc. 3 (MBR with sludge incineration).

Input / output data	Unit	Sc. 3
INPUTS		
Greywater	m ³	1.00
Reagents		
Polyacrylamide	kg FU ⁻¹	6.30·10 ⁻⁴
Air	m ³ FU ⁻¹	2072
Energy		
Aeration	MJ FU ⁻¹	41.4
Pumping	MJ FU ⁻¹	20.3
Sludge treatment	MJ FU ⁻¹	1.00·10 ⁻¹
OUTPUTS		
Sludge	kg FU ⁻¹	7.00·10 ⁻²
Treated water (90.0% SDBS removal)	m ³ FU ⁻¹	1.00

5.2.1. Estimation of the natural resources consumption

The energy intake in Sc. 3 was 162 MJ. Table 5.8 shows that after the normalization process $X_{1,1}$ took a value of $4.00 \cdot 10^{-2}$. It is remarkable that $X_{1,1}$ displayed negative values in the sludge treatment due to the thermal energy obtained during incineration.

Sc. 3 had a significantly higher materials demand, 2481 kg, than Sc. 1 and Sc. 2. This was due to the high intake of materials to produce the energy for the aeration required in the MBR, representing near the 100% of the total natural resources consumed in Sc. 3. Thus, the manufacture of polyacrylamide, the sludge treatment, and the transport showed a negligible contribution to $X_{1,2}$.

Table 5.8. Normalized NRs (dimensionless) for Sc. 3 (MBR with sludge incineration).

	Sc. 3
Energy: $X_{1,1}^*$	$4.00 \cdot 10^{-2}$
Materials: $X_{1,2}^*$	$6.80 \cdot 10^{-1}$
Water: $X_{1,3}^*$	1.00
Total: X_1	$5.70 \cdot 10^{-1}$

Regarding the indicator $X_{1,3}$, although the intakes of water for the reagents production and for cleaning were considered, the main contributor was the water required for the primary energy transformation. According to Table 5.9, the value was 100% for Sc. 3, being the participation of other stages minimal.

Comparing Sc. 3 with the two scenarios previously studied it could be checked that it had the highest total consumption of NRs ($X_1 = 5.70 \cdot 10^{-1}$), being 1.62 times higher than the one of Sc. 1 ($X_1 = 3.50 \cdot 10^{-1}$) and 1.46 times higher than the one of Sc. 2 ($X_1 = 3.90 \cdot 10^{-1}$). This behavior, as it was stated above, was consequence of the high demand of energy to produce the aeration required in the MBR.

Table 5.9. Contribution of the main stages to Sc. 3 (MBR with sludge incineration) to their NRs.

	Contribution (%)		
	Energy	Materials	Water
MBR treatment	100	100	100
Polyacrylamide production	$2.00 \cdot 10^{-2}$	0.00	$7.00 \cdot 10^{-2}$
Sludge treatment	$-9.00 \cdot 10^{-2}$	$1.00 \cdot 10^{-2}$	$-9.00 \cdot 10^{-2}$
Transport	0.00	0.00	0.00

5.2.2. Determination of the environmental burdens

It has to be highlighted that in the energy consumption for this scenario the electricity grid mix chosen might have an important impact on the quantity of greenhouse gas emitted and in the derived results. Hence, the Spanish electricity mix of 2016 was selected.

Before the normalization process, the score obtained for the GW (4.42 kg CO₂ eq.) was almost 3-fold smaller than in Sc. 1 but 2-fold higher than in Sc. 2. Regarding the aquatic indicators, the EU showed the highest impact in the scenario owing to the emissions of ammonia, chemical oxygen demand, nitrogen, and phosphate in energy production.

Table 5.10 shows the EBs to air and water after the normalization process using the European threshold values (E-PRTR, 2006). The HHE and POF became the most important categories among air metrics, as it happened in the other two scenarios. Sc. 3 showed a higher total aquatic EBs than Sc.1 and Sc. 2 owing to its high NMeCo value, which was associated with the disposal process of the sludge incineration waste (Pretel *et al.*, 2016).

Table 5.10. EBs dimensionless variables for Sc. 3 (MBR with sludge incineration).

Environmental burden	Unit	Threshold values	
		(kg year ⁻¹) (E-PRTR, 2006)	Sc. 3
To air: X*_{2,1}			4.70·10⁻⁶
AA: X* _{2,1,1}	kg SO ₂ eq.	150000	1.06·10 ⁻⁷
GW: X* _{2,1,2}	kg CO ₂ eq.	100000000	4.42·10 ⁻⁸
HHE: X* _{2,1,3}	kg benzene eq.	1000	2.34·10 ⁻⁶
POF: X* _{2,1,4}	kg ethylene eq.	1000	1.59·10 ⁻⁶
SOD: X* _{2,1,5}	kg CFC-11 eq.	1.00	6.23·10 ⁻⁷
To water: X*_{2,2}			1.81·10⁻⁷
AOD: X* _{2,2,1}	kg O ₂ eq.	50000	6.73·10 ⁻¹¹
AqA: X* _{2,2,2}	kg H ⁺ eq.	100	2.84·10 ⁻¹¹
MEco: X* _{2,2,3,1}	kg Cu eq.	50.0	1.41·10 ⁻⁹
NMEco: X* _{2,2,3,2}	kg formaldehyde eq.	50.0	1.52·10 ⁻⁷
EU: X* _{2,2,4}	kg phosphate eq.	5000	2.80·10 ⁻⁸

5.2.3. MBR variation assessment

Since the EBs to water in Sc. 3 were slightly higher than in the other two scenarios due to the landfilling process of the sludge, a variation in the MBR to assess the environmental impact of an alternative sludge treatment was applied. In this new scenario, Sc. 3b, the sludge generated in the MBR was used as fertilizer after a composting process, adding a new function to the system.

The MBR scenario was a multi-functional process, where the greywater treatment was the main function and the energy recovery in the landfill site and in the incinerator were additional functions. In these systems, the environmental burdens related to a particular process had to be partitioned over the several functional flows of that process (Margallo *et al.*, 2014b). According to the ISO recommendation, the existence of additional functions was solved gaining credit by the reduction of the emissions related to the co-products. So the impact of the co-product production was subtracted from the original systems. In this case, for energy and material valorization, the ‘avoided’ emissions of conventional production of electricity and fertilizer were subtracted from those produced during waste treatment. This method required the identification of the kind of material substituted or displaced. In Sc. 3, the Spanish energy mix was the substituted process, whereas in Sc. 3b the displaced fertilizer was the ammonium sulfate.

As it can be seen in Fig. 5.6, the sludge was thickened and dewatered on-site following the same procedure than in Sc. 3 and, then, it was stabilized by a composting process, transported, stored for several days and finally used for land stabilization. Fig. 5.3 also shows the flow diagram and the system boundaries considered for Sc. 3b. The main system flows considered were the energy input, water input, production of the reagents used (extraction of resources, manufacture, and transport), and their outputs to the environment. As with the rest of scenarios, in order to simplify the application of the LCA tool, the infrastructure related to the scenario was not considered.

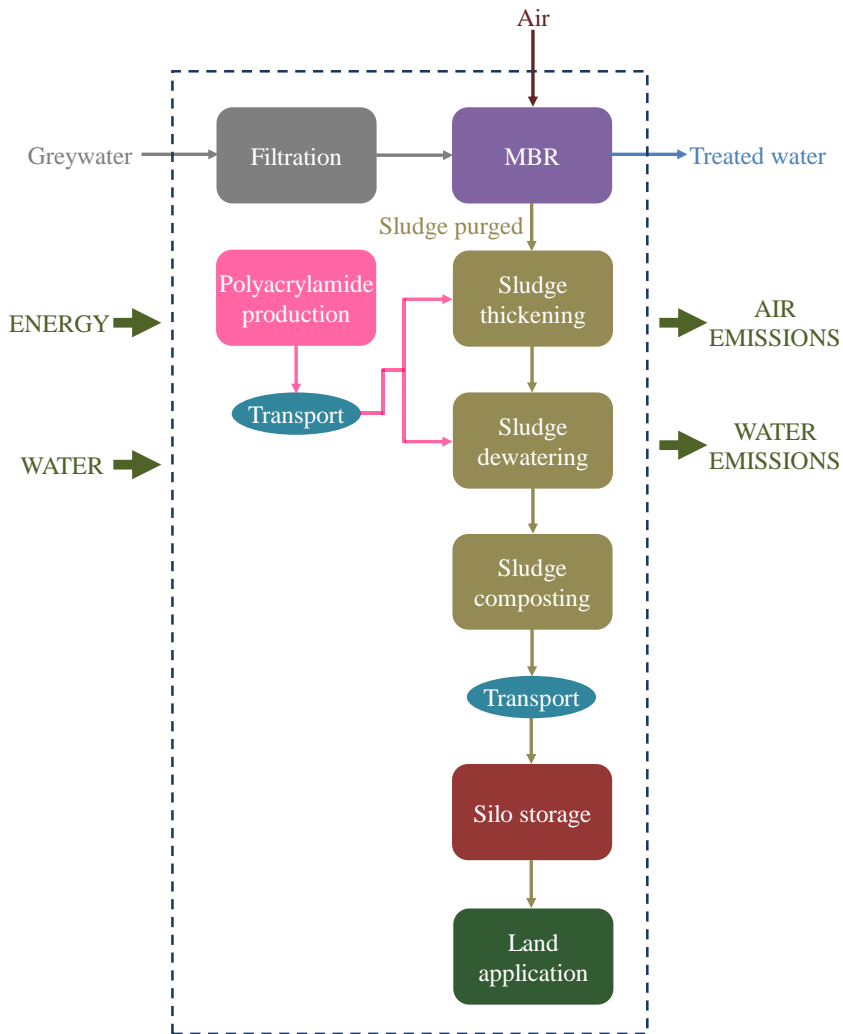


Fig. 5.6. System boundaries for the greywater treatment in Sc. 3b (MBR with sludge composting).

All the data used for the analysis were taken from literature (Hospido *et al.*, 2005; Suh and Rousseaux, 2002). Fig. 5.7 depicts the results obtained. As it can be observed, although the NRs and EBs were expected to be reduced in Sc. 3b, both alternatives had an analogous environmental performance. This was due to the fact that in both scenarios

the energy necessary for the aeration of the reactor was the variable that originated higher consumption of resources and generation of environmental burdens and, therefore, the loads avoided, both by incineration and by composition, were minimal compared to the aeration.

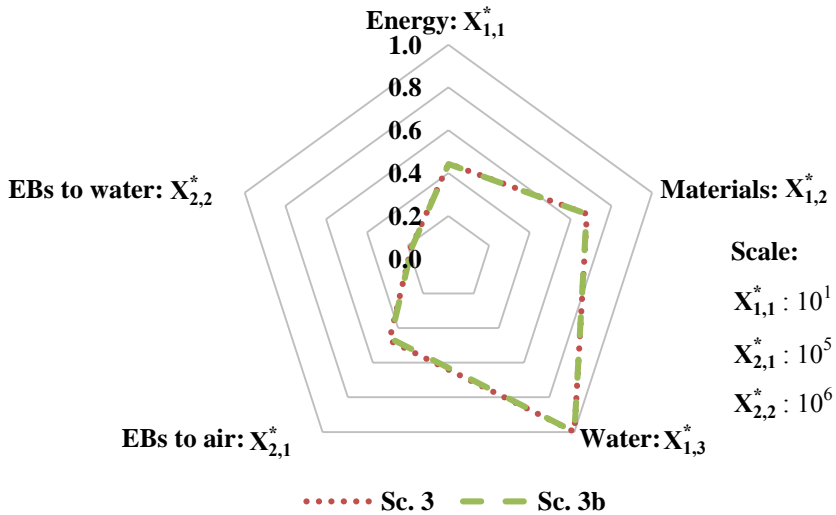


Fig. 5.7. NRs and EBs dimensionless variables for Sc. 3 (MBR with sludge incineration) and Sc. 3b (MBR with sludge composting).

Table 5.11 details the EBs obtained for both scenarios. It can be seen that Sc. 3 had slightly higher EBs than Sc. 3b. This trend was observed for all the indicators with the exception of the water aquatic ecotoxicity, which was higher in Sc. 3b because the sludge applied to the agricultural fields contains heavy metals. Nonetheless, it has to be mentioned that the presence of heavy metals in air was more important than in water because in the first one there were more possibilities of contact between the heavy metals and human beings. Regarding the air burdens, Sc. 3 showed a higher global warming indicator due to the emission of greenhouse gases during

the incineration stage. The highest impact in Sc. 3 was due to the human toxicity, owing to the presence of heavy metals in the gaseous effluent created in the sludge incineration (Suh and Rousseaux, 2002). Furthermore, in Sc. 3 the stratospheric ozone layer depletion also had a high value owing to the landfill gas emissions generated when the incinerated sludge was landfilled. Thus, taking all this into account, the Sc. 3b could be considered the most environmental friendly alternative for the MBR treatment of greywater.

Table 5.11. EBs dimensionless variables for Sc. 3b (MBR with composting).

Environmental burden	Unit	Threshold values	
		(kg year ⁻¹)	Sc. 3b
To air: X*_{2,1}			4.60·10⁻⁶
AA: X _{2,1,1}	kg SO ₂ eq.	150000	1.04·10 ⁻⁷
GW: X* _{2,1,2}	kg CO ₂ eq.	100000000	4.22·10 ⁻⁸
HHE: X* _{2,1,3}	kg benzene eq.	1000	2.30·10 ⁻⁶
POF: X* _{2,1,4}	kg ethylene eq.	1000	1.53·10 ⁻⁶
SOD: X* _{2,1,5}	kg CFC-11eq.	1.00	6.18·10 ⁻⁷
To water: X*_{2,2}			1.78·10⁻⁷
AOD: X* _{2,2,1}	kg O ₂ eq.	50000	6.19·10 ⁻¹¹
AqA: X* _{2,2,2}	kg H ⁺ eq.	100	2.67·10 ⁻¹¹
MEco: X* _{2,2,3,1}	kg Cu eq.	50.0	1.42·10 ⁻⁹
NMEco: X* _{2,2,3,2}	kg formaldehyde eq.	50.0	1.51·10 ⁻⁷
EU: X* _{2,2,4}	kg phosphate eq.	5000	2.57·10 ⁻⁸

5.3. Final remarks

Three alternatives for the treatment of greywater, photocatalysis, photovoltaic solar-driven photocatalysis and MBR, were assessed using the LCA methodology to determine their environmental impacts.

From the results obtained it could be concluded that Sc.2, photovoltaic solar-driven photocatalysis, was the most environmental friendly alternative. Within this scenario it is remarkable that the variable with the highest contribution to the demand of natural resources and the generation of environmental burdens was the energy consumption originated by the high energy requirements of the light source. Thus, in this chapter the main hot-spot of photocatalysis was determined. Moreover, the results obtained allowed to promote the deployment of the photocatalytic process through its combination with photovoltaic solar energy.

Considering the comments given in Chapter 5, future technological challenges have to be addressed for the studied scenarios. In spite of the high potential of photocatalysis for greywater treatment, the energy consumption has to be optimized to operate in a sustainable manner. Hence, more energy efficient light sources need to be developed. However, in order to reduce to a minimum its environmental burdens, the most desirable scenario would come from using solar light as light source but further research is required to overcome some important challenges related to solar photocatalysis, including poor photocatalyst interaction, long term reliability, and the need of large areas of operation.

5.4. References

- [1] Chai, H., Bao, Y., Lin, H., 2013. Engineering applications on reclaimed water treatment and reuse of hotel's high grade gray water. *Adv. Mat. Res.* 610–613, 2391–2396.
- [2] Corona, B., Escudero, L., Quéméré, G., Luque-Heredia, I., San Miguel, G., 2017. Energy and environmental life cycle assessment of a high concentration photovoltaic power plant in Morocco. *Int. J. Life Cycle Assess.* 22, 364–373.
- [3] De Gisi, S., Casella, P., Notarnicola, M., Farina, R., 2016. Grey water in buildings: a mini-review of guidelines, technologies and case studies. *Civ. Eng. Environ. Syst.* 33, 35–54.
- [4] Derypol. <http://www.derypol.com/> (accessed 03.02.2017).
- [5] Dhouib, A., Hdiji, N., Hassaïri, I., Sayadi, S., 2005. Large scale application of membrane bioreactor technology for the treatment and reuse of an anionic surfactant wastewater. *Process Biochem.* 40, 2715–2720.
- [6] EC JCR, 2010. *ILCD Handbook: general guide for life cycle assessment - provisions and action steps.* Publications office of the European Union, Luxembourg.
- [7] E-PRTR, 2006. Regulation (EC) No 166/2006 of the European Parliament and of the Council of 18 January 2006 concerning the establishment of a European pollutant release and transfer register and amending council directives 91/689/EEC and 96/61/EC.
- [8] Evonik Industries. <http://corporate.evonik.com> (accessed 03.02.2017).
- [9] Filimonau, V., Dickinson, J., Robbins, D., Huijbregts, M.A.J., 2011. Reviewing the carbon footprint analysis of hotels: life cycle energy

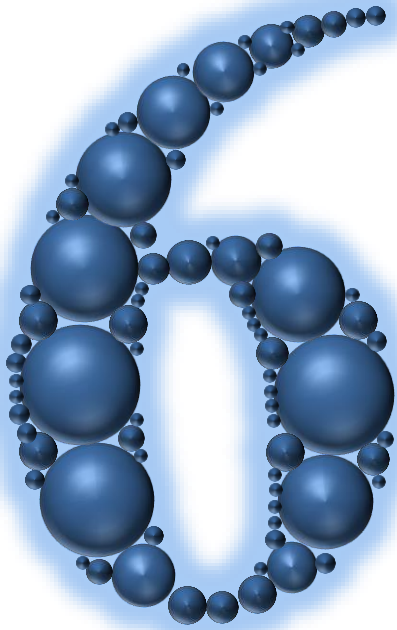
- analysis (LCEA) as a holistic method for carbon impact appraisal of tourist accommodation. *J. Clean. Prod.* 19, 1917–1930.
- [10] Fountoulakis, M.S., Markakis, N., Petousi, I., Manios, T., 2016. Single house on-site grey water treatment using a submerged membrane bioreactor for toilet flushing. *Sci. Total Environ.* 551–552, 706–711.
- [11] Gabarró, J., Batchellí, L., Balaguer, M.D., Puig, S., Colprim, J., 2013. Grey water treatment at a sports centre for reuse in irrigation: a case study. *Environ. Technol.* 34, 1385–1392.
- [12] Gander, M., Jefferson, B., Judd, S., 2000. Aerobic MBRs for domestic wastewater treatment: a review with cost considerations. *Sep. Purif. Technol.* 18, 119–130.
- [13] García, V., Margallo, M., Aldaco, R., Urtiaga, A., Irabien, A., 2013. Environmental sustainability assessment of an innovative Cr (III) passivation process. *ACS Sustainable Chem. Eng.* 1, 481–487.
- [14] Garcia-Herrero, I., Laso, J., Margallo, M., Bala, A., Gazulla, C., Fullana-i-Palmer, P., Vázquez-Rowe, I., Irabien, A., Aldaco, R., 2017a. Incorporating linear programming and life cycle thinking into environmental sustainability decision-making: a case study on anchovy canning industry. *Clean Techn. Environ. Policy.* 19(7), 1897–1912.
- [15] Garcia-Herrero, I., Margallo, M., Onandía, R., Aldaco, R., Irabien, A., 2017b. Environmental challenges of the chlor-alkali production: seeking answers from a life cycle approach. *Sci. Total Environ.* 580, 147–157.
- [16] Giménez, J., Bayarri, B., González, Ó., Malato, S., Peral, J., Esplugas, S., 2015. Advanced oxidation processes at laboratory scale:

- environmental and economic impacts. *ACS Sustainable Chem. Eng.* 3, 3188–3196.
- [17] Gori, R., Cammilli, L., Petrovic, M., Gonzalez, S., Barceló, D., Lubello, C., Malpei, F., 2010. Fate of surfactants in membrane bioreactors and conventional activated sludge plants. *Environ. Sci. Technol.* 44, 8223–8229.
- [18] Hospido, A., Moreira, M.T., Martín, M., Rigola, M., Feijoo, G., 2005. Environmental evaluation of different treatment processes for sludge from urban wastewater treatments: anaerobic digestion versus thermal processes. *Int. J. LCA* 10, 336–345.
- [19] IChemE, 2002. The sustainability metrics. Sustainable development progress metrics recommended for use in the process industries. The Institution of Chemical Engineers, Rugby
- [20] Irabien, A., Aldaco, R., Dominguez-Ramos, A., 2009. Environmental sustainability normalization of industrial processes. *Comput. Aided Chem. Eng.* 26, 1105–1109.
- [21] ISO, 2006a. ISO 14040: environmental management - Life cycle assessment – Principles and framework.
- [22] ISO, 2006b. ISO 14044: environmental management - Life cycle assessment – Requirements and guidelines.
- [23] Khan, S.J., Hankins, N.P., Shen, L.-C., 2016. Submerged and attached growth membrane bioreactors and forward osmosis membrane bioreactors for wastewater treatment. *Emerging membrane technology for sustainable water treatment*, 277–296. Singh, R., Hankins, N.P., Elsevier B.V, Amsterdam, Netherlands.
- [24] Liberman, N., Shandalov, S., Forgacs, C., Oron, G., Brenner, A., 2016. Use of MBR to sustain active biomass for treatment of low

- organic load grey water. *Clean Techn. Environ. Policy* 18, 1219–1224.
- [25] Margallo, M., Aldaco, R., Irabien, A., Carrillo, V., Fischer, M., Bala, A., Fullana, P., 2014b. Life cycle assessment modelling of waste-to-energy incineration in Spain and Portugal. *Waste Manag. Res.* 32, 492–499.
- [26] Margallo, M., Dominguez-Ramos, A., Aldaco, R., Bala, A., Fullana, P., Irabien, A., 2014a. Environmental sustainability assessment in the process industry: a case study of waste-to-energy plants in Spain. *Resour. Conserv. Recy.* 93, 144–155.
- [27] Margallo, M., Taddei, M.B.M., Hernández-Pellón, A., Aldaco, R., Irabien, Á., 2015. Environmental sustainability assessment of the management of municipal solid waste incineration residues: a review of the current situation. *Clean Techn. Environ. Policy* 17(5), 1333–1353.
- [28] Máša, V., Bobák, P., Kuba, P., Stehlík P., 2013. Analysis of energy efficient and environmentally friendly technologies in professional laundry service. *Clean Techn. Environ. Policy* 15, 445–457.
- [29] Merz, C., Scheumann, R., El Hamouri, B., Kraume, M., 2007. Membrane bioreactor technology for the treatment of greywater from a sports and leisure club. *Desalination* 215, 37–43.
- [30] Muñoz, I., 2003. Life cycle assessment as a tool for green chemistry: application to kraft pulp industrial wastewater treatment by different advanced oxidation processes. *Universitat Autònoma de Barcelona*.
- [31] Muñoz, I., Peral, J., Ayllón, J.A., Malato, S., Passarinho, P., Domènech, X., 2006. Life cycle assessment of a coupled solar photocatalytic–biological process for wastewater treatment. *Water Res.* 40, 3533–3540.

- [32] Muñoz, I., Rieradevall, J., Torrades, F., Peral, J., Domènech, X., 2005. Environmental assessment of different solar driven advanced oxidation processes. *Sol. Energy* 79, 369–375.
- [33] PE International, 2016. Gabi 6 Software and Database on Life Cycle Assessment. Leinfelden-Echterdingen, Germany.
- [34] Pretel, R., Robles, A., Ruano, M.V., Seco, A., Ferrer, J., 2016. Economic and environmental sustainability of submerged anaerobic MBR-based (AnMBR-based) technology as compared to aerobic-based technologies for moderate-/high-loaded urban wastewater treatment. *J. Environ. Manage.* 166, 45–54.
- [35] Real Decreto 1620/2007, de 7 de diciembre, por el que se establece el régimen jurídico de la reutilización de las aguas depuradas, BOE no. 294, 2007.
- [36] Rivero, M.J., Parsons, S.A., Jeffrey, P., Pidou, M., Jefferson, B., 2006. Membrane chemical reactor (MCR) combining photocatalysis and microfiltration for grey water treatment. *Water Sci. Technol.* 53, 173–180.
- [37] Sanchez, M., Rivero, M.J., Ortiz, I., 2010. Photocatalytic oxidation of grey water over titanium dioxide suspensions. *Desalination* 262, 141–146.
- [38] Santasmasas, C., Rovira, M., Clarens, F., Valderrama, C., 2013. Grey water reclamation by decentralized MBR prototype. *Resour. Conserv. Recy.* 72, 102–107.
- [39] Serra, A., Brillas, E., Domènech, X., Peral, J., 2011. Treatment of biorecalcitrant α -methylphenylglycine aqueous solutions with a solar photo-Fenton-aerobic biological coupling: biodegradability and environmental impact assessment. *Chem. Eng. J.* 172, 654–664.

- [40] Song, K., Mohseni, M., Taghipour, F, 2016. Application of ultraviolet light-emitting diodes (UV-LEDs) for water disinfection: a review. *Water Res.* 94, 341–349.
- [41] Spasiano, D., Marotta, R., Malato, S., Fernandez-Ibañez, P., Di Somma, I., 2015. Solar photocatalysis: materials, reactors, some commercial, and pre-industrialized applications. a comprehensive approach. *Appl. Catal. B-Environ.* 170–171, 90–123.
- [42] Suh, Y.-J., Rousseaux, P., 2002. An LCA of alternative wastewater sludge treatment scenarios. *Resour. Conserv. Recy.* 35, 191–200.



CONCLUSIONS

Chapter 6

Conclusions

Abstract

This thesis aims to contribute to the progress of knowledge and development of the photocatalysis technology through the identification and resolution of its main challenges. This chapter summarizes the main results attained, draws the conclusions derived from the analysis of these results, and highlights future challenges that would be necessary to overcome for the adequate scale-up and industrial implementation of photocatalytic processes.

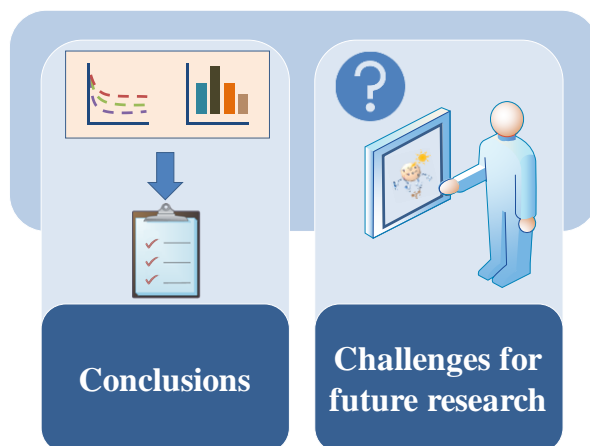


Fig. 6.1. Graphical abstract.

6.1. Conclusions

This thesis is focused on advance the knowledge of the photocatalysis technology for the removal of emerging contaminants through the identification and resolution of its mains challenges. As it was shown, several issues still remain challenging for its scale-up and industrial implementation worldwide.

The easy and low cost recovery of the photocatalyst after the treatment and the development of photocatalysts with activity under sunlight are two of the main challenges. Thus, the synthesis, characterization and testing of magnetic $\text{TiO}_2\text{-WO}_3$ composites, $\text{Fe}_3\text{O}_4@\text{SiO}_2@\text{TiO}_2\text{-WO}_3$, were performed. The photocatalytic activity was studied for the removal of the emerging contaminant bisphenol A (BPA) in two water matrixes, ultrapure water (UP) and real wastewater, under simulated solar light (photoreactor 1 (Xe lamp)). A decrease in the activity of the photocatalysts was observed in the treatment of BPA in the wastewater owing to its complex chemical composition. For both cases, the commercial photocatalyst TiO_2 P25 showed best results, however, the synthesized photocatalyst was easily recovered after treatment. In the case of UP water, the determination of the reaction intermediates was performed to propose a degradation pathway for the photocatalytic removal of BPA. When any of the photocatalysts synthesized in this thesis were used, 2-(4-hydroxyphenyl)-2-propanol was the only aromatic ring compound that was identified, while with TiO_2 P25 the compounds observed were different. It is worth mentioning that, further work is required to increase the activity of the synthesized photocatalysts to improve the trade-off between loss of activity and photocatalyst recovery.

Due to the existence of countless photoreactor designs aiming to the optimal configuration for the performance of the photocatalytic degradation, another key issue related to the scale-up of photocatalysis is the lack of robust parameters that allow the comparison of the obtained photocatalytic results. Taking into account that the rate of hydroxyl radicals ($\cdot\text{OH}$) generation has a great influence in the overall photocatalytic oxidation rate, it was proposed as an index for comparison purposes. Hence, this thesis contributes to the progress of knowledge in photocatalysis by proposing a methodology to describe $\cdot\text{OH}$ generation kinetic models including as main variable the radiation intensity. The methodology was applied to two light emitting diodes (LEDs) photoreactors with adjustable radiation intensity, photoreactor 3 (1st generation LEDs) and photoreactor 4 (upgraded LEDs), for the removal of sodium dodecylbenzenesulfonate (SDBS). It is worth noticing that the last one allowed the evaluation of the influence of the radiation intensity in a wider range, accomplishing higher SDBS degradation.

When using artificial light sources, another challenge in photocatalysis is the reduction of the energy consumed by the light source. Therefore, three photoreactors with different types of lights sources, photoreactor 2 (Hg lamp), photoreactor 3 (1st generation LEDs), and photoreactor 4 (upgraded LEDs) were evaluated for the photocatalytic removal of SDBS and the assessment of the energy efficiency was performed through the parameter electrical energy per order (E_{EO}). It was observed that photoreactor 2 (Hg lamp) was the best alternative from a kinetic perspective, nevertheless, photoreactor 4 (upgraded LEDs) showed the minimum E_{EO} , implying that it was the best global option from a kinetic and energy consumption coupled point of view.

Finally, since for the scale-up of photocatalysis it is necessary to consider not only the degree of degradation and mineralization attained during the treatment but also the environmental impacts generated, a complete environmental assessment was performed using the life cycle assessment (LCA) approach. The LCA of the photocatalytic treatment of greywater generated in a hotel laundry was performed. Additionally, the LCA results were compared to those attained with two alternatives, photovoltaic solar-driven photocatalysis and membrane biological reactor. The results showed that photovoltaic solar-driven photocatalysis was the most environmentally friendly alternative and that the hot-spot of this alternative was the energy consumption derived from the high energy intake of the light source.

To sum up this thesis addresses four of the most important challenges for the development of photocatalysis at industrial scale, contributing to make progress in its technology readiness.

6.2. Challenges for future research

This thesis aims to contribute to the development of photocatalysis for the removal of emerging contaminants. However, despite the achievements already described, there are still new challenges ahead that must be overcome to improve the present research:

- Study in depth of the synthesis process of magnetic photocatalysts in order to increase the activity of the photocatalysts keeping the capacity of magnetic recovery.

- Development of a mathematical model that considers the radiation emission field of the light source and includes the absorption and scattering radiation phenomena.
- Design of an optimal photoreactor that allows working with maximum illumination efficiency and minimum mass transfer limitations.

6.3. Conclusiones

Esta tesis se centra en el progreso de la tecnología de fotocatalisis para la eliminación de contaminantes emergentes a través de la identificación y resolución de sus principales desafíos. Como se demostró, varias cuestiones siguen siendo un reto para el cambio de escala e implementación industrial en todo el mundo.

La recuperación del fotocatalizador fácil y económica después del tratamiento y el desarrollo de fotocatalizadores con actividad bajo la luz solar son dos de los principales desafíos. Por lo tanto, se realizó la síntesis, caracterización y prueba de fotocatalizadores magnéticos de $\text{TiO}_2\text{-WO}_3$ ($\text{Fe}_3\text{O}_4@\text{SiO}_2@\text{TiO}_2\text{-WO}_3$). La actividad fotocatalítica se estudió para la eliminación del contaminante emergente bisfenol A (BPA) en dos matrices de agua, agua ultrapura (UP) y aguas residuales reales, bajo luz solar simulada (fotorreactor 1 (lámpara Xe)). Se observó una disminución en la actividad de los fotocatalizadores en el tratamiento del BPA en las aguas residuales debido a su compleja composición química. Para ambos casos, el fotocatalizador comercial TiO_2 P25 mostró mejores resultados, sin embargo, el fotocatalizador sintetizado se recuperó fácilmente después del tratamiento. En el caso del agua UP, la determinación de los intermedios

de reacción se realizó para proponer una ruta de degradación para la eliminación fotocatalítica de BPA. Cuando se utilizó cualquiera de los fotocatalizadores sintetizados en esta tesis, el 2-(4-hidroxifenil)-2-propanol fue el único compuesto con anillo aromático identificado, mientras que con el TiO₂ P25 los compuestos observados fueron diferentes. Vale la pena mencionar que se requiere trabajo futuro para aumentar la actividad de los fotocatalizadores sintetizados para encontrar una solución de compromiso entre la pérdida de actividad y la recuperación del fotocatalizador.

Debido a la existencia de innumerables diseños de fotorreactores que tienen como objetivo obtener una configuración óptima para la fotocatálisis, otra cuestión clave relacionada con el cambio de escala de la tecnología es la falta de parámetros robustos que permitan comparar los resultados fotocatalíticos obtenidos. Teniendo en cuenta que la velocidad de generación de radicales hidroxilo ([•]OH) tiene una gran influencia en la velocidad global de oxidación fotocatalítica, la primera se propuso como índice para propósitos de comparación. Por lo tanto, esta tesis contribuye al progreso de la fotocatálisis al proponer una metodología para obtener modelos cinéticos de generación de [•]OH que incluyan como variable principal la intensidad de la radiación. La metodología se aplicó a dos fotorreactores con diodos emisores de luz (LEDs) con intensidad de radiación ajustable, fotorreactor 3 (LEDs de primera generación) y fotorreactor 4 (LED mejorados), para la eliminación de dodecibencenosulfonato de sodio (SDBS). Vale la pena destacar que el último permitió la evaluación de la influencia de la intensidad de la radiación en un rango más amplio, logrando mayor degradación de SDBS.

Cuando se usan fuentes de luz artificiales, otro desafío en la fotocatalisis es la reducción de la energía consumida por la fuente de luz. Consecuentemente, tres fotorreactores con diferentes tipos de fuentes de luz, fotorreactor 2 (lámpara Hg), fotorreactor 3 (LED de primera generación) y fotorreactor 4 (LEDs mejorados) fueron evaluados para la eliminación fotocatalítica de SDBS y se realizó una evaluación de su eficiencia energética a través de el parámetro “electrical energy per order (E_{EO})”. Se observó que el fotorreactor 2 (lámpara Hg) fue la mejor alternativa desde una perspectiva cinética, sin embargo, el fotorreactor 4 (LEDs mejorados) mostró el E_{EO} mínimo, lo que implica que fue la mejor opción global desde un punto de vista combinado cinético y de consumo energético.

Finalmente, dado que para el cambio de escala de la fotocatalisis es necesario considerar no solo el grado de degradación y mineralización alcanzado durante el tratamiento sino también los impactos ambientales generados, se realizó la evaluación ambiental completa utilizando el enfoque de análisis de ciclo de vida (ACV). Se realizó el ACV del tratamiento fotocatalítico de aguas grises generadas en la lavandería de un hotel. Además, los resultados del ACV se compararon con los obtenidos con dos alternativas, fotocatalisis solar fotovoltaica y reactor biológico de membrana. Los resultados mostraron que la fotocatalisis solar fotovoltaica es la alternativa más respetuosa con el medio ambiente y que el cuello de botella de esta alternativa es el consumo de energía derivado del elevado requerimiento energético de la fuente de luz.

En resumen, esta tesis aborda cuatro de los desafíos más importantes para el desarrollo de la fotocatalisis a escala industrial, contribuyendo a su maduración de tecnológica.

6.4. Retos futuros

Esta tesis pretende contribuir al desarrollo de la fotocatalisis para la eliminación de contaminantes emergentes. Sin embargo, a pesar de los logros descritos en la misma, todavía hay nuevos desafíos por delante que deben superarse para mejorar la presente investigación:

- Estudiar en profundidad el proceso de síntesis de los fotocatalizadores magnéticos para aumentar la actividad de los fotocatalizadores manteniendo la capacidad de recuperación magnética.
- Desarrollo de un modelo matemático que considere el campo de emisión de radiación de la fuente de luz e incluya los fenómenos de absorción y dispersión de la radiación.
- Diseño de un fotorreactor óptimo que permita trabajar con máxima eficiencia de iluminación y mínimas limitaciones de transferencia de materia.

ANNEXES

Annex I. Nomenclature

AA atmospheric acidification

AOD aquatic oxygen demand

AOPs advanced oxidation processes

AqA aquatic acidification

BET Brunauer-Emmett-Teller

BPA bisphenol A

[BPA] concentration of bisphenol A

CB conduction band

CO₂ carbon dioxide

CTAB Cetyl trimethyl ammonium bromide

DMSO dimethyl sulfoxide

DNPH 2,4-dinitrophenylhydrazine

DNPHo 2,4-dinitrophenylhydrazine hydrazine

DOC dissolved organic carbon

[DOC] concentration of dissolved organic carbon

EBs environmental burdens

EDCs endocrine-disrupting compounds

EDS Electron dispersion spectroscopy

E_{EO} electrical energy per order

E_g band gap energy

EU eutrophication

e⁻ electron

e⁻/h⁺ electron-hole pair

GC-MS gas chromatography with mass spectrometry

GW global warming

Hg mercury

HHE human health effects

HPLC high performance liquid chromatography
HR-TEM high-resolution transmission electron microscope
H₂O water
H₂O₂ hydrogen peroxide
h⁺ hole
IC inorganic carbon
k_{app} pseudo-first order kinetic constant
k_{[•OH]_{gen}} hydroxyl radicals generation kinetic constant
LCA life cycle assessment
LCI life cycle inventory
LCIA life cycle impact assessment
LC-Q-TOF/MS quadrupole time of flight/mass spectrometer
LEDs light emitting diodes
m experimental fitted parameter
MBR membrane biological reactor
MEco ecotoxicity to aquatic life (metals to seawater)
M_s magnetization saturation
n experimental fitted parameter
NDIR non-dispersive infrared
NMEco ecotoxicity to aquatic life (other substances)
NRs natural resources
O₃ ozone
O₂^{-•} superoxide anion radicals
•OH hydroxyl radicals
•OH_{gen} hydroxyl radicals generated
[•OH]_{gen} concentration of hydroxyl radicals generated
P_{el} electrical power
POF photochemical ozone formation

R^2 regression coefficient
Rad radiation intensity
 $r_{[\cdot\text{OH}]_{\text{gen}}}$ rate of hydroxyl radicals generation
SDBS sodium dodecylbenzenesulfonate
[SDBS] concentration of sodium dodecylbenzenesulfonate
[SDBS]_{rem} concentration of sodium dodecylbenzenesulfonate removed
SEM scanning electron microscope
SOD stratospheric ozone depletion
TC total carbon
TEOS tetraethyl orthosilicate
 TiO_2 titanium dioxide
[TiO_2] concentration of titanium dioxide
TOC total organic carbon
TTIP titanium (IV) isopropoxide
UP ultrapure
UV ultraviolet
VB valence band
 WO_3 tungsten (VI) oxide
WWTPs wastewater treatment plants
XRD X-ray diffraction
Xe xenon
 $X_{1,1}$ consumption of energy
 $X_{1,2}$ consumption of materials
 $X_{1,3}$ consumption of water
 $X_{2,1}$ primary burdens to air
 $X_{2,2}$ primary burdens to water
 $X_{2,3}$ primary burdens to land
 λ wavelength

Annex II. Scientific contributions

List of papers published in indexed journals

1. **Dominguez, S.**, Laso, J., Margallo, M., Aldaco, R., Rivero, M.J., Irabien, Á., Ortiz, I., 2017. Comparative LCA of greywater management within a water circular economy restorative thinking framework. *Sci. Total Environ.*, article in press (JCR impact factor 2016: 4.900, Q1, position 22 of 229 in the Environmental Sciences category).



2. Gómez-Pastora, J., **Dominguez, S.**, Bringas, E., Rivero, M.J., Ortiz, I., Dionysiou, D.D., 2017. Review and perspectives on the use of magnetic nanophotocatalysts (MNPCs) in water treatment. *Chem. Eng. J.* 310, 407–427 (JCR impact factor 2016: 6.216, Q1, position 6 of 135 in the Chemical Engineering category).



3. **Dominguez, S.**, Huebra, M., Han, C., Campo, P., Nadagouda, M.N., Rivero, M.J., Ortiz, I., Dionysiou, D.D., 2017. Magnetically recoverable TiO₂-WO₃ photocatalyst to oxidize bisphenol A from model wastewater under simulated solar light. *Environ. Sci. Pollut. R.* 24, 12589–12598 (JCR impact factor 2016: 2.741, Q2, position 79 of 229 in the Environmental Sciences category).



4. Escudero, C.J., Iglesias, O., **Dominguez, S.**, Rivero, M.J., Ortiz, I., 2017. Performance of electrochemical oxidation and photocatalysis in terms of kinetics and energy consumption. new insights into the p-cresol degradation. *J. Environ. Manage.* 195, 117–124 (JCR impact factor 2016: 4.010, Q1, position 39 of 229 in the Environmental Sciences category).



5. **Dominguez, S.**, Rivero, M.J., Gomez, P., Ibañez, R., Ortiz, I., 2016. Kinetic modeling and energy evaluation of sodium dodecylbenzenesulfonate photocatalytic degradation in a new LED reactor. *J. Ind. Eng. Chem.* 37, 237–242 (JCR impact factor 2016: 4.421, Q1, position 14 of 135 in the Chemical Engineering category).



6. **Dominguez, S.**, Ribao, P., Rivero, M.J., Ortiz, I., 2015. Influence of radiation and TiO_2 concentration on the hydroxyl radicals generation in a photocatalytic LED reactor. Application to dodecylbenzenesulfonate degradation. *Appl. Catal. B - Environ.*, 178, 165–169 (JCR impact factor 2015: 8.328, Q1, position 3 of 135 in the Chemical Engineering category).



Related papers published prior to this thesis

7. Rivero, M.J., Alonso, E., **Dominguez, S.**, Ribao, P., Ibañez R., Ortiz I., Irabien, A., 2014. Kinetic analysis and biodegradability of the Fenton mineralization of bisphenol A. J. Chem. Technol. Biot. 89:8, 1228–1234 (JCR impact factor 2014: 2.738, Q1, position 28 of 135 in the Chemical Engineering category).



Contributions to scientific meetings

1. **Dominguez, S.**, Mueses, M.A., Rivero, M.J., Ortiz, I., Li Puma, G. Modeling of radiant field in a light emitting diodes photocatalytic reactor using TiO₂. 3rd Iberoamerican Conference on Advanced Oxidation Technologies – III CIPOA, Guatapé, Colombia, 11/(14-17)/2017. Poster presentation.



2. Rivero, M.J., **Dominguez, S.**, Ortiz, I. Comparative energy assessment of two UV light advanced oxidation processes. 10th World Congress of Chemical Engineering – WCCE 2017, Barcelona, Spain, 10/(1-5)/2017. Oral presentation.



3. Rancaño, L., **Dominguez, S.**, Rivero, M.J. Combination of coagulation-flocculation and photocatalysis for the treatment of landfill leachate. 10th World Congress of Chemical Engineering – WCCE 2017, Barcelona, Spain, 10/(1-5)/2017. Poster presentation.



4. Rivero, M.J., **Dominguez, S.**, Ortiz, I. Conceptual design of a photocatalytic LED reactor for grey water treatment. 5th European Conference on Environmental Applications of Advanced Oxidation Processes – EAAOP5, Prague, Czech Republic, 6/(25-29)/2017. Poster presentation.



5. Dominguez, S., Han, C., Nadagouda, M.N., Rivero, M.J., Ortiz, I., Dionysiou, D.D. Magnetically Recoverable TiO_2/WO_3 Photocatalyst to oxidize bisphenol A from model wastewater under simulated solar light. 9th European meeting on Solar Chemistry and Photocatalysis: Environmental Applications – SPEA9, Strasbourg, France, 06/(13-17)/2016. Poster and oral flash presentations.



6. Rivero, M.J., Ribao, P., **Dominguez, S.**, Ortiz, I. Influence of the synthesis method on the photocatalytic activity of graphene oxide/titanium dioxide composites. 4th European Conference on Environmental Applications of Advanced Oxidation Processes – EAAOP4, Athens, Greece, 10/(21-24)/2015. Oral presentation.



7. Rivero, M.J., Escudero, C.J., Iglesias, O., **Dominguez, S.**, Ortiz, I. New insights into the electro-oxidation of a model phenolic compound, p-cresol: effect of electrode material and electrolyte. 4th European Conference on Environmental Applications of Advanced Oxidation Processes – EAAOP4, Athens, Greece, 10/(21-24)/2015. Poster presentation.



8. **Dominguez, S.**, Rivero, M.J., Ortiz, I. Photocatalytic removal of bisphenol A with a magnetically separable TiO₂ nanocomposite. 4th European Conference on Environmental Applications of Advanced Oxidation Processes – EAAOP4, Athens, Greece, 10/(21-24)/2015. Poster presentation.



9. **Dominguez, S.**, **Rivero, M.J.**, Gomez, P., Ibañez, R., Urtiaga, A.M., Ortiz, I. New LED reactor designs for photocatalysis applied to water treatment. 7th European Meeting on Chemical Industry and Environment – EMChIE, Tarragona, Spain, 06/(10-12)/2015. Oral presentation.



10. Ribao, P., **Dominguez, S.**, Rivero, M.J., Ortiz, I. Influence of the inoculum in the respirometric biodegradability of oxidized waters. 13th Mediterranean Congress of Chemical Engineering – 13MCCE, Barcelona, Spain, 09/30/2014 - 10/03/2014. Poster presentation.

13MCCE

11. **Dominguez, S.**, Ribao, P., Rivero, M.J., Ortiz, I. Influence of TiO₂ concentration on the OH radicals generation. Photocatalytic removal of dodecylbenzenesulfonate. ANQUE·ICCE·BIOTEC 2014 Congresses on Chemistry, Chemical Engineering and Biotechnology, Madrid, Spain, 07/(01-04)/2014. Poster presentation.



12. Ribao, P., **Dominguez, S.**, Ramirez, F., Gonzalez-Barriuso, M., Rivero, M.J., Yedra, A., Ortiz, I. New catalysts based on nanocomposites of graphene oxide-TiO₂ for photocatalytic applications. ANQUE·ICCE·BIOTEC 2014 Congresses on Chemistry, Chemical Engineering and Biotechnology, Madrid, Spain, 07/(01-04)/2014. Poster presentation.



13. **Rivero, M.J., Dominguez, S.**, Ribao, P., Ortiz, I. Influence of radiation on the ·OH generation in a photocatalytic LED reactor. Application to Removal of dodecylbenzenesulfonate. 8th European Meeting on Solar Chemistry and Photocatalysis: Environmental Applications – SPEA8, Thessaloniki, Greece, 06/(25-28)/2014. Oral presentation.



Related contributions prior to this thesis

14. Rivero, M.J., **Dominguez, S.**, Ortiz, I. Biodegradability enhancement of bisphenol A solutions after advanced oxidation processes. 3rd European Conference on Environmental Applications of Advanced Oxidation Processes – EAAOP3, Almería, Spain, 10/(28-30)/2013. Poster presentation.



15. Dominguez, S., Rivero, M.J., Ortiz, I. Photocatalytic degradation of bisphenol with titanium dioxide. XXXIV Reunión Bienal de la Real Sociedad Española de Química, Santander, Spain, 09/(15-18)/2013. Poster presentation.



16. Rivero, M.J., **Dominguez, S.**, Perez, M.A., Ortiz, I. Feasibility of a UV-LED reactor for dodecylbenzenesulphonate photocatalytic degradation. Oxidation Technologies for Water and Wastewater Treatment – AOP6, Goslar, Germany, 05/(07-09)/2012. Poster presentation.



About the author



Sara Domínguez (Santander, 1989) is Chemical Engineer (2007-2012) and Technical Industrial Engineer specialized in industrial chemistry (2012-2013) by the University of Cantabria (Spain). Moreover, she did a Master's Degree in Chemical Engineer (2012-2013) at the University of Cantabria.

In 2012 she joined the Chemical and Biomolecular Engineering Department of the University of Cantabria as researcher. After one year, she was granted with a Personnel Research Training Program of the Spanish Ministry of Economy and Competitiveness to develop her Ph.D. studies, under the supervision of Prof. Dr. Inmaculada Ortiz and Dr. María José Rivero.

In the framework of her Ph.D. she performed two short research stays. During the first one, she was under the supervision of Prof. Dr. Dionysios D. Dionysiou in the Department of Biomedical, Chemical and Environmental Engineering of the University of Cincinnati (United States of America). The second research was in the Department of Chemical Engineering of Loughborough University (United Kingdom) under the supervision of Prof. Dr. Gianluca Li Puma.

She is the author of 7 scientific articles in indexed journals and 16 contributions to international conferences.

The sustainable management of the available water resources represents one of the most important issues that the scientific community has to face. One promising solution is the treatment and reuse of wastewater. Thus, the development of environmental friendly technologies that allow to treat wastewater with low-cost and high efficiency results vital.

Emerging contaminants, which are not completely removed by conventional wastewater treatments, have become a social concern due to their presence in aquatic environments and their negative impact on ecological or human health.

Advanced oxidation processes seem to be an appropriate group of technologies for wastewater treatment that have shown high effectiveness in the removal of several emerging contaminants. Among them, photocatalysis arises as a sustainable alternative for the removal of these contaminants. However, although its technical viability has been assessed, some challenges still need to be overcome to develop an efficient and sustainable photocatalytic process implemented at industrial scale.

This thesis aims at the development of the photocatalysis technology through the identification and approach of solutions of its main challenges for the degradation of emerging contaminants.